APPENDIX I: ANALYTICAL SIMULATION

INTRODUCTION

For certain simplifying assumptions, the radial flow equation can be solved analytically. Application of analytical simulation can be extended to a wide combination of wells and reservoir geometries. The development of analytical simulation will be discussed herein; the approach has been discussed by several authors in the past; van Everdingen and Hurst(1940), Matthews et al(1954), and Collins(1961), however, the most comprehensive, succinct, and most recent approach is contained in a monograph on well testing written by Earlougher(1977). Much of the material presented herein closely follows that development. Where the works of others are utilized, they are appropriately referenced.

Basic Equations and Assumptions

In order to understand the principles of analytic solutions, one must deal directly with the partial differential equations which govern fluid flow in porous media. Matthews and Russell(1967) give the basic fundamentals for deriving the radial flow equation for a single well.

The resulting partial differential equation is a combination of the law of conservation of matter, a simple equation-of-state, and Darcy's law. This equation is commonly referred to as the diffusivity equation and is:

$$\frac{\partial^2 p}{\partial r^2} + \frac{1}{r}\frac{\partial p}{\partial r} = \frac{1}{0.0002637}\frac{\phi \mu c}{k}\frac{\partial p}{\partial t} \qquad \text{(I-1)}$$

The assumptions utilized in the development of this equation are horizontal flow, negligible gravity effects, a homogeneous and isotropic porous medium (reservoir rock), and a single phase fluid of small and constant compressibility. Darcy's law must be applicable i.e. laminar flow, and the fluid and rock properties must be constant and independent of pressure. The temperature of the rock/fluid system must be constant, i.e. isothermal flow.

The parameters in the above equation are:

p = pressure, psia

r = radial position from well, ft.

ϕ = porosity of rock, fraction

μ = fluid viscosity, centipoise

k = permeability of rock, millidarcies

c = compressibility, volume/volume/psi

where

$$c = -\frac{1}{v}\frac{\partial v}{\partial p}$$

where

v = fluid volume in consistent units

The constant 0.0002637 is required to render consistency in oil field units between the right and left hand sides of the equation. The group of terms, $\frac{\phi \mu c}{k}$ is termed the hydraulic diffusivity, thereby giving rise to the equation name. Similar analogs exist in heat and electrical potential equations. All equations of this type are known as diffusivity equations.

Solutions of this equation fall into three classifications with respect to boundary conditions. All three cases assume a centrally located well flowing at a constant rate. The three basic cases are: 1) infinite reservoir, i.e. $p \longrightarrow p_{initial}$ as $r \longrightarrow \infty$, 2) bounded cylindrical reservoir, $[\partial p / \partial r]_{r_e} = 0$, and 3) constant pressure outer boundary at edge of cylindrical drainage area, $p = p_{initial}$ at $r = r_e$. Figure I-1, taken from Matthews and Russell(1967) illustrates the three cases.

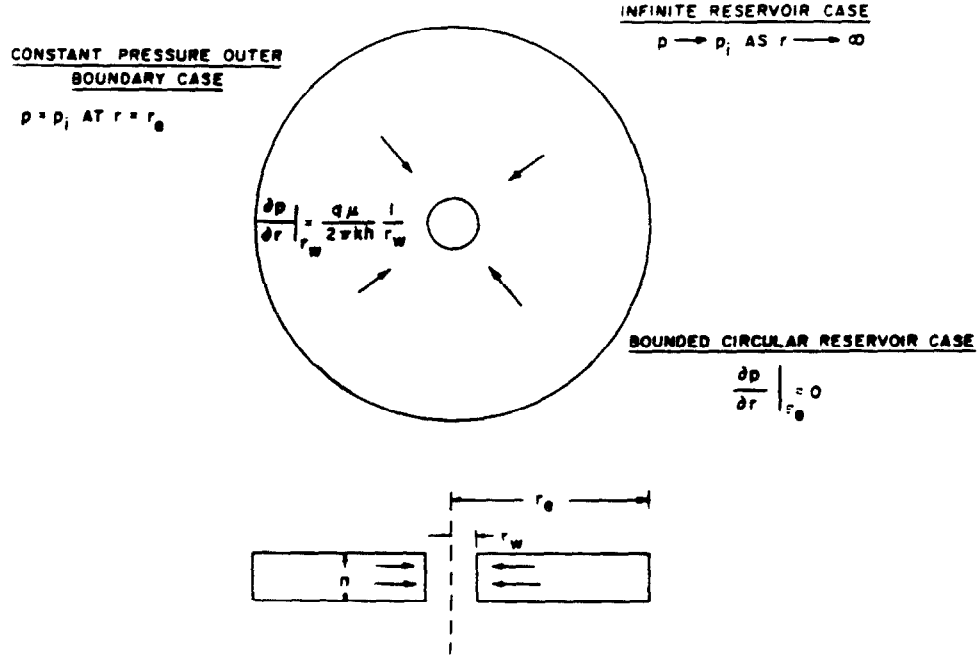

Figure I-1

For the infinite reservoir case the initial and wellbore boundary conditions are: 1) $p = p_i$ at $t = 0$ for all r and 2) from Darcy's law in terms of flow rate (q, Bbls/day) at the reservoir sandface:

$$q = \frac{2\pi kh}{\mu}\left(r\frac{\partial p}{\partial r}\right)\Bigg|_{r_w} \quad \text{or}$$

$$\left(\frac{\partial p}{\partial r}\right)_{r_w} = \frac{q\mu}{2\pi kh}\frac{1}{r_w} \tag{I-2}$$

For this case the well known exponential-integral solution of Theis (1935) exists.

$$p(r,t) = p_i - \frac{q\mu}{2\pi kh}\left\{-\frac{1}{2}\,Ei\left(\frac{-\phi\mu cr^2}{4kt}\right)\right\} \tag{I-3}$$

where

$$-Ei(-x) = \int_x^{\infty}\frac{e^{-u}}{u}\,du$$

This solution is also referred to as the line source solution (A single well in an infinite medium.).

While the solutions for a bounded reservoir and a constant pressure outer boundary are useful, we will only pursue the development of the exponential integral solution here. For additional details regarding the other cases, the reader is referred to Matthews and Russell(1967) and Earlougher(1977).

Dimensionless Pressure and Time

In future sections of this discussion we will be performing manipulations of the Theis solution to calculate pressure drops for multiple rates, multiple wells, and different geometries. In order to facilitate the ease with which these combinations are performed, it will be useful to have the solution for pressure as a function of spatial location in time [p(r,t)] in dimensionless form. Therefore, we introduce the concept here, before proceeding to the more complicated combinations.

The steady-state radial equation for incompressible flow is:

$$q = 0.007082 \frac{kh(p_e - p_w)}{B\mu \ln (r_e/r_w)} \qquad \text{(I-4)}$$

All terms have been previously defined except h, which is reservoir thickness in ft, and B, which is the formation volume factor for reservoir fluid, reservoir volume/surface volume. For water this factor is approximately unity. Subscript "e" designates the reservoir boundary, "w" designates the wellbore. Derivation of this solution requires integration of a constant flow rate across a cylindrical element log reservoir.

With some algebraic rearrangement the pressure drop ($p_e - p_w$) between r_w and r_e is:

$$p_e - p_w = 141.2 \frac{qB\mu}{kh} \ln (r_e/r_w) \qquad \text{(I-5)}$$

Equating to $p_D \ln (r_e/r_w)$ this equation becomes

$$p_e - p_w = 141.2 \frac{qB\mu}{kh} p_D \qquad \text{(I-6)}$$

Therefore the actual pressure drop $(p_e - p_w)$ in the steady-state radial flow equation becomes equal to the dimensionless pressure drop, p_D, times a scaling factor. The scaling factor is a function of flow rate and reservoir properties. This same concept applies to unsteady-state flow and to more complex situations. In those cases the form of the dimensionless pressure is different.

In general the pressure at any point in a single-well reservoir being produced at a constant rate, q, is described by the generalized solution

$$p_i - p(t,r) = 141.2 \frac{qB\mu}{kh} \left[p_D(t_D, r_D, c_D, \text{geometry}) + s \right] \qquad \text{(I-7)}$$

where

t_D = dimensionless time,

r_D = dimensionless radius,

c_D = storage coefficient of the well string,

s = skin at sandface

geometry = circle, square, triangle, etc.

Skin may represent additional pressure drop due to damage if the sandface is plugged with particulates or swelling clays. Skin may also represent a reduction in pressure drop if the well is fractured or acidized. The skin effect only appears in this equation when

$$r_D = 1, \text{ (where } r_D = r/r_w\text{)}.$$

In transient or unsteady-state flow, p_D is always a function of t_D, the dimensionless time. The dimensionless time, t_D is:

$$t_D = \frac{0.0002637\ kt}{\phi \mu c r_w^2} \qquad \text{(I-8)}$$

when based upon the wellbore radius, r_w. Other forms of dimensionless time can be defined, for instance if t_D is based upon drainage area, A, then $t_{DA} = t_D \left[\frac{r_w^2}{A} \right]$.

Dimensionless Pressure and the Line Source Solution

We are now ready to incorporate the concepts of dimensionless pressure and time into the exponential-integral solution that was previously found to be a solution of the diffusivity equation for a well with a constant flow rate in an infinite medium (Or during an "infinite acting" flow period.).

The solution for dimensionless p_D for the line source or Theis(1935) solution Eqn. (I-3) is shown in Figure I-2. This figure shows p_D to be a function of dimensionless radial distance, r_D, and dimensionless time, t_D for an infinite acting system. In dimensionless form Eqn. (I-3) becomes

$$p_D\ (t_D,\ r_D) \quad = \quad -\frac{1}{2}\ Ei\left[\frac{-r_D{}^2}{4t_D}\right] \tag{I-9}$$

When $r_D \geq 20$ and $t_D/r_D{}^2 \geq 0.5$ or alternatively when $t_D/r_D{}^2 \geq 25$ the solution of p_D for $r_D = 20$ and the exponential-integral solution become essentially the same. Mueller & Witherspoon(1965) have provided an expanded graph of the exponential-integral solution to include dimensionless distances beyond that of Theis; see Figure I-3.

When $t_D/r_D{}^2 > 100$ the exponential-integral solution may be closely approximated (within 2%) by

$$p_D\ (t_D,\ r_D) \simeq \frac{1}{2}\left[\ln\ (t_D/r_D{}^2) + 0.80907\right] \tag{I-10}$$

For intermediate values of $t_D/r_D{}^2$ or smaller values of r_D Figure I-3 should be utilized. The early time and near well solutions have been calculated strictly from the exponential-integral solution and are accurately graphed in Figure I-2.

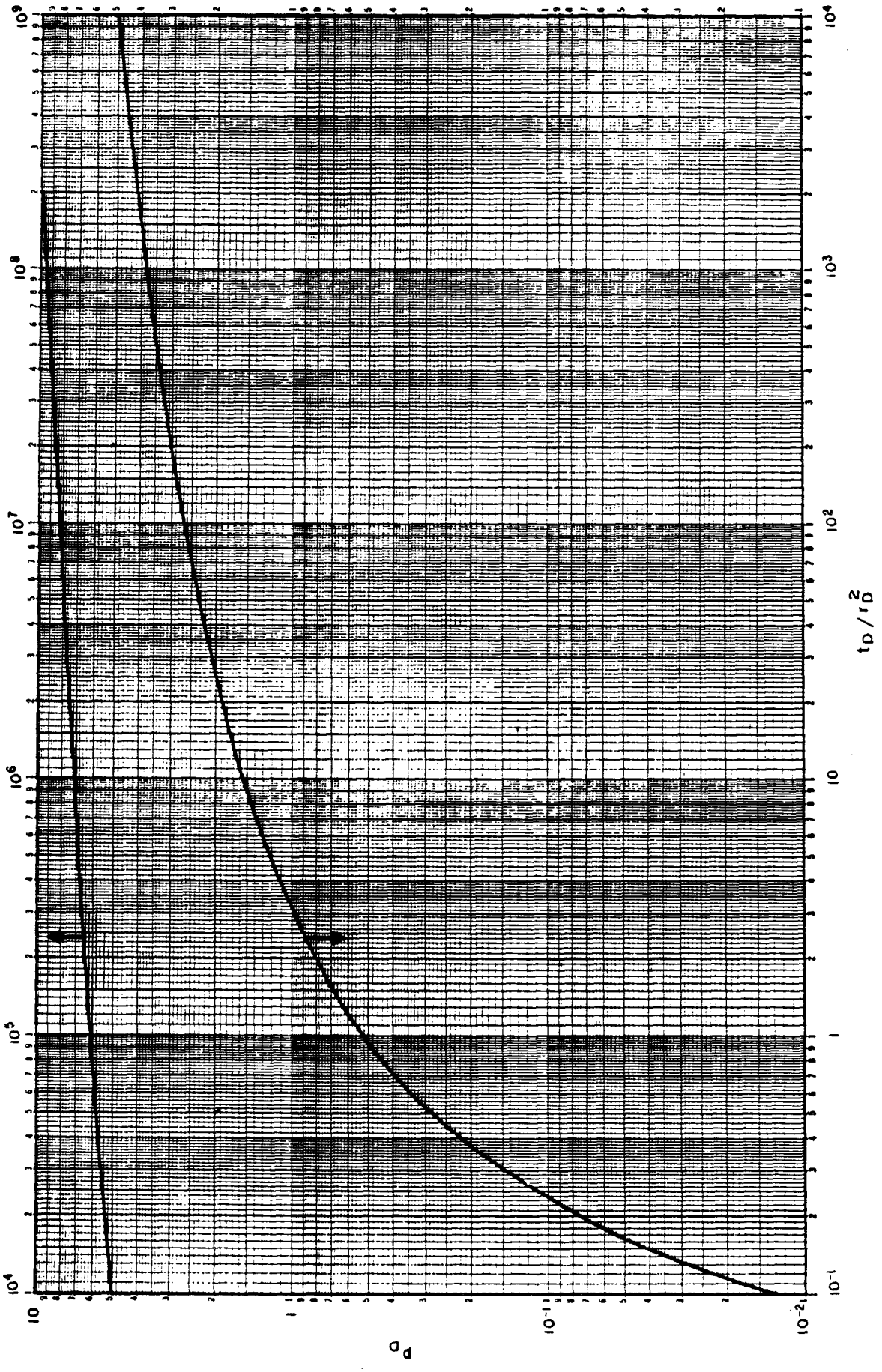

Figure I-2

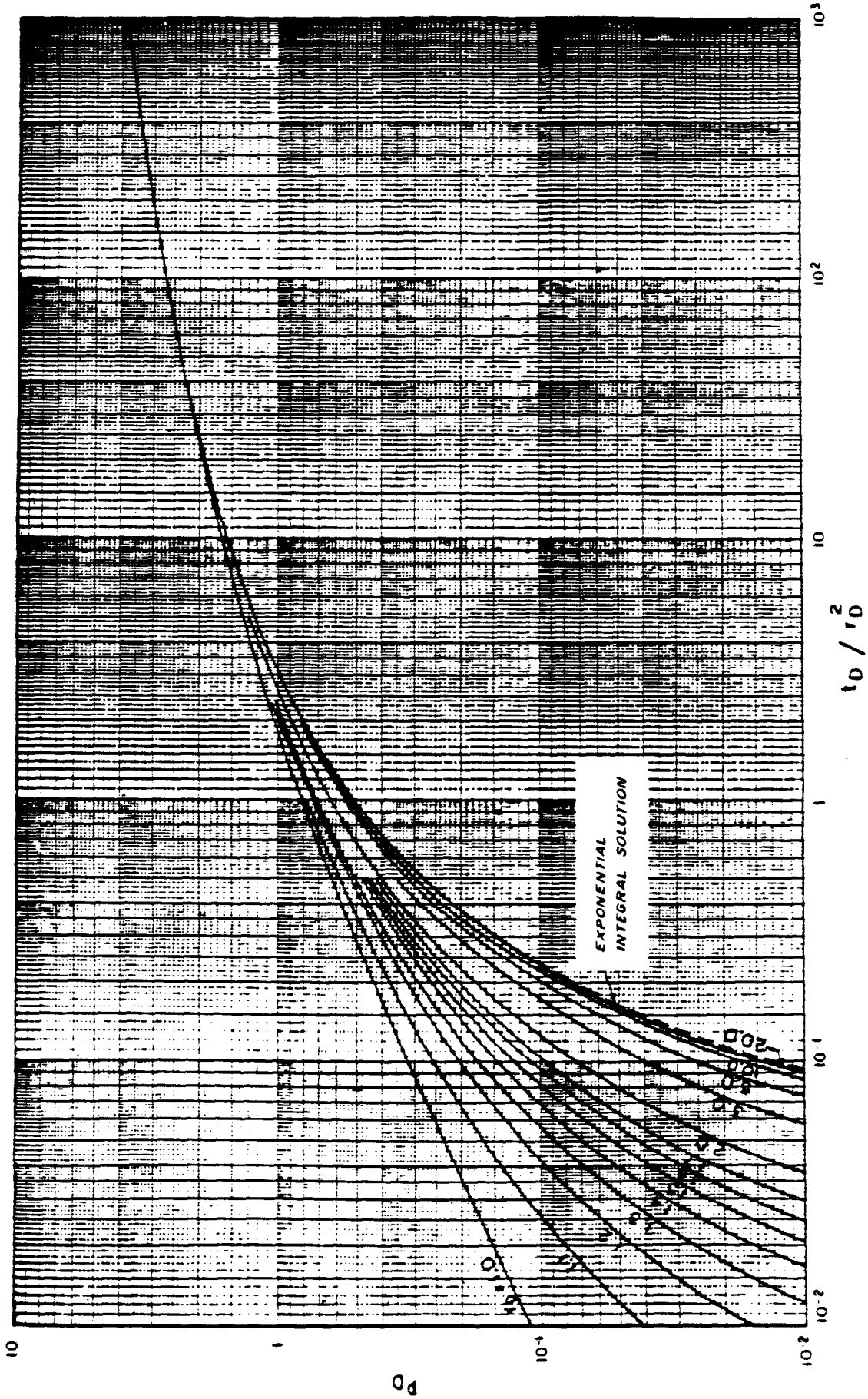
EXPONENTIAL
INTEGRAL SOLUTION
t_D / r_D^2
Q_d
10
1
10^{-1}
10^{-2}
10^2
10^3
10
$r_D = 1.0$

Figure I-3

Example Problem #1

Use the dimensionless exponential-integral solution of Figure I-2 and the following oil reservoir data to estimate the pressure vs. time relationship for single well in an infinite-acting system. (Note: taken directly from Earlougher(1977).

p_i	= 3265 psi	ϕ	= 0.17
K	= 90 md	C	= 2×10^{-5} psi^{-1}
μ	= 13.2 cp	r_w	= 0.5 ft
B	= 1.02 RB/STB	A	= 40 acres
h	= 47 ft.	S	= 0

We will calculate p_w at 1 minute and again at 10 hrs. to illustrate the procedure. All additional results are shown in Figure I-4. We first calculate t_D, then using p_D from Figure I-2 we calculate p_{wf}, the wellbore pressure at flowing conditions.

$$t_D = \frac{(0.0002637)(90)t}{(0.17)(13.2)(2. \times 10^{-5})(0.5)^2} = 2115.\ t \qquad \text{(I-11)}$$

At one minute, $t_D = (2115)(1/60) = 35.25$. For this value of $t_D/r_D^2 = 35.25 < 100$ so the log approximation for p_D should not be used. Evaluating p_D from Figure I-2 at $t_D/r_D^2 = 35.25$ we get $p_D = 2.18$. Solving for p_{wf} from Eqn. (I-7) we get

$$p_{wf}(1 \text{ minute}) = 3265. - \frac{(141.2)(135)(1.02)(13.2)}{(90)\ (47)}\ (2.18)$$

$$p_{wf} = 3265. - (60.67)(2.18) = 3133.\ \text{psi}$$

For 10 hrs, $t_D = (2115)(10) = 21{,}150.$ and the log approximation Eqn. (I-10) can be used:

$$p_D = \frac{1}{2}\left[\ln (21{,}150/1) + 0.80907\right] = 5.384 \text{ and}$$

$$p_{wf}(10 \text{ hrs}) = 3265. - (60.67)(5.384) = 2938.\ \text{psi}$$

Both the log approximation and the results from the exponential-integral solution are presented in Figure I-4. It can be readily observed that agreement between the log approximation and the exponential-integral solution to the diffusivity equation are quite comparable within the ranges of t_D/r_D^2 described earlier.

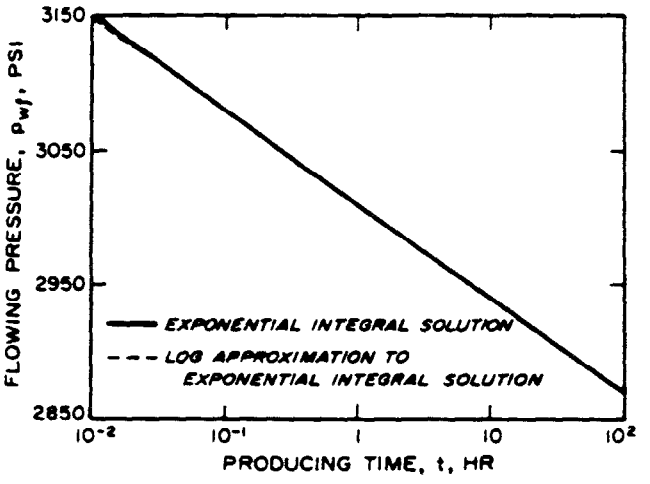

Figure I-4

Superposition Principle

So far we have considered only the pressure behavior for a single well operating at constant rate in an infinite porous medium. However, actual reservoir systems are composed of multiple wells operating at multiple and varying rates. Because the diffusivity equation is linear, these more complex problems can be solved utilizing the principle of superposition. For more fundamental mathematical treatment the reader should consult van Everdingen and Hurst(1949), Collins (1961), and others.

As we will use it, the superposition principle simply states that summing the solutions to a linear differential equation will also provide a solution to the equation. Superposition can be utilized to include multiple wells, to accommodate changing rates, and to impose physical boundaries. We will approach the treatment in two separate parts; first we will concern ourselves with multiple wells, and changing

rates in an infinite system, and second we will address the problem of physical boundaries.

Multiple Wells, Constant Rates

Consider the three well infinite system in Figure I-5.

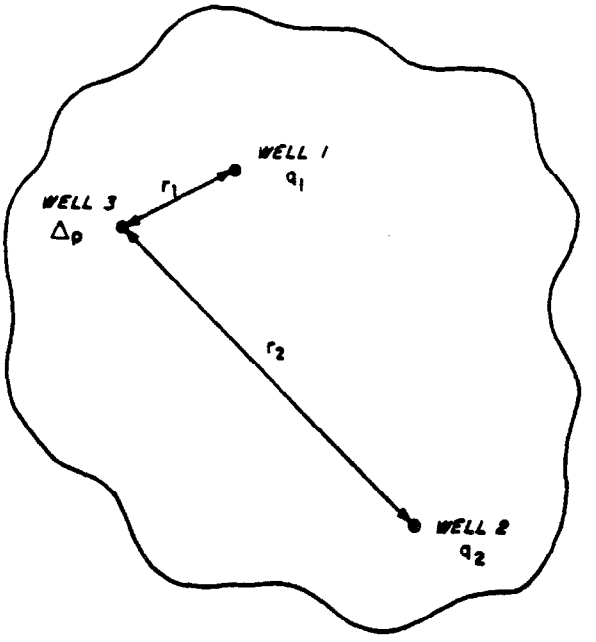

Figure I-5

At zero time Well #1 starts producing at rate q_1, and Well #2 starts producing at rate q_2. We would like to know the pressure at shut-in Well #3. In order to do this we add the pressure change at Well #3 caused by Well #1 to the pressure change at Well #3 caused by Well #2;

$$\Delta p_3 = \Delta p_{3,1} + \Delta p_{3,2}$$

Substituting Eqn. (I-7) for $\Delta p_{3,1}$ and $\Delta p_{3,2}$ we have;

$$\Delta p_3 = 141.2 \frac{B\mu}{kh} \left[q_1 \, p_{D_1}(t_D, r_{D_1}) + q_2 p_{D_2}(t_D, r_{D_2}) \right]$$

or, for any arbitrary number of wells;

$$\Delta p(t,r) = 141.2 \frac{B\mu}{kh} \sum_{j=1}^{n} q_j p_D(t_D, r_{D_j}) \qquad \text{(I-12)}$$

where r_{D_j} is the dimensionless distance from Well j to the point of interest. Note that pressure drops are being summed, not pressures. Figure I-6 illustrates the concept in this example. If the location of interest happens to be an operating well, then one has to consider skin for that well in the calculation. This is not necessary at observation wells since skin is only meaningful in producing or injecting wells.

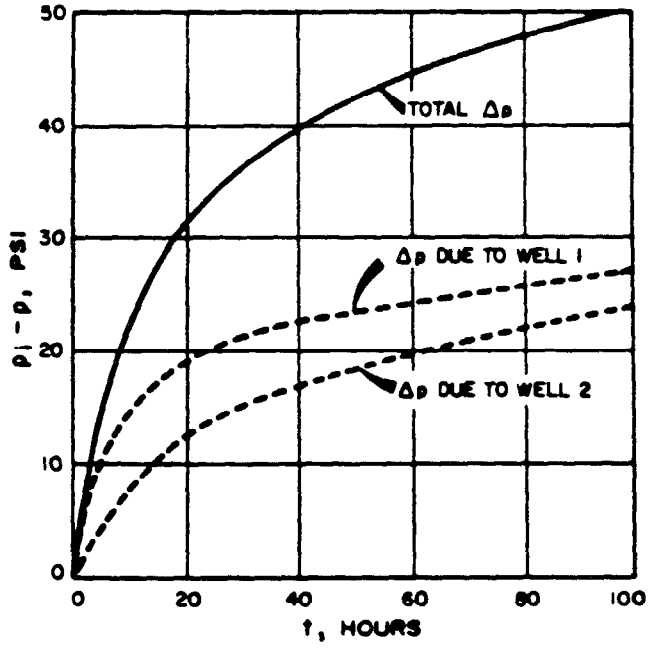

Figure I-6

Single Well, Changing Rate

Consider the well of Figure I-7.

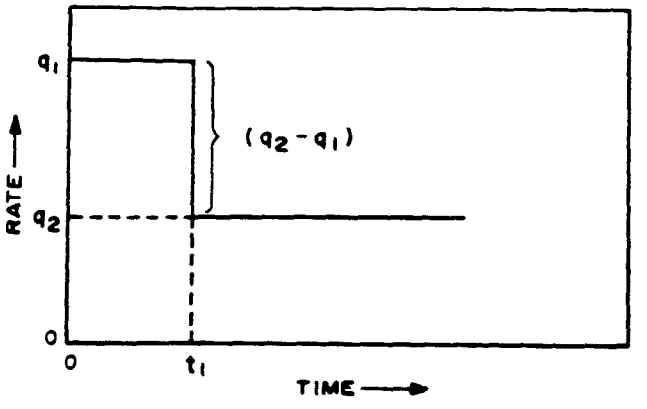

Figure I-7

This well produces at rate q_1 until time t_1 and then produces at rate q_2 thereafter. In order to calculate the pressure drop in the well at some time later than t_1 one can utilize superposition. One way to visualize this situation is to consider two wells at the same location. The first well produces at rate q_1 from t=0 into the future; the second well begins producing at time $t=t_1$, at a lower rate (q_2-q_1). As in the example of multiple wells the Δp's can be added for this situation. The general form of the equation is:

$$p = \frac{141.2\ B\mu}{kh} \sum_{j=1}^{N} \left\{ (q_j - q_{j-1}) \left[p_D \left[(t-t_{j-1})_D \right] + S \right] \right\} \qquad (I-13)$$

In Eqn. (I-13) $(t-t_1)_D$ is the dimensionless time calculated at time $(t-t_1)$. For the example in Figure I-7 only two terms are required in the summation. Figure I-8 illustrates the example.

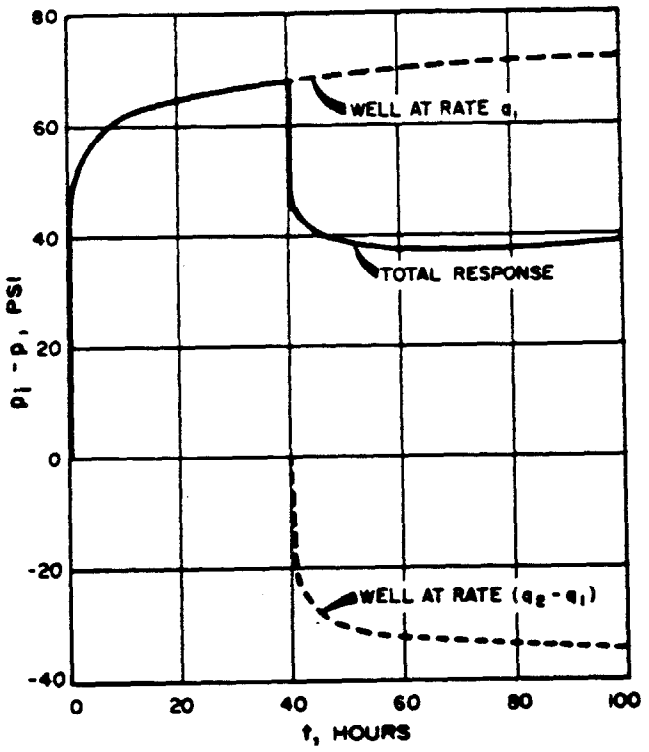

Figure I-8

The upper curve (including the dashed portion) is the pressure change (or drop) caused by the rate q_1. The lower dashed curve is the pressure change caused by the rate $q_2 - q_1$ after 40 hours; that Δp is negative because $(q_2 - q_1) < 0$. The sum of the two dashed curves, the solid curve labeled "total response" is the pressure response for the two rate schedule of the single well. It is well to note here that production rates are treated as positive quantities, however, these same principles apply to injection rates when treated as negative quantities.

If both varying rates and multiple wells are included in the situation of interest, apply Eqn. (I-13) first for varying rates; then apply Eqn. (I-12) for different wells to obtain the total Δp caused by all wells and all rates. The double summation process is conceptually simple, but becomes tedious in application. We illustrate the process now with the following example which is taken directly from Earlougher(1977).

Example - Principle of Superposition

Figure I-9 illustrates two wells, spaced 100 ft. apart with different producing histories.

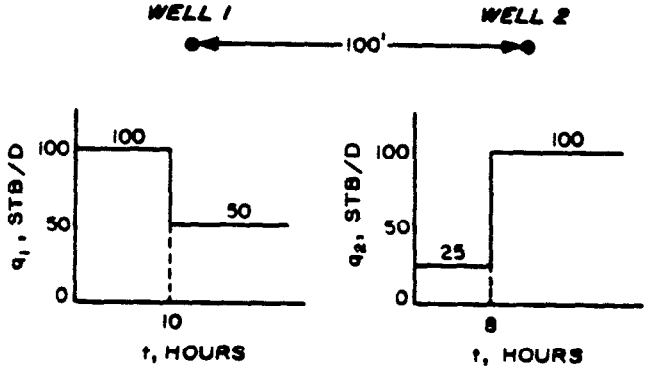

Figure I-9

The data for the two wells are: Well #1: r_w = 1 ft, s = 5.0; Well #2: r_w = 1 ft, s = 1.7. General reservoir and fluid properties are: k = 76 md, μ = 1.0 cp, ϕ = 0.20, C_t = 10 x 10^{-6} psi $^{-1}$, B = 1.08 RB/STB, h = 20. ft, and p_i = 2200 psi.

For the conditions shown in Figure I-9, estimate the pressure at Well #1 after 7 hours and at Well #2 after 11 hours. Assume that the system behaves as an infinite one at these short times.

Start by computing the coefficients in the Δp and t_D equations, Eqns. (I-7) and (I-8). Then, at a given time, estimate Δp at the desired well caused by both Well #1 and Well #2; that calculation of Δp may require use of Eqn. (I-13) to account for varying rates.

From Eqn. (I-8),

$$t_D = \frac{0.0002637\ kt}{\phi \mu c_t r_w^2} = \frac{0.0002637(76)t}{(0.2)(1)(10 \times 10^{-6})(1)^2} = 10{,}000\ t$$

From Eqn. (I-7),

$$\Delta p = \frac{141.2\ qB\mu}{kh}\ p_D(t_D,\ldots) = \frac{(141.2)(1.08)(1)q}{(76)(20)}\left[p_D(t_D,r_D\ldots)\right]$$

$$= 0.1\ q\left[p_D(t_D,r_D,\ldots)\right].$$

Recall that s_j must be added to p_D to get Δp at Well j. The appropriate r also must be used to calculate r_D, depending on the p_D function we use.

At t = 7 hours, there is a Δp contribution at Well #1 from a single rate at Well #1 and a single rate at Well #2; so the over-all pressure change from Eqn. (I-12) would be

$$\Delta p \text{ (7 hours, } r_D = 1)$$

$$= \frac{141.2\ q_1 B\mu}{kh}\left[p_D(t_D, r_D = 1) + s\right]$$

$$+ \frac{141.2\ q_2 B\mu}{kh}\left[p_D(t_D, r_D = 100/1)\right].$$

For the contribution of Well #1, $t_D = (10{,}000)(7) = 70{,}000$. Since $t_D > 100$ Eqn. (I-10) is used:

$$p_D(t_D = 70{,}000,\ r_D = 1)$$

$$= \frac{1}{2}\left[\ln (70{,}000) + 0.80907\right]$$

$$= 5.98.$$

For the contribution of Well #2, at a distance of 100 ft.

$$\frac{t_D}{r_D^2} = \frac{(70{,}000)}{(100/1)^2} = 7.$$

Since $r_D > 20$, we can use the line-source solution, Eqn. (I-3) from Figure I-2, but we should not use the log approximation unless $t_D/r_D^2 > 100$. From Figure I-2 or Figure I-3 for $t_D/r_D^2 = 7$ and $r_D = 100$,

$$p_D(t_D = 7,\ r_D = 100) = 1.40.$$

Calculating Δp at Well #1,

$$\Delta p(\text{Well \#1, 7 hours}) = (0.1)(100)(5.98 + 5) + (0.1)(25)(1.40) = 113.3 \text{ psi.}$$

The pressure at Well #1 at 7 hours is

$$p_w \text{ (7 hours, } r_D = 1) = p_i - \Delta p = 2{,}200 - 113.3 = 2{,}086.7 \text{ psi}$$

At t = 11 hours, we wish to estimate p at Well #2. We must consider two rates at each well:

$$\Delta p(11 \text{ hours}, r_D = 1) = (0.1)(100)[p_D(\text{Well \#1, t = 11 hours, } r_D = 100)] + (0.1)(50-100)[p_D(\text{Well \#1, t = [11-10] hours, } r_D = 100)] + (0.1)(25)[p_D(\text{Well \#2, t = 11 hours, } r_D = 1) + s] + (0.1)(100-25)[p_D(\text{Well \#2, t = [11-8] hours, } r_D = 1) + s]$$

For Well #1, use Figure I-2.

$$t_D(11 \text{ hours})/r_D^2 = \frac{(10{,}000)(11)}{(100)^2} = 11.$$

$$p_D(\text{Well \#1, } t_D = 11, r_D = 100) = 1.61.$$

$$t_D(11\text{-}10 \text{ hours})/r_D^2 = \frac{(10{,}000)(1)}{(100)^2} = 1.$$

$$p_D(\text{Well \#1, } t_D = 1, r_D = 100) = 0.522.$$

For Well #2, $r_D = 1$:

$$t_D(11 \text{ hours}) = (10{,}000)(11) = 110{,}000.$$

Since $t_D > 100$, we use the log approximation

$$p_D(\text{Well \#2}, t_D = 110{,}000, r_D = 1)$$

$$= \frac{1}{2}[\ln(t_D) + 0.80907] = 6.21.$$

$$t_D(11\text{-}8 \text{ hours}) = (10{,}000)(3) = 30{,}000.$$

$$p_D(t_D = 30{,}000, r_D = 1)$$

$$= \frac{1}{2}[\ln(30{,}000) + 0.80907] = 5.56.$$

Estimating Δp at Well #2,

$$\Delta p(\text{Well \#2, 11 hours}) =$$

$$(0.1)(100)(1.61) + (0.1)(50\text{-}100)(0.522)$$

$$+ (0.1)(25)(6.21 + 1.7)$$

$$+ (0.1)(100\text{-}25)(5.56 + 1.7) = 87.7 \text{ psi.}$$

$$p_w(\text{Well \#2, 11 hours}) = 2{,}200 - 87.7 = 2{,}112.3 \text{ psi.}$$

Final Note: Multiple Rates with Log Approximation

Before leaving this section to address physical boundaries, it might be well to note one additional form of Eqn. (I-13) for multiple rates, when the log approximation of the exponential-integral can be applied.

Figure I-10 illustrates a multiple rate history for a single well. Within the nomenclature of the figure production (or injection) starts at time t=0; the rate remains constant at q_1 until t_1, and so on. Rate q_j always ends t at time t_j and the last and most current rate is q_N. We may calculate the pressure at the well (or at any other location for which we know p_D) at any time during rate q_N by using superposition.

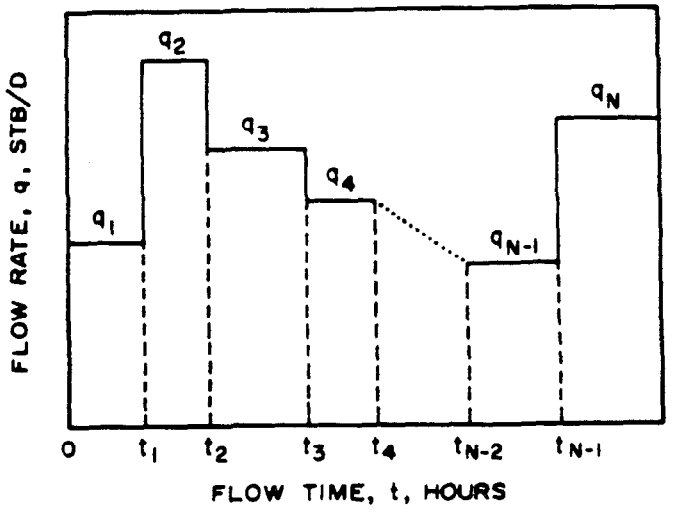

Figure I-10

If the logarithmic approximation is applicable it can be shown that:

$$\frac{p_i - p_{wf}^{(t)}}{q_N} = \frac{162.6\ B}{kh}\left\{\sum_{j=1}^{N}\left[\left(\frac{q_j - q_{j-1}}{q_N}\right) x \log\left(t - t_{j-1}\right)\right] + \log\left(\frac{k}{\phi\mu c_t r_w^2}\right) - 3.2275 + 0.868595\right\} \qquad \text{(I-14)}$$

Physical Boundaries - General

Up to now, all of our superposition solutions for pressures at multiple rates and multiple wells have been generated for infinite porous mediums. If physical boundaries exist near enough to wells, they affect the pressure behavior resulting from rate behavior and must be accounted for.

Two prevalent situations that must be dealt with are barriers to flow, and boundaries which are constant pressure boundaries. An example of a barrier could be a sealing fault or a permeability pinch-out. A constant pressure boundary could exist at the edge of a small waste disposal area, which is situated in a large aquifer with recharge. A more easily visualized example might be a natural gas reservoir underlain by an aquifer with large recharge. Water influx, in either case, serves to keep boundaries at constant pressure.

We can again rely upon the solutions from the exponential-integral for our demonstration. Superposition calculations can utilize the dimensionless pressure solutions for an infinite medium even when the

goal is to describe pressure behavior in a closed system. Several references exist describing the process; Earlougher(1977), Matthews and Russell(1967), Theis(1935), and Mueller and Witherspoon(1965).

No-Flow (Barrier) Boundaries

Figure I-11 illustrates the method of images when used to create a no-flow boundary.

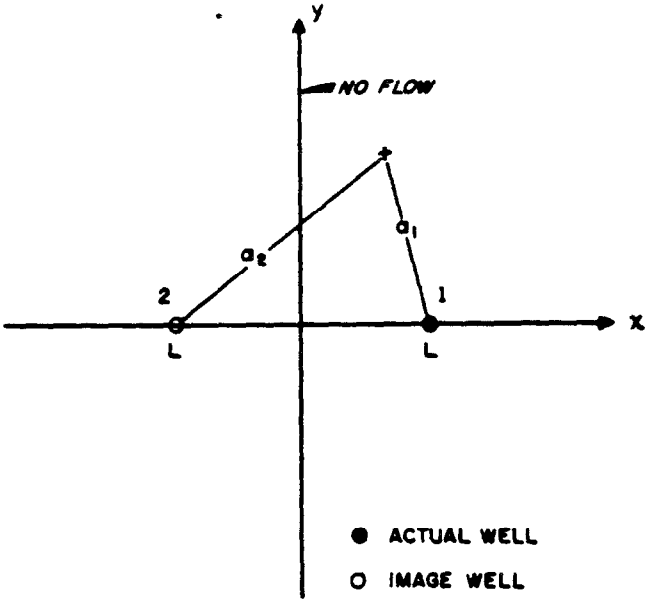

Figure I-11

Well #1 operates on a constant flow rate q, at distance L from a single impermeable boundary, represented by the y-axis in the figure. An image well, Well #2, located at distance -L from the y-axis and operating at the same rate as Well #1, generates an isopotential line along the y-axis across which no fluid flows. Note that if Well #1 is a producing well then Well #2 must also be a producing well. The image well could also be an injector if Well #1 is an injector. By applying

superposition, we can calculate any pressure in the x-y plane of the figure.

$$p(t,x,y) = p_i - \frac{141.2\ q\ B\mu}{kh}\left[p_{D_1}(t_D,a_{D_1}) + p_{D_2}(t_D,a_{D_2})\right] \quad \text{(I-15)}$$

Constant Pressure Boundaries

If the y-axis is to be a constant pressure boundary, then the image well becomes an injection well with the same rate as the production well. In the case of a constant pressure boundary, superposition gives

$$p(t,x,y) = p_i - \frac{141.2\ q\ B\mu}{kh}\left[p_{D_1}(t_D,a_{D_1}) - p_{D_2}(t_D,a_{D_2})\right] \quad \text{(I-16)}$$

Since $a_{D_1} = a_{D_2}$ at x = o for all y, then

$$p_{D_1}(t_D,a_{D_1}) = p_{D_2}(t_D,a_{D_1}) \quad \text{(I-17)}$$

and the pressure p(t,0,y) at all points along the boundary (y-axis) is p_i. A similar proof can be shown for the no-flow case, but the mathematics are more complex. For those readers who are interested, Earlougher(1977) provides the demonstration in Appendix B of his monograph.

In both cases above the dimensionless distances a_{D_1} and a_{D_2} are:

$$a_{D_1} = \frac{a_1}{r_w} = \frac{1}{r_w}\sqrt{(x-L)^2 + y^2} \text{ and} \quad \text{(I-18)}$$

$$a_{D_2} = \frac{a_2}{r_w} = \frac{1}{r_w}\sqrt{(x+L)^2 + y^2} \quad \text{(I-19)}$$

where r_w is the same for both wells.

Multiple Barriers

The method of images clearly extends to multiple barrier and/or constant pressure boundary situations. The general approach uses superposition and adds or subtracts dimensionless pressures.

The application of the technique becomes quite tedious and careful work is required. A few examples will be illustrated, but the details are beyond the scope of this Appendix. For further details the reader is referred to Earlougher(1968) or Ramey, Kumar, and Gulati(1973).

Figure I-12 illustrates a single well located between two parallel boundaries which are no-flow barriers.

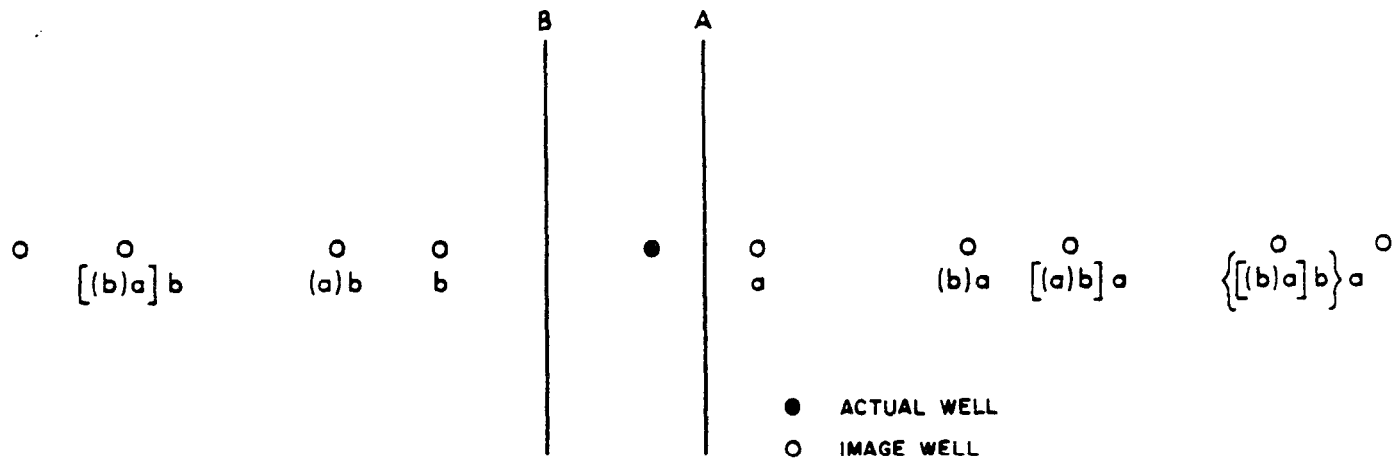

Figure I-12

Also shown are the image wells required to produce those two parallel no-flow barriers. Well a (open circle) is the image of the actual well in Boundary A. Well b (open circle) is the image of the actual well in Boundary B. Since each image well would cause flow across the opposite barrier for which it is an image well, additional image wells are required. Well (a)b is the image of well a in Boundary B and is required to keep Well a from causing fluid to flow across Boundary B. Well (b)a is the counterpart of Well (a)b for the A boundary. Once there is more than one boundary the method of images is theoretically infinite (as Figure I-12 illustrates). As a practical matter the effects of image wells several positions away from the boundaries usually becomes negligible. This assessment has to be made for each specific situation. The general expression for summation is:

$$p\,(t_D, x_D, y_D) = \sum_{i=1}^{\infty} p_D(t_D, a_{D_i}) \qquad \text{(I-20)}$$

In order to give the reader a flavor of the situation for several boundaries Figure I-13 is presented.

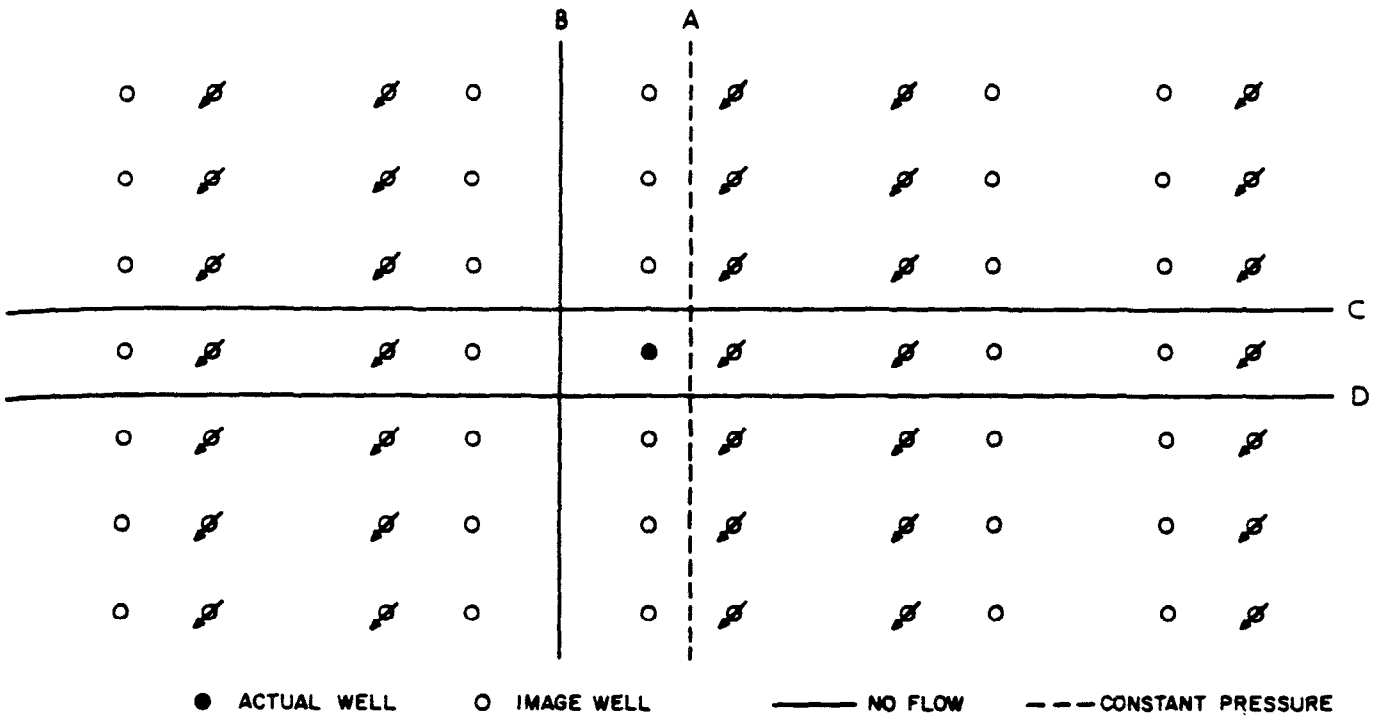

Figure I-13

In this case the actual well (solid black dot) is enclosed between three no-flow boundaries and one constant pressure boundary. As mentioned earlier there are several excellent references in the literature for those readers so inclined to pursue the principles of superposition further. As an adjunct to superposition Gringarten, Ramey, and Raghavan(1974) have developed a desuperposition approach using Green's functions. This approach incorporates storage and skin values for a well with a vertical fracture into the calculation and is considerably more sophisticated mathematically than superposition.

REFERENCES

Collins, Royal Eugene: Flow of Fluids Through Porous Materials, Reinhold Publishing Corp., New York (1961), 109-113, 116-118.

Earlougher, Robert C. Jr.: "Advances in Well Test Analysis," Monograph Volume 5, Society of Petroleum Engineers, Dallas, Texas (1977).

Earlougher, Robert C. Jr., Ramey, H. J. Jr., Miller, F. G., and Mueller, T. D.: "Pressure Distributions in Rectangular Reservoirs," Journal of Petroleum Technology, February 1968, 199-208.

Gringarten, Alain C., Ramey, Henry J. Jr., and Raghaven, R.: "Unsteady-State Pressure Distributions Created by a Well with a Single Infinite-Conductivity Vertical Fracture," Society of Petroleum Engineers Journal, August, 1974, 347-360.

Matthews, C. S., Brons, F., and Hazebroek, P.: " A Method for Determination of Average Pressure in a Bounded Reservoir," Trans. AIME (1954), Vol. 201, 182-191.

Matthews, C. S. and Russell, D. G.: "Pressure Buildup and Flow Tests in Wells," Monograph Volume One, Society of Petroleum Engineers, Dallas, Texas (1967).

Mueller, Thomas D., and Witherspoon, Paul A.: "Pressure Interference Effects Within Reservoirs and Aquifers," Journal of Petroleum Technology, April, 1965, 471-474.

Ramey, Henry J. Jr., Kumar, Anil, and Gulati, Mohinder S.: Gas Well Test Analysis Under Water Drive Conditions, American Gas Association, Arlington, Virginia (1973).

Theis, Charles V.: "The Relation Between the Lowering of the Piezometric Surface and the Rate and Duration of the Discharge of a Well Using Ground-Water Storage," Trans. American Geophysical Union (1935), 519-524.

REFERENCES (Cont.)

Van Everdingen, A. F. and Hurst, W.: "The Application of the Laplace Trnsformation to Flow Problems in Reservoirs," Trans. AIME (1949), Vol. 186, 304-324.

PROBLEM 1 - VERTICAL LEAKAGE THROUGH AQUITARDS

This problem set outlines one method of performing calculations to determine vertical transport of waste products during a 50 year injection period and a 10,000 year dormant period. The calculations were based on reservoir simulation models designed to determine waste concentration as a function of the vertical distance above the injection interval. The simulations assume that the wellbore of the injection well is completely isolated from upper zones and there are no local faults with an effective vertical permeability capable of transferring fluids to upper zones. The operating conditions of the model were designed such that the injection pressure did not exceed the fracture gradient of the injection interval at any time during the simulation.

General Description of the Simulation Models

Vertical leakage caused by injection of hazardous waste was analyzed using two separate numerical reservoir simulation models. A two-dimensional(2-D) radial model was used to simulate a 50 year period of waste disposal (Figure 1). A one-dimensional(1-D) vertical model (Figure 2) was used to simulate the diffusion of waste material for a period of 10,000 years following the injection period in a region directly above the wellbore. The vertical concentration profile of the injected waste product obtained from the 2-D radial model was used to initialize the 1-D vertical model. Additional reservoir simulation data is contained in Table 1.

The 2-D radial model was constructed of 4 coarse grid radial blocks and 75 vertical layers. A no-flow condition was assumed for all outer boundaries. The radial blocks were sized such that the pressure at the injection well would not exceed an assumed fracture gradient. The thickness and permeability of the injection interval was 15 ft and 200 md respectively. The vertical leakage of hazardous waste was calculated based on convection, and molecular dispersion was assumed to be negligible. The aquitard was divided into 50 one-foot layers and the upper aquifer was divided into 24 two-foot layers. The permeability of the aquitard was varied from 1.0 md to 0.0001 md in five separate simulation cases. The permeability of the upper aquifer was assumed to be 10 md. The reservoir simulator used to model these test problems automatically adjust time step size to assure a proper material balance and maintain numerical stability. The model was constructed such that waste products did not leak into the top layer of the over-lying aquifer during the injection or diffusion period to avoid numerical disturbance due to the top no-flow boundary.

The 1-D vertical model used to simulate the 10,000 year diffusion period was divided into 50 layers. A 50 ft aquitard over-lying the injection interval was defined by thirty 1-foot layers and four 5-foot layers. A 130 ft upper aquifer was divided into six 5-foot layers and ten 10-foot layers. Each layer was 100 ft by 100 ft. The initial block pressures were assumed to be hydrostatic at a gradient of 0.433 psi/ft. The simulations were performed for an injection interval 3550 ft in depth at a pressure of 1540 psig. The initial waste product

concentration of each layer was based on the results at the end of a 50 year simulation of the injection period.

The concentration of waste products above the injection interval for the 2-D model was based on an observation point 1 ft from the well-bore. The concentration profile obtained from the 2-D simulation of the injection period was used as the initial condition for the 1-D simulation of the 10,000 year diffusion period. Since waste concentration was not allowed to disperse in the horizontal direction in the 10,000 year case the waste concentration profiles will define the upper limit of vertical leakage or a "worst case condition".

During the 50 year simulation of waste injection the concentration of waste product was controlled by convection only. Following the injection period the concentration of waste product was controlled solely by molecular diffusion as a stabilized pressure gradient was assumed throughout the reservoir system. The effective molecular diffusion in porous media was assumed to be 0.0001 ft^2/day as discussed by Morganwalp(1988) on vertical leakage in porous media. Additional simulations were performed based on an effective diffusion coefficient of 0.0000083 ft^2/day. Molecular diffusion in porous media will be discussed in a later section.

The bottomhole injection pressure was limited to 3000 psi which is based on an arbitrary fracture gradient of 0.85 psi/ft at an injection depth of 3550 ft. This fracture gradient is low for a disposal well in

the Gulf Coast but could be high for a well in an older area where severe faulting has occurred. The fracture of a waste disposal well should not be exceeded during periods of injection if waste material is to be properly contained. Empirical correlation can be used to predict fracture gradients in certain areas but pressure leak off testing is the preferred method of measuring the fracture gradient. Pressure transient testing is the preferred method of verifying that the well was not fractured during periods of waste injection.

Discussion of Results

The discussion of results will be based on concentration profiles of the waste product above the injection interval. The concentration of injected waste product was normalized to a value of 1.0 making the profiles dimensionless. The actual waste concentration C(x,t) is calculated by multiplying the dimensionless concentration profile-(C/C_o) by the initial waste product concentration(C_o) of the injection stream.

Table 2 and Figure 3 was based on an injection rate of 500 bbls/day for 50 years. The vertical permeability of the injection interval and the aquitard was assumed to be 200 md and 1.0 md respectively. Waste was transported 86 ft above the injection interval during the 50 year injection period. Following the injection period the waste product was transported, as a result of diffusion, an additional 84 ft above the injection interval for a total vertical transport distance of 170 ft.

The migration of waste products after injection was dependent on molecular diffusion. Post injection pressure transient effects are negligible and do not contribute to vertical transport during extended shut-in periods.

The concentration profile obtained from the simulation of the injection period was used as the initial condition for the simulation of the 10,000 yr diffusion period. After termination of injection, waste material can neither be lost nor gained. The vertical concentration of waste material may only be redistributed during the 10,000 yr diffusion period. Referring to Figure 3, during the diffusion period the waste product concentration decreases near the injection interval and increases above the injection interval. In other words, the waste products are redistributed as a result of molecular diffusion. Integration of the area below the 50 yr concentration curve (sum C/C_o x vertical distance) must equal the area below the 10,000 yr concentration curve to preserve a mass balance.

Additional simulations assuming an injection rate of 1000 bbls/day were made for confining permeabilities of 1.0 md and 0.001 md to examine the sensitivity of vertical leakage as a function of injection rate. Referring to Figure 3 and 6 an increase in injection rate has negligible effect on vertical leakage assuming injection pressures are below the formation fracture gradient. The average pressure of the reservoir system increased for the higher injection rate as expected.

Given a confining permeability of 1.0 md the vertical pressure drops for both injection rates were constant. The difference in pressure from the lower layer to the upper layer at radial block 1(Vertical pressure drop) was 95 psi and 97 psi for 500 bbls/day and 1000 bbls/day respectively after 50 years. Since the vertical pressure drop is constant the vertical migration near the wellbore will also be constant. The wellbore pressure after 50 years of injection at 1000 bbls/day is 2990 psig which is approaching the estimated fracture pressure of 3000 psig.

The vertical transport for both injection rates is also constant given a confining permeability of 0.001 md. The injection pressure exceeded the fracture pressure of 3000 psi after 8400 days of injection at 1000 bbls/day which imposed a different operating condition. The vertical pressure drop just prior to exceeding the fracture pressure was 171 psi and the vertical waste product migration was 9 ft. Upon exceeding the fracture pressure the operating conditions of the model were changed to maintain a constant bottomhole injection pressure below the fracturing gradient. The injection rate was reduced accordingly to maintain the injection pressure of 3000 psig. Figure 6-A illustrates the injection rate as a function of injection time for this case. The total amount of fluids injected for this simulation was 10.24 million barrels as opposed to 18.25 million barrels had the pressure constraint not been imposed. The final vertical pressure drop after 50 years of injection was 25 psi at a injection rate of 7 bbls/day. The final vertical migration was 10 ft. The reduced vertical pressure drop

is consistent with a reduced injection rate. The final vertical pressure drop at an injection rate of 500 bbls/day was 100 psi and the final vertical migration was 9 ft after a total of 9.125 million barrels of waste injection.

The leakage of waste material for the simulations performed and illustrated by Figures 3-7 and Tables 2-6 are summarized in the following table.

qinj , kc (bbls/d),(md)	Vertical Leakage Injection Period (ft)	Vertical Leakage Diffusion Period (ft)
500, 1.0	83	170
1000, 1.0	86	170
500, 0.1	29	150
500, 0.01	20	130
500, 0.001	9	120
1000, 0.001	10	120
500, 0.0001	4	80

Where:

qinj = Injection Rate - bbls/day

kc = Aquitard Permeability - md

Figure 8 illustrates the effect of the permeability of the aquitard on vertical leakage during 50 years of injection at 500 bbls per day. Note aquitards with permeabilities of less than 0.0001 md are essentially impermeable and will confine all waste products during

periods of injection as long as fracture gradients are not exceeded. Figure 9 illustrates the effect of confining permeability on vertical leakage during the 10,000 year diffusion period for a constant diffusion coefficient. As would be expected, waste transport as a result of diffusion during extended shut-in periods is not directly dependent on the permeability of the aquitard. The concentration profile of the waste material during the diffusion period is indirectly related to the permeability of the aquitard in that the concentration profile after 50 years of injection was used to initialize the simulation of the diffusion period.

Figure 10 illustrates the sensitivity of vertical leakage to vertical permeability for both the injection and diffusion periods. The vertical leakage for the injection period is directly dependent on vertical permeability. The leakage data was curve fit using a power law relation of the form Ax^B. The leakage due to diffusion is only indirectly related to the vertical permeability. The leakage due to molecular diffusion follows a straight line relation on the semi-log plot. The leakage due to diffusion is directly related to the amount and distribution of the waste products after injection is terminated. Waste products are not confined to the 50 ft aquitard after 50 years assuming an aquitard permeability of 1.0 md. This lack of confinement is most likely the cause of the abnormally high leakance assigned to the 1.0 md vertical permeability during the injection period.

Analytical Estimates of Vertical Leakage

An analytical solution for estimating vertical leakage was proposed by Miller et al.(1986) which was partly based on work performed by Hantush and Jacob(1955). A formula for calculating vertical leakage as a function of radial distance from the injection well is as follows:

$$\delta(r) = \frac{Q}{2\pi B^2 \phi c} Ko(r/B) \quad (1)$$

$$B^2 = \frac{k \cdot h \cdot b}{kc} \quad (2)$$

Where:

$\delta(r)$	=	Vertical Distance at C/C_o=1.0	- (ft)
k	=	Permeability of the Injection Interval	- (md)
kc	=	Permeability of the Aquitard	- (md)
h	=	Thickness of the Injection Interval	- (ft)
b	=	Thickness of the Aquitard	- (ft)
Q	=	Total Volume of Liquid Injected	- (bbls)
ϕ c	=	Porosity of the Aquitard	- (fraction)
Ko	=	Modified Bessel Function of the Second Kind	

Using Equation 1 for a comparison of leakage estimated from the simulations performed yields the following results:

Aquitard Permeability (md)	For C/C_o=1.0 Miller Et. Al. (ft)	Numerical Simulations (ft)
1.0	144	24
0.1	17	18
0.01	2	11
0.001	0.3	2
0.0001	0.0026	0.5

Equation 1 over-predicts vertical leakage for large values of aquitard permeability and under-predicts leakage for low values of aquitard permeability. The aquitard was divided into 50 one-foot layers, reducing numerical dispersion to a minimum, even at the lower permeabilities. The waste product concentrations were controlled by convection only, therefore the leakage calculated from the simulations are minimum values for the radial observation point of 1 foot.

Discussion of Molecular Diffusion In Porous Media

The migration of fluids in porous media at static conditions is dependent on molecular diffusion of the fluids and formation properties as described by Perkins and Johnston(1963). This relation is defined by:

$$De = \frac{Do}{F\phi} \qquad (3)$$

Where:

De = Effective Diffusion Coefficient - ft^2/day

Do = Molecular Diffusion - ft^2/day

F = Formation Electrical Resistivity Factor

ϕ = Formation Porosity - fraction

The term ($Do/F\phi$) is defined as the effective diffusion coefficient in porous media. The term (F) is commonly called the tortuosity of the formation. Equation 3 simply states that the fluid diffusion in porous media will be controlled by the concentration gradient of the fluid and the associated rock geometry.

The value of ($F\phi$) ranges from 1.414 to 2.000 for permeable formations where the pore structure of the formation is interconnected [Frick(1962)]. The tortuosity ($F\phi$) of an impermeable formation such as shale has not been determined experimentally as yet, but it follows that the tortuosity of a confining shale must be much higher than that of a permeable zone as the pore structure of the shale platlets is very complex and less interconnected.

Figure 9 illustrates that vertical leakage during the diffusion period is weakly dependent on the permeability of the aquitard for a constant effective diffusion coefficient. A simulation was performed assuming an effective diffusion coefficient of the aquitard to be 0.00000833 ft^2/day. The results of the simulation were plotted on Figure 9 for comparison. Note that the total vertical leakage after 10,000 years was reduced to 35 ft from a comparable value of 120 ft for an effective diffusion og 0.0001 ft^2/day. The aquitard permeability was 0.001

md. The diffusion coefficient for a zone with low permeability was estimated by first calculating the effective diffusion coefficient for a permeable zone.

Do = 1.25x10-3 ft^2/day Molecular diffusion of salt water in fresh water.

Assuming $F\phi$ = 1.5

Deff = 1.25x10-3/1.5

= 8.33X10-4 ft^2/day for a permeable zone.

The effective diffusion coefficient for a less permeable zone, such as shale, was estimated by arbitrarily reducing the effective diffusion by a factor of 100. The effective diffusion coefficient of a confining shale of very low permeability was assumed to be $8.33x10^{-6}$ ft^2/day.

Figure 11 is a plot of the sensitivity of vertical leakage to the effective diffusion coefficient of the aquitard. The confining permeability was held constant at a value of 0.001 md. The data generated by the sensitivity cases were curve fit using a power law relation of the form of Ax^B. The power law constants listed on Figure 11 are only valid for an aquitard with a permeability of 0.001 md. As an extension to this approach a series of sensitivity runs could be performed as a function of aquitard permeability and the resulting power law constants analyzed to obtain a general relation for total vertical leakage as a function of both aquitard permeability and effective diffusion. This correlation would be very useful to validate calculations

submitted to the EPA in conjunction with requests for disposal permits.

Conclusions

A 50 ft aquitard with an effective vertical permeability of 0.10 md or less will confine injected waste products during a 50 year injection period given the fracture pressure is not exceeded during injection. A 50 ft aquitard with an effective permeability of 1.0 md or greater will not confine waste products during periods of injection.

Vertical leakage of waste products is independent of injection rate.

The equation proposed by Miller et.al.(1986) under-predicts vertical leakage for aquitards with high a permeabilities and under-predicts vertical leakage for aquitards with low permeabilities.

A reliable method for estimating the effective diffusion coefficient for impermeable formations such as shales is not available at this time.

An empirical correlation relating vertical leakage to the effective diffusion coefficient and permeability of the aquitard could be formulated from numerical simulations.

REFERENCES

Miller C. et al.:" Flow and Containment of Injected Wastes", Underground Injection Practice Council - 1986 Symposium, New Orleans La.

Hantush, M.S. and Jacob, C.E.:"Nonsteady Radial Flow in an Infinite Leaky Aquifer", Transactions of the American Geophysical Union, v. 36 no. 1, 1955, pp 95-100.

Perkins, T.K. and Johnson, O.C.: "A Review of Diffusion and Dispersion in Porous Media", SPEJ March 1963, 70-84.

Frick T.C.: "Petroleum Production Handbook", Volume II - Reservoir Engineering - Chapter 23, 1962, pp 34-40.

Morganwalp D.W, Smith R.E.: "Modeling of Representative Injection Sites", 1988.

Table 1

Reservoir Data Used for Simulations

Top of Injection Zone: 3550 ft

Reservoir Pressure: Hydrostatic (0.433 psi/ft)

Formation Volume Factor of the Liquids: 1.0 STBW/Reservoir Barrels

Rock Compressibility: 1.0×10^{-5}

Reservoir Temperature: 103 ^{o}F

Injection Zone Data:

k_x	=	200 md
k_z	=	200 md
ø	=	20 pct
h	=	15 ft
C/C_o	=	1.0

Confining Aquitard Data:

k_x	=	1.0 to 0.0001 md
k_z	=	1.0 to 0.0001 md
ø	=	40 pct
h	=	50 ft

Zone Over-lying Aquitard Data:

k_x	=	10 md
k_z	=	10 md
ø	=	20 pct
h	=	130 ft

Where:

k	=	Formation Permeability (md)
ø	=	Formation Porosity
h	=	Formation Thickness (ft)

Table 2

Concentration Profiles
k_c = 1.0 md

50 Year Injection Phase

Vertical Distance Above Injection Zone (ft)	Dimensionless Concentration C / C_o
0	1.0000
24	1.0000
28	0.9986
32	0.9904
36	0.9427
40	0.9117
44	0.8050
50	0.6816
60	0.4502
70	0.1950
80	0.0598
83	0.0144
90	0.0000

10,000 Year Diffusion Phase

5	0.6853
10	0.6798
20	0.6527
30	0.6064
40	0.5451
50	0.4737
75	0.2868
100	0.1385
125	0.0526
150	0.0152
160	0.0084
170	0.0042
180	0.0000

Table 3

Concentration Profiles
k_c = 0.1 md

50 Year Injection Phase

Vertical Distance Above Injection Zone (ft)	Dimensionless Concentration C / C_o
0	1.0000
18	1.0000
21	0.9400
22	0.7974
23	0.5852
24	0.3755
25	0.2124
26	0.1050
27	0.0437
28	0.0135
29	0.0021
30	0.0000

10,000 Year Diffusion Phase

1	0.4107
5	0.4086
20	0.3736
30	0.3307
40	0.2896
50	0.2343
75	0.1111
100	0.0428
120	0.0148
130	0.0079
150	0.0014
160	0.0000

Table 4

Concentration Profiles
k_c = 0.01 md

50 Year Injection Phase

Vertical Distance Above Injection Zone (ft)	Dimensionless Concentration C / C_o
0	1.0000
11	1.0000
13	0.9945
15	0.8213
16	0.5179
17	0.2224
18	0.0711
19	0.0170
20	0.0021
21	0.0000

10,000 Year Diffusion Phase

1	0.2851
5	0.2836
20	0.2580
30	0.2268
40	0.1971
50	0.1576
75	0.0590
100	0.0154
120	0.0042
130	0.0017
140	0.0000

Table 5

Concentration Profiles
k_c = 0.001 md

50 Year Injection Phase

Vertical Distance Above Injection Zone (ft)	Dimensionless Concentration C / C_o
0	1.0000
2	1.0000
3	0.9997
4	0.9933
5	0.9147
6	0.5671
7	0.1629
8	0.0227
9	0.0012
10	0.0000

10,000 Year Diffusion Phase

1	0.1054
5	0.1048
20	0.0950
30	0.0830
40	0.0716
75	0.0249
100	0.0084
120	0.0019
130	0.0000

Table 6

Concentration Profiles
k_c = 0.0001 md

50 Year Injection Phase

Vertical Distance Above Injection Zone (ft)	Dimensionless Concentration C / C_o
0	1.0000
1	0.8899
2	0.4187
3	0.0739
4	0.0055
5	0.0000

10,000 Year Diffusion Phase

1	0.0257
20	0.0233
30	0.0200
60	0.0072
80	0.0015
90	0.0000
130	0.0000

Figure 1

Schematic of 2D Radial Model

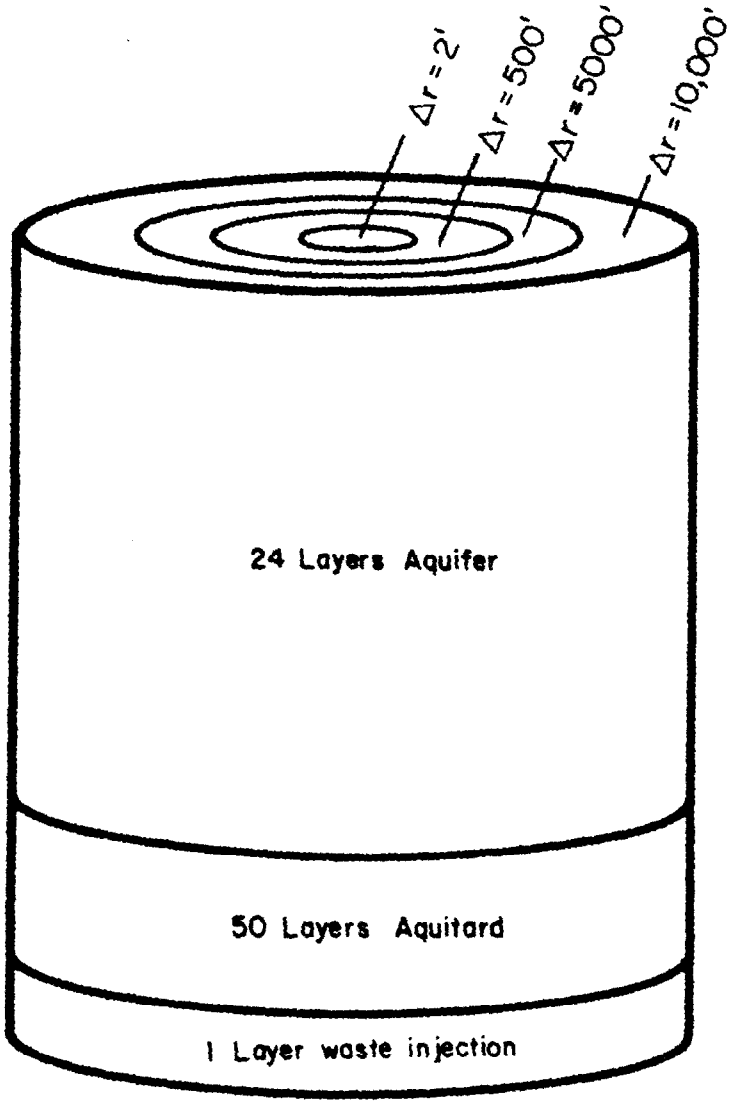

	h, ft.	k, md	layer thickness, ft.
Overlying aquifer	48	10	2
Aquitard	50	1.0	1
Waste injection	15	200	15

Figure 2

Schematic of 1D Vertical Model

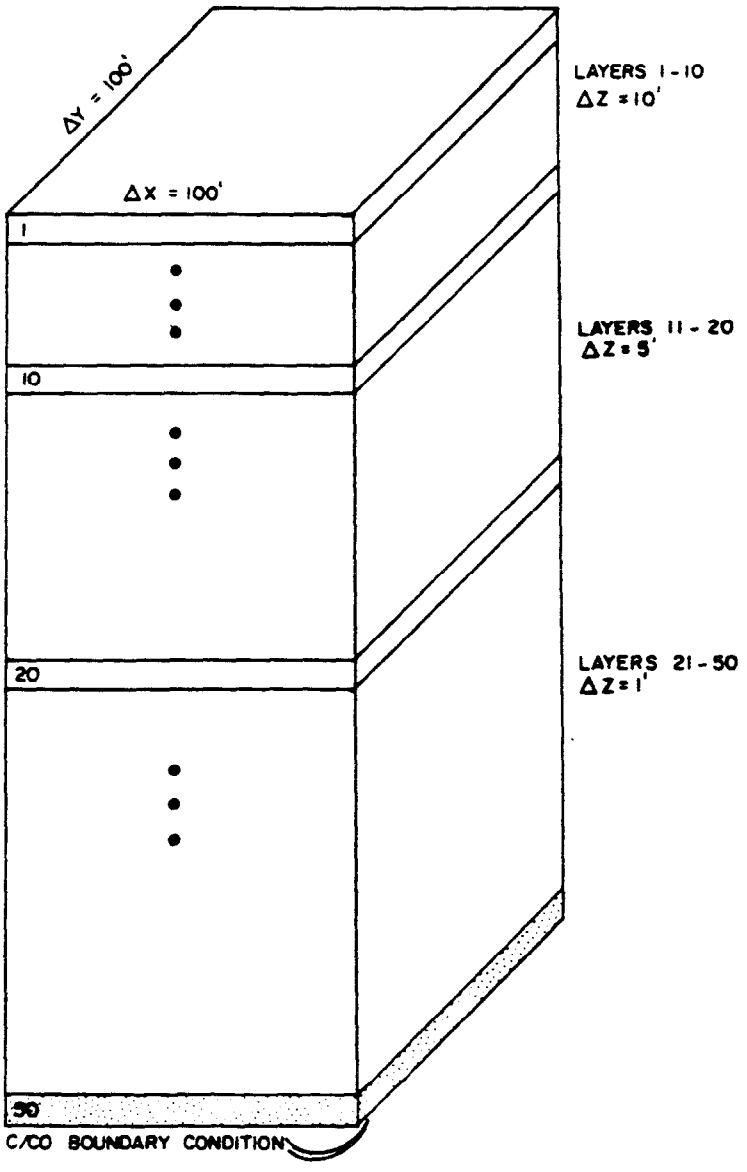

AQUITARD = 50', Layers 17-50
AQUIFER = 130', Layers 1-16

Figure 3
Concentration Profile Versus Vertical Distance

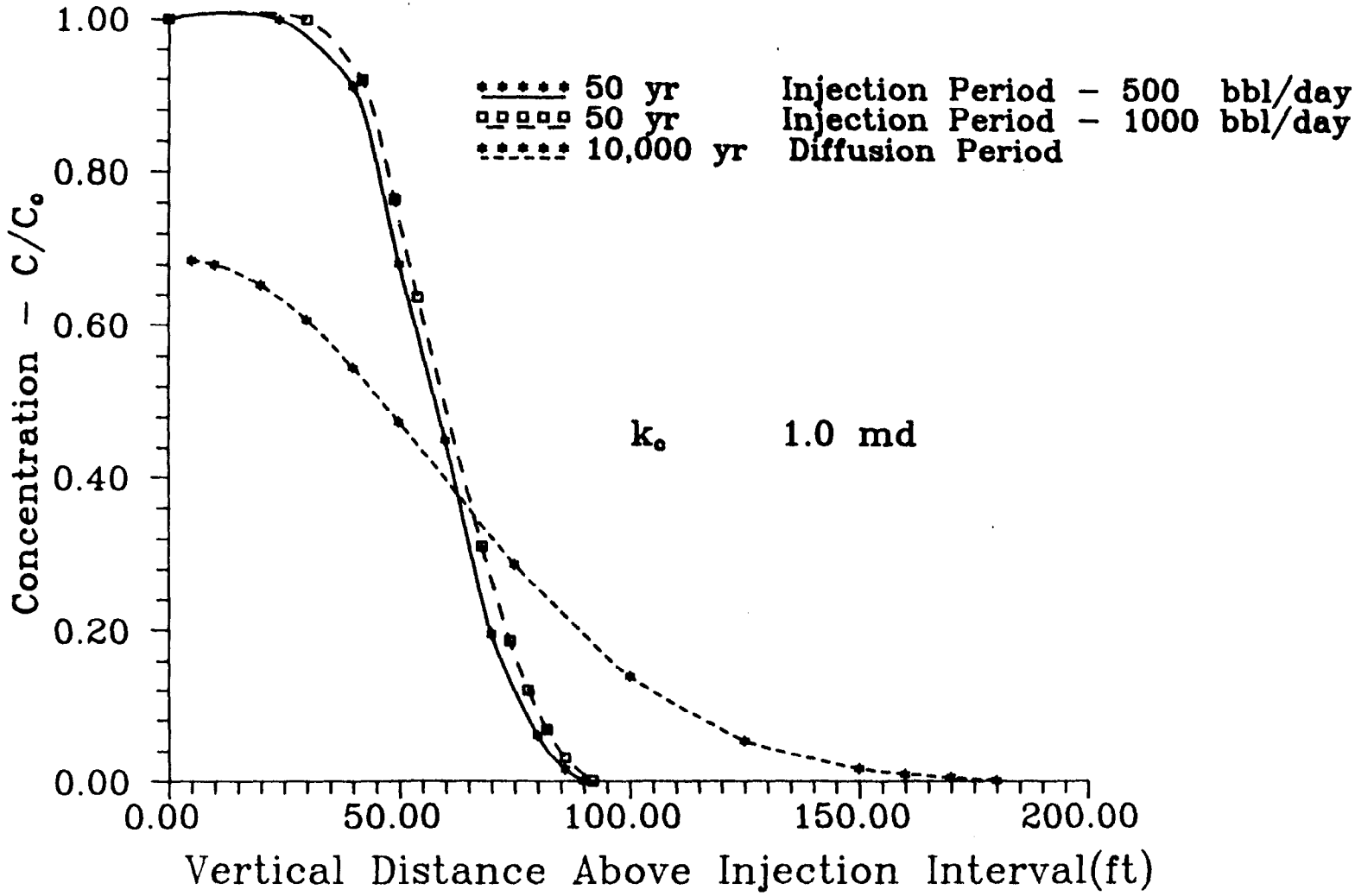

Figure 4
Concentration Profile Versus Vertical Distance

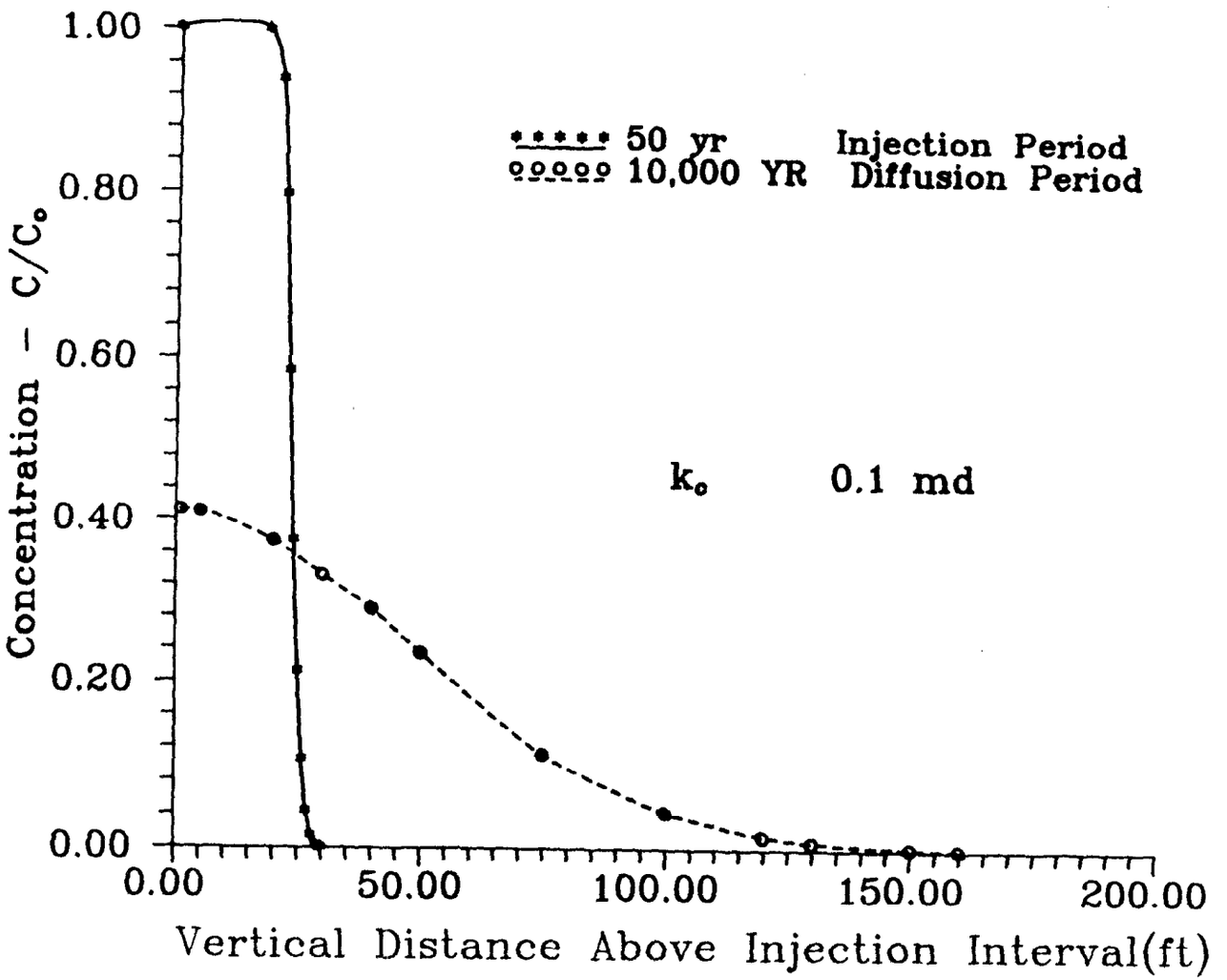

Figure 5
Concentration Profile Versus Vertical Distance

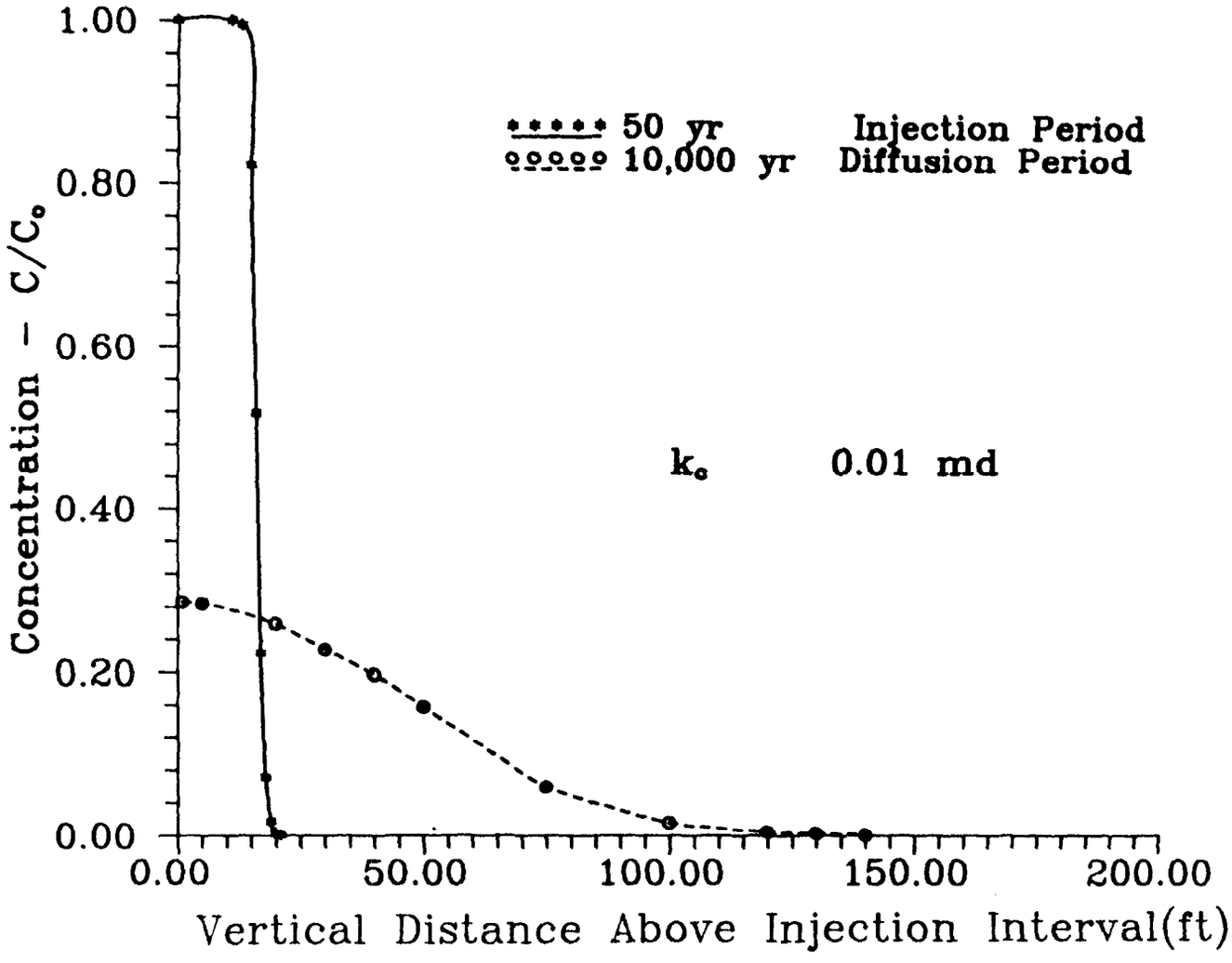

Figure 6
Concentration Profile Versus Vertical Distance

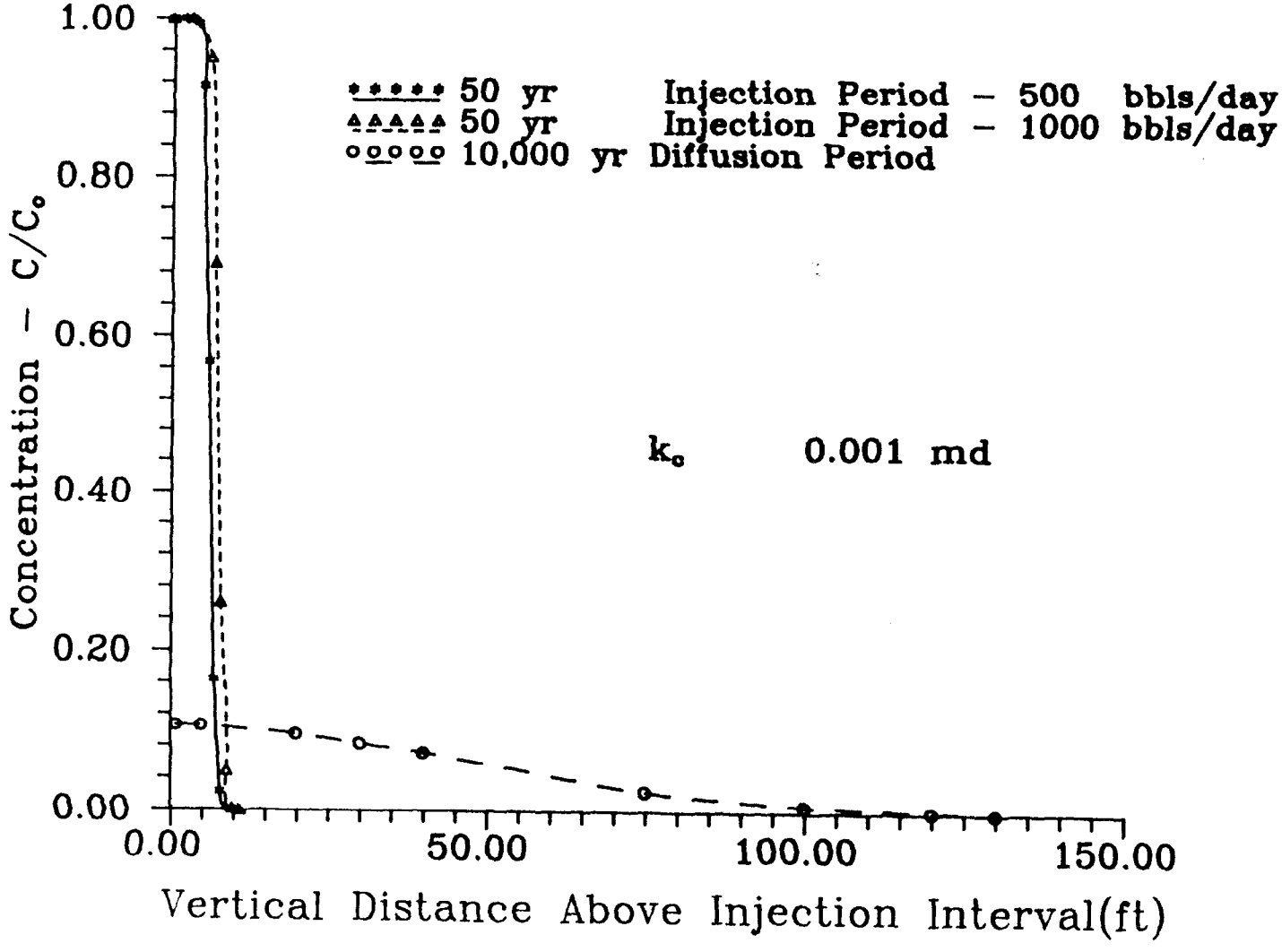

Figure 6-A
Injection Rate Versus Injection Time

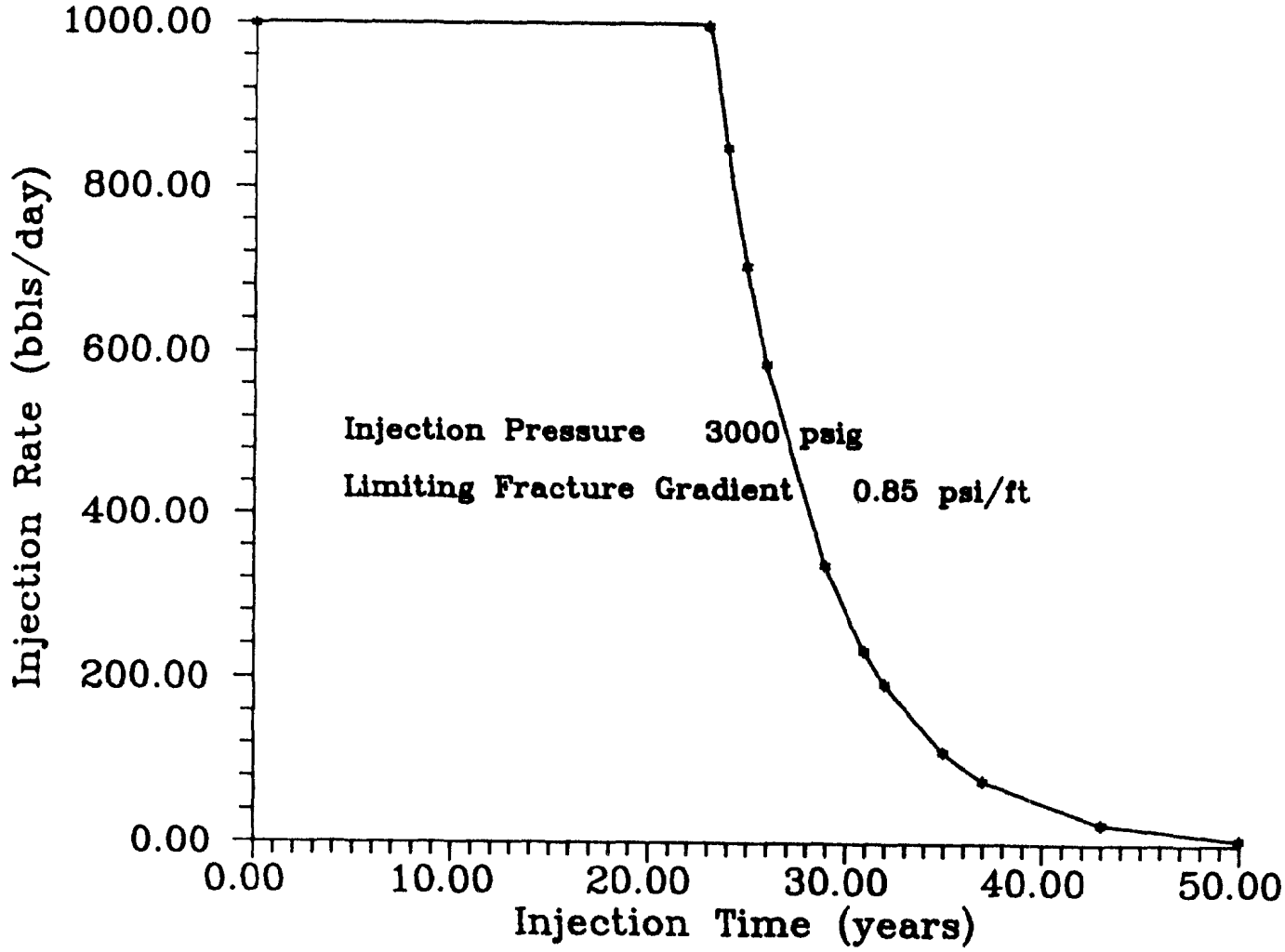

Figure 7
Concentration Profile Versus Vertical Distance

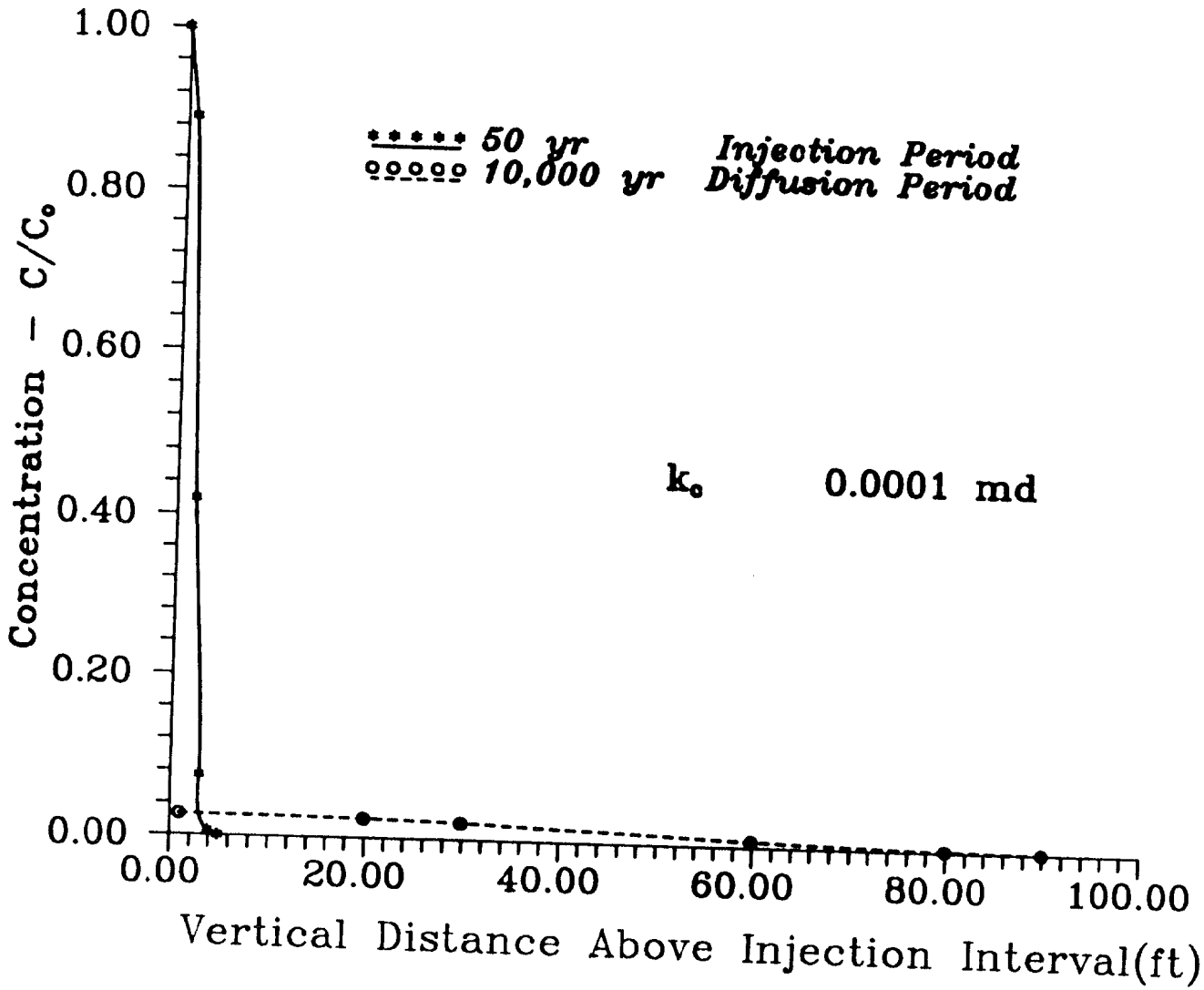

Figure 8
Leakage During Injection Versus Vertical Permeability

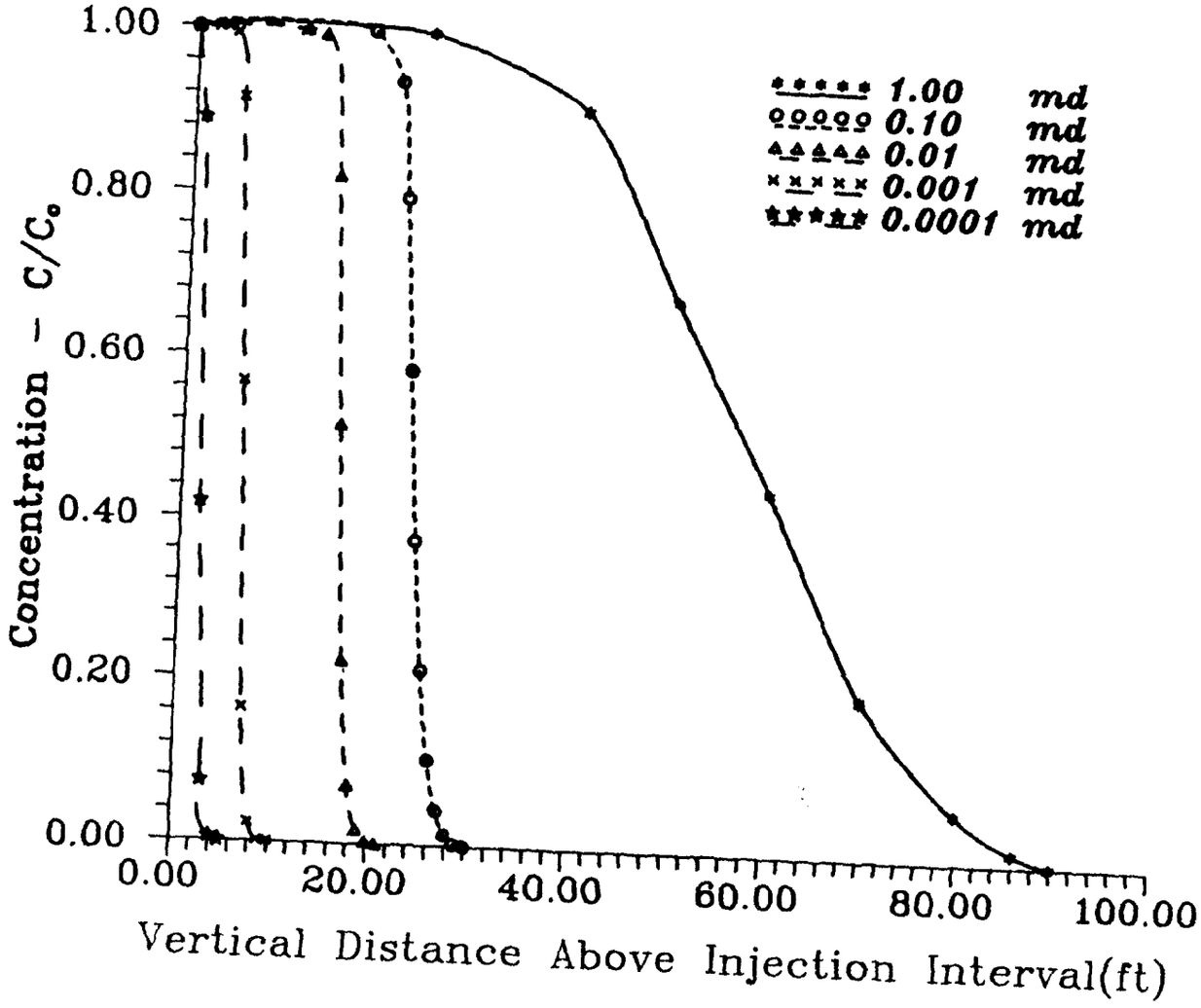

Figure 9
Leakage by Diffusion

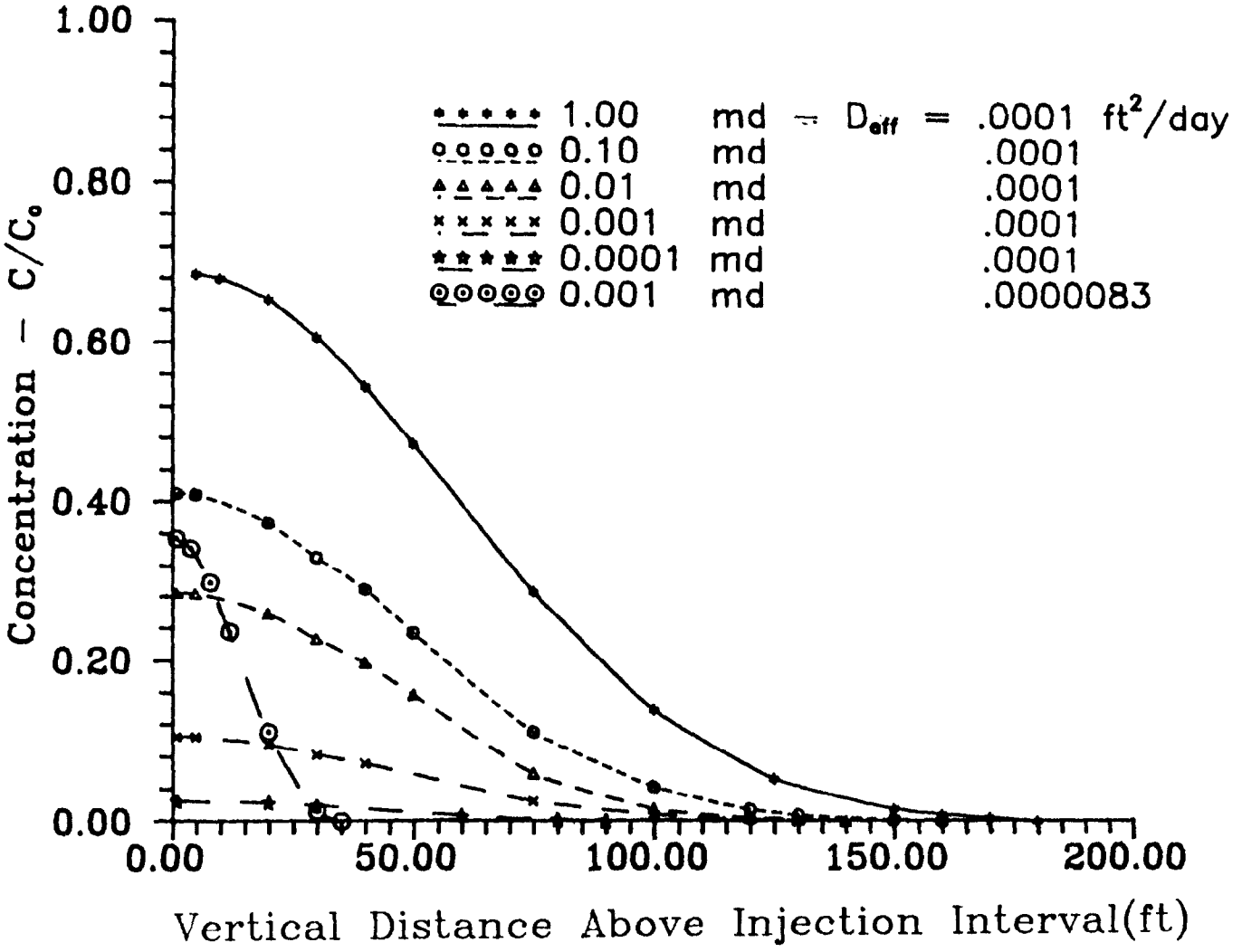

Figure 10
Leakage Versus Vertical Permeability

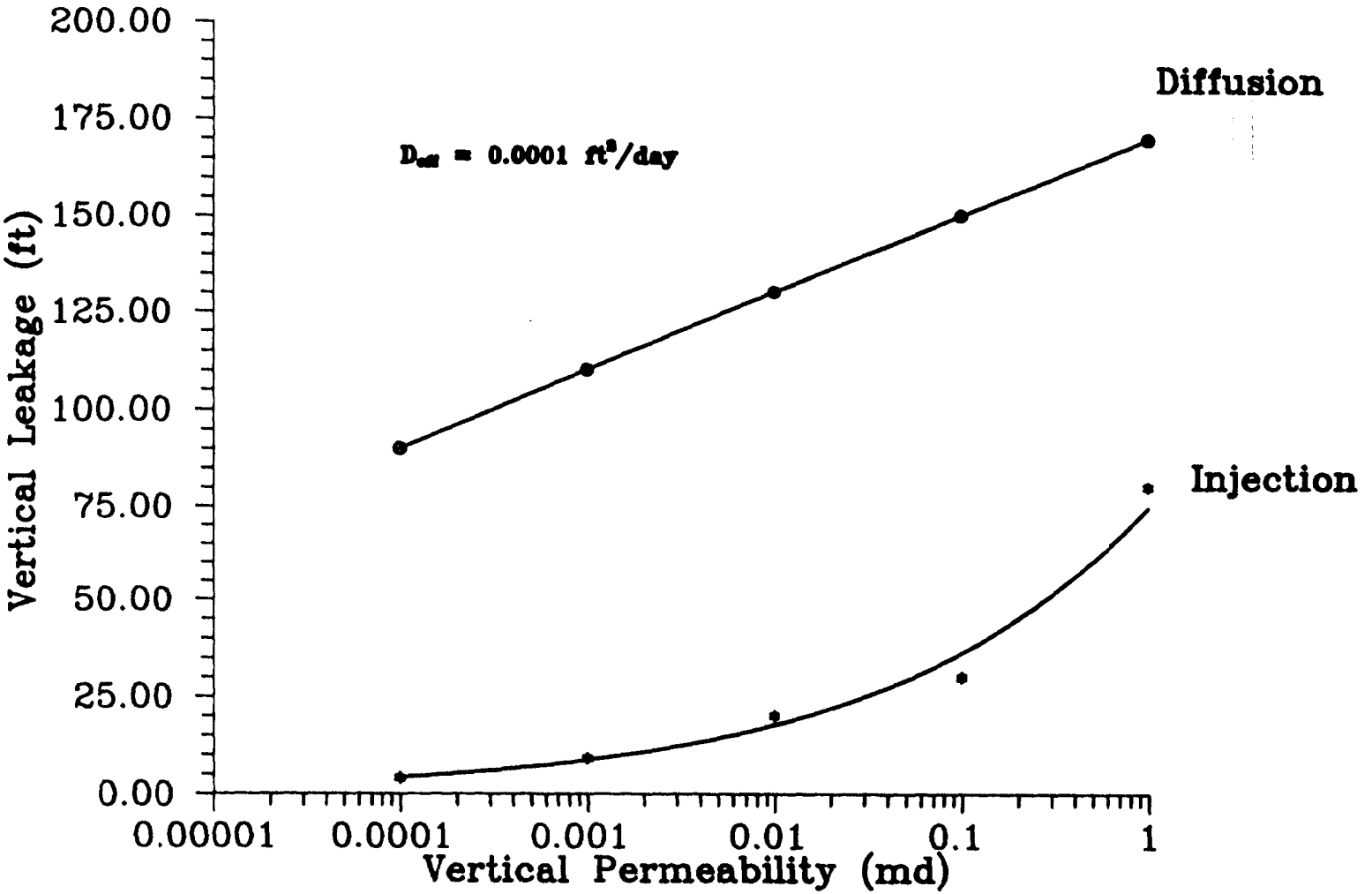

Figure 11
Leakage Versus Effective Diffusion

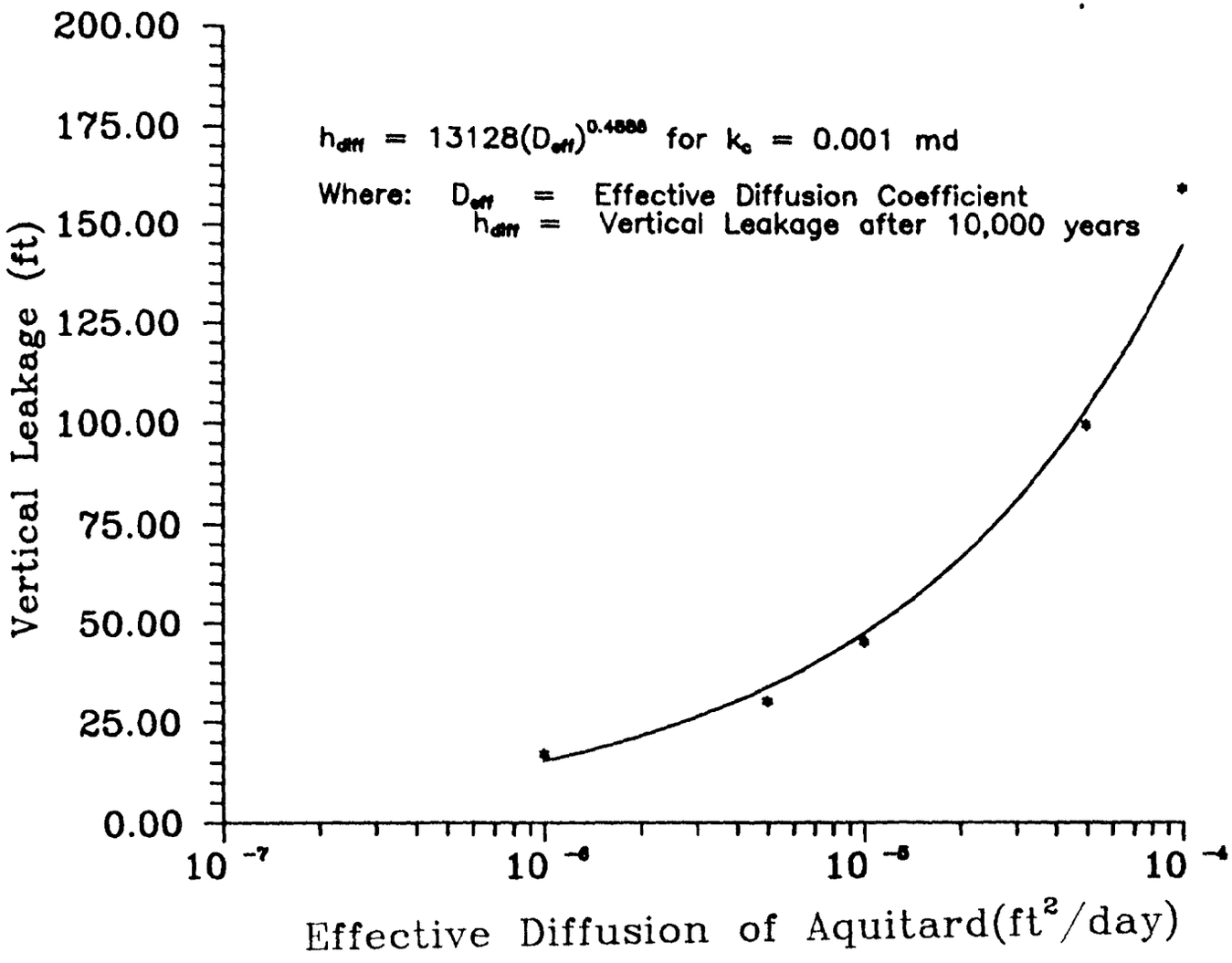

PROBLEM 2 - LINEAR DISPLACEMENT

Introduction

The displacement of resident aquifer water by injected waste water is accompanied by mixing of the waste and in situ water at the leading edge of the waste water plume. This mechanical mixing is caused by the fact that the pore space of the rock in which the aquifer resides is tortuous, and the length of various tortuous pore pathways varies on a microscopic scale. Waste water circulating through various length pore pathways is mixed with the in situ reservoir water according to the amount of "dispersion" caused by mechanical mixing in the unequal length pore pathways. The width, or dimension, of the mixed zone will become larger at longer displacement distances. The amount of dispersion is proportional to the velocity of the displacement and the microscopic geometry of the pore space. The purpose of this example problem is to demonstrate the general features of this phenomenon. A one-dimensional problem is utilized to simplify the concepts.

The Linear Problem

Figure 1 schematically illustrates the one-dimensional reservoir problem. The linear strip is 50 ft. wide (Δy) by 10 ft. thick (Δz). There are 100 grid blocks, or cells, in the x-direction. Each Δx is 2.0 ft. long, therefore the overall length is 200 ft. The

porosity of the rock is 20% and the permeability is 250 md. The reservoir system is filled with water (100% saturation), and the linear strip has an initial pressure of 1100 psi.

Waste water is injected at 5 Bbl/D (at a pore water velocity of 0.28 ft/day) and produced at the same steady-state rate. The purpose of the simulation is to observe the development of the dispersed interface between the injected waste and the resident aquifer water. The simulator utilized for this purpose is OMEGA. OMEGA's frontal displacement simulation is based upon the method-of-characteristics with an associated front tracking algorithm. Since there is no numerical dispersion associated with the calculation, displacement fronts are accurate, and stability considerations regarding time step and spatial increment size do not apply. OMEGA is unconditionally stable because of the method-of-characteristics solution.

Background on Diffusion/Dispersion

Perkins and Johnston(1963) describe hydrodynamic dispersion as related to molecular diffusion and frontal velocity as follows:

$$D_\ell^* = \frac{D_o}{\tau} + 1.75\, V_\ell\, d_p \qquad (1)$$

where:

D_ℓ^* = longitudinal dispersion, ft^2/day,

D_o = molecular diffusion coefficient, ft^2/day,

τ = tortuosity of the rock, dimensionless,

V_ℓ = displacement velocity, ft/day,

d_p = particle diameter, ft.

The diffusion coefficient, D_o, is for a liquid in the absence of porous media. Divided by τ, the tortuosity of the rock, an effective diffusion coefficient in porous media can be obtained,

$$D_e = \frac{D_o}{\tau} \tag{2}$$

For salt water diffusing into pure water, Perry(1950) gives $D_o = 1.256 \times 10^{-3}$ ft^2/D. Dividing by a tortuosity of 1.5, $D_e = 0.837 \times 10^{-3}$ ft^2/day. Perkins and Johnston give particle size diameter of approximately 0.0164 ft. for Berea and Boise sandstones.

With the addition of real data Equation (1) now becomes;

$$D_\ell^* = \underbrace{8.37 \times 10^{-4}}_{\text{diffusion}} + \underbrace{2.87 \times 10^{-2}}_{\text{convection}} v_\ell \tag{3}$$

The first term on the right-hand side of Equation (3) is the contribution to D_ℓ^* of diffusion. The second term is the contribution to D_ℓ^* of convection. At an interstitial velocity of 0.0292 ft/day the two terms are equally important to longitudinal dispersion.

Equation (1) may be rewritten in slightly different terms as:

$$D_\ell^* = \frac{D_o}{\tau} + \alpha_\ell v_\ell \tag{4}$$

where α_ℓ is the longitudinal dispersivity, ft. As developed by Perkins and Johnston for laboratory displacements is smaller in magnitude than found in field scale environments. As reported by Lake and Hirasaki(1981) field measured values vary from 0.002 to 0.11 ft. in single well tests and up to 8.1 ft. in two well tests. The dispersivity utilized in this problem is 2.863 ft.

OMEGA utilizes the form of this relationship, and in two- and three-dimensional problems the directional velocity at the face of each grid block is calculated at each time step and the velocity dependency calculated using Equation (4) before solving for the resulting frontal movement at the next time step.

Method of Characteristics Development

The equation for advective-dispersion flow in porous media is:

$$\phi \frac{\partial C}{\partial t} = D \frac{\partial^2 C}{\partial x^2} - v_x \frac{\partial C}{\partial x} \qquad (5)$$

where:

C	=	concentration, function of (x,t),
t	=	time,
x	=	spatial position,
D	=	diffusion or dispersion coefficient,
v_x	=	bulk velocity in the x-direction,
ϕ	=	porosity

This equation contains both a hyperbolic term $v_x \frac{\partial C}{\partial x}$

and a parabolic term $D \frac{\partial^2 C}{\partial x^2}$

In most reservoir problems the hyperbolic or advective flow term is much larger than the parabolic or dispersion-diffusion term, so any error in the solution to the hyperbolic advective term may have a serious impact on the solution to the diffusive parablic term. Richtmeyer(1957) shows that when the forward difference approximation is used, the numerical dispersion errors are:

error = $O(\Delta t, \Delta x^2)$ for a parabolic equation

error = $O(\Delta t, \Delta x)$ for a hyperbolic equation

Where "O" means "the order of" and the higher the power, the lesser the error, i.e., Δx is a worse approximation than Δx^2. Therefore, in general the numerical dispersion error is greater in the hyperbolic term and, since on a true physical basis, the advective term is much larger than the diffusion term, the numerical dispersion error may completely mask out the true physical dispersion. One method of reducing the numerical dispersion is to use higher order finite difference approximations. For example, Richtmeyer(1957) also shows that for a Crank-Nicholson finite difference equation,

error = $O(\Delta t^2, \Delta x^2)$ for a parabolic equation

error = $O(\Delta t, \Delta x)$ for a hyperbolic equation

In general this is more accurate, however, the hyperbolic term is still large so this tends to reduce but not eliminate the numerical dispersion and therefore is unsatisfactory for most problems. For these reasons, the model developed for this study was based upon the Method of Characteristics by which it is possible to reduce numerical dispersion to an acceptable level. More discussion of numerical dispersion may be found in the chapter entitled "Model Construction" in Volume I.

The Method of Characteristics

The Method of Characteristics is basically a procedure for splitting the advective-dispersive equation into two equations, one describing the advective flow and another describing the transport due to diffusion. A proof of the validity of the method is well described in a paper by Garder, Peaceman and Pozzi(1964). A heuristic explanation of the method is given here for one dimensional flow. The extension to three dimensions is straight forward. Consider a particle of fluid existing in the reservoir at spatial position x at any time t. The change in spatial position is given by the velocity of the point,

$$\frac{dx}{dt} = \frac{v_x}{\phi} \tag{6}$$

The concentration of the particle is C which is a function of position and time, so

$$C = C(x,t) \tag{7}$$

Expanding the concentration expression by the chain rule for derivatives

$$dC = \left[\frac{\partial C}{\partial x}\right] dx + \left[\frac{\partial C}{\partial t}\right] dt \tag{8}$$

$$\frac{dC}{dt} = \left[\frac{\partial C}{\partial x}\right] \frac{dx}{dt} + \frac{\partial C}{\partial t} \tag{9}$$

Combining equations and simplifying, the result is:

$$\frac{dC}{dt} = D \frac{\partial^2 C}{\partial x^2} \tag{10}$$

$$\frac{dx}{dt} = \frac{v_x}{\phi} \tag{11}$$

Equations (10) and (11) now represent the system of equations to be solved (Method of Characteristics). The movement of the particle of gas due to advective flow is obtained by integrating Equation (11) and the change in concentration due to diffusion is obtained by solving Equation (10). Note that since Equation (11) is an ordinary differential equation, numerical dispersion is eliminated so the

advective transport solution introduces no error. The solution to Equation (10) requires a finite difference approximation solution, however, the error is now negligible since it is based only on the diffusion equation.

Of particular interest is the comparison of the simulator to the analytical solution describing diffusion in a one-dimensional porous medium in the absence of bulk flow (zero velocity):

$$D_o \frac{\partial^2 C}{\partial x^2} = \phi \frac{\partial C}{\partial t} \tag{12}$$

where:

D_o = the molecular diffusion coefficient,

$C(x,t)$ = concentration of injected waste,

x = distance coordinate,

t = time coordinate, and

ϕ = porosity of rock

The solution to this equation for constant D_o and is:

$$\frac{C(x,t)}{C_o} = \frac{1}{2} \left\{ 1 - \text{erf} \left[\frac{x}{\sqrt{4D_o t/\phi}} \right] \right\} \tag{13}$$

where:

erf = error function

The solution to the problem when bulk flow occurs with a constant velocity (v), is equivalent to solving the diffusion problem in a moving coordinate system. In order to account for the flow, it is only necessary to replace the distance (x) in Equation (13) by the amount a point would move over time (t) with a constant Darcy velocity (v), i.e.

$$x = x - vt/\phi \tag{14}$$

Under conditions of steady flow the solution to the diffusion equation as presented by Peaceman and Rachford(1962) is:

$$\frac{C(x,t)}{C_o} = \frac{1}{2}\left\{1 - \text{erf}\left[\frac{x-vt/\phi}{\sqrt{4Dt/\phi}}\right]\right\} \tag{15}$$

where D/ϕ is now is now an effective diffusion or dispersion coefficient depending upon the flow regime.

The boundary conditions are:

C/C_o = 0.0 for all x at t = 0.

C/C_o = 1.0 for x = 0 at t>0.

C/C_o = 0.0 for x = L and t>0.

Other analytical solutions to the infinite and semi-infinite strip problem are available for comparison of numerical results.

OMEGA utilizes wellbore boundary conditions at each end of the strip; i.e., a steady-state Darcy's Law boundary condition which dictates the same constant injection and production rate is utilized. In this simple problem, the violation of the boundary condition at x = L apparently does not cause significant distortion in the numerical solution as compared to the analytical solution.

Comparison of Numerical Results in Analytical Solution

Figure 2 illustrates the comparison of the numerical solution from OMEGA with the analytical error function solution of Equation (8). The dimensionless concentration vs. dimensionless distance profile is for 0.50 PV (pore volume) injected at 5 Bbl/D rate (v/ϕ = 0.28 ft/day). In this case the convective term of Equation (4) is controlling. D_ℓ^* for this problem is 0.818 ft^2/day.

If there were no physical dispersion the injected fluid would travel as a plug and the displacement front would be a vertical line at a dimensionless distance of 0.50. The argument of the error function is zero when $x = vt/\phi$, a condition that is satisfied when enough injection time has passed so that the fluid front is at distance x. At one quarter pore volume injected x/L = 0.25, at one-half pore volume injected x/L = 0.50, at three quarters pore volume injected x/L = 0.75, etc. The error function of argument equal to zero is zero itself. Therefore, from the form of Equation (8) C/C_0 = 0.500 when ($x - vt/\phi$) = 0.0.

In addition, a property of error functions is that they are symmetric; i.e. erf (-z) = -erf (z). The dispersed front is symmetric about C/C_0 = 0.500. Superimposed on a pore velocity (in this case 0.28 ft/day) the dispersed band is symmetric, i.e. the mixing zone trails as far behind the midpoint of the front as it precedes the front. The agreement between OMEGA and the analytical function is quite good. This

agreement indicates a good numerical solution unperturbed by round-off or truncations of Taylor's series representation of derivatives has been achieved. (We shall see in a later problem that this is not always the case.)

In Figure 3 the dimensionless concentration profiles are shown for 0.25, 0.50, and 0.75 pore volume injected at 0.28 ft/day. Although somewhat difficult to perceive in this figure the width of the dispersed front is becoming wider as injectant moves farther in distance along the linear strip. One may quantify this widening of the dispersed band by measuring the width between C/C_o = 0.90, and C/C_o = 0.10 for each of the three profiles. At 0.25 PV, x/L (10-90) = 0.43; at 0.50 PV, x/L (10-90) = 0.66; at 0.75 PV, x/L (10-90) = 0.80.

The problem of Figure 3 (0.28 ft/day pore velocity) was rerun for D_ℓ^* = 0.0818 ft^2/D and also for 8.18 ft^2/D. The results of these two runs are compared to the prior simulation with D_ℓ^* = 0.818 ft^2/D in Figure 4 at 0.50 pore volume injected. The effect of dispersion on spreading of the advancing waste front is now apparent. Higher dispersion spreads the front faster than lower dispersion at the same velocity. The C/C_o profile at D_ℓ^* = 8.18 ft^2/day appears to be somewhat distorted in that it does not intersect C/C_o = 0.50 at 0.50 at x/L = 0.50 as the error function solution does.

Effluent Measurements

If samples of the mixed fluids were taken at the end of the strip (x/L = 1.0) and their concentrations measured, the effluent concentration profile would appear as in Figure 5. Comparison with the analytical error function solution is again quite good.

There are some additional features to this curve that are distinctly different from the concentration profiles graphed versus x/L. Recall that the profiles graphed vs. x/L were symmetric because they were superimposed on a bulk velocity. In other words the viewer is travelling at the same bulk velocity so the profiles appear symmetric. When profiles are measured at a stationary point, say x/L = 1.0, the effluent profile is asymmetric. At one pore volume of injection C/C_o is still 0.50; however the higher C/C_o values are "strung out" or present a longer "tail" on the effluent. This effect is caused by the fact that dispersion in the direction of the bulk velocity runs ahead of the advancing front while dispersion counter to the velocity stretches the concentration profile out. (i.e. The net velocity of the advancing "toe" benefits from a component from dispersion where the lagging "tail" has a negative velocity component from dispersion).

Figure 6 is the effluent analog of the three simulations in Figure 4. Here we measure the effluent concentrations at the end of the strip. Again we observe that higher levels of dispersion, D_ℓ^*, cause spreading fo the emerging concentration profiles at constant velocity.

REFERENCES

Gardner, A.O. Jr., Peaceman, D.W., and Pozzi, A.C. Jr.; "Numerical Calculation of Multidimensional Displacement by the Method of Characteristics," Society of Petroleum Engineers Journal, March, 1964, p 26.

Lake, Larry W., and Hirasaki, George J.; "Taylor's Dispersion in Stratified Porous Media," Society of Petroleum Engineer's Journal, August 1981, pp. 459-468.

Peaceman, D. W., and Rachford, H. H. Jr.; "Numerical Calculation of Multidimensional Miscible Displacement," Society of Petroleum Engineers Journal, December, 1962, pp. 327-339.

Perkins, T. K. and Johnston, O. C.; "A Review of Diffusion and Dispersion in Porous Media," Society of Petroleum Engineers Journal, March 1963, pp. 70-84.

Perry, John H.; Chemical Engineer's Handbook, page 540, McGraw-Hill Book Company, Inc., 1950.

Richtmeyer, R.D.; Difference Methods for Initial Value Problems, Interscience Publishers, Inc., New York, 1957.

Figure 1

Schematic of One Dimensional Model

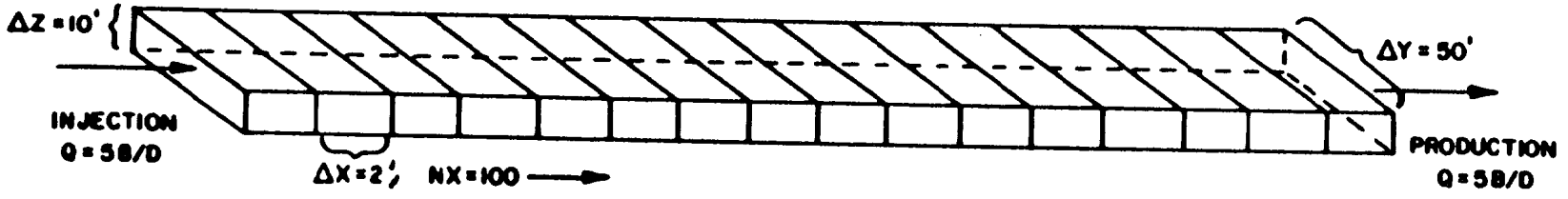

K = 250 md
ϕ = 0.20
S_w = 100%
p_i = 1100 psi
V/ϕ = 0.2857 ft/day

Figure 2
Concentration Profile Versus Distance

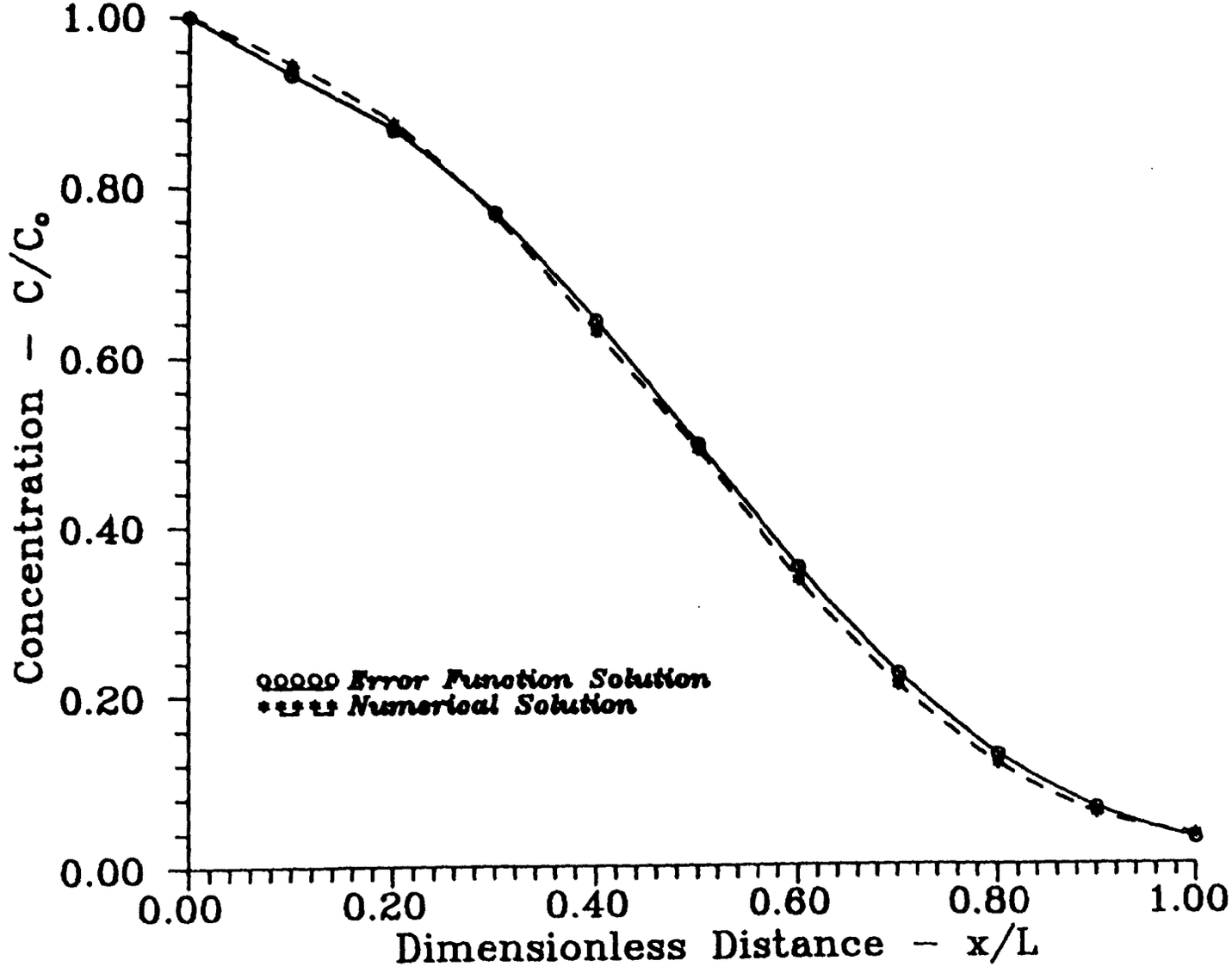

Figure 3
Concentration Profile Versus Pore Volume Injected

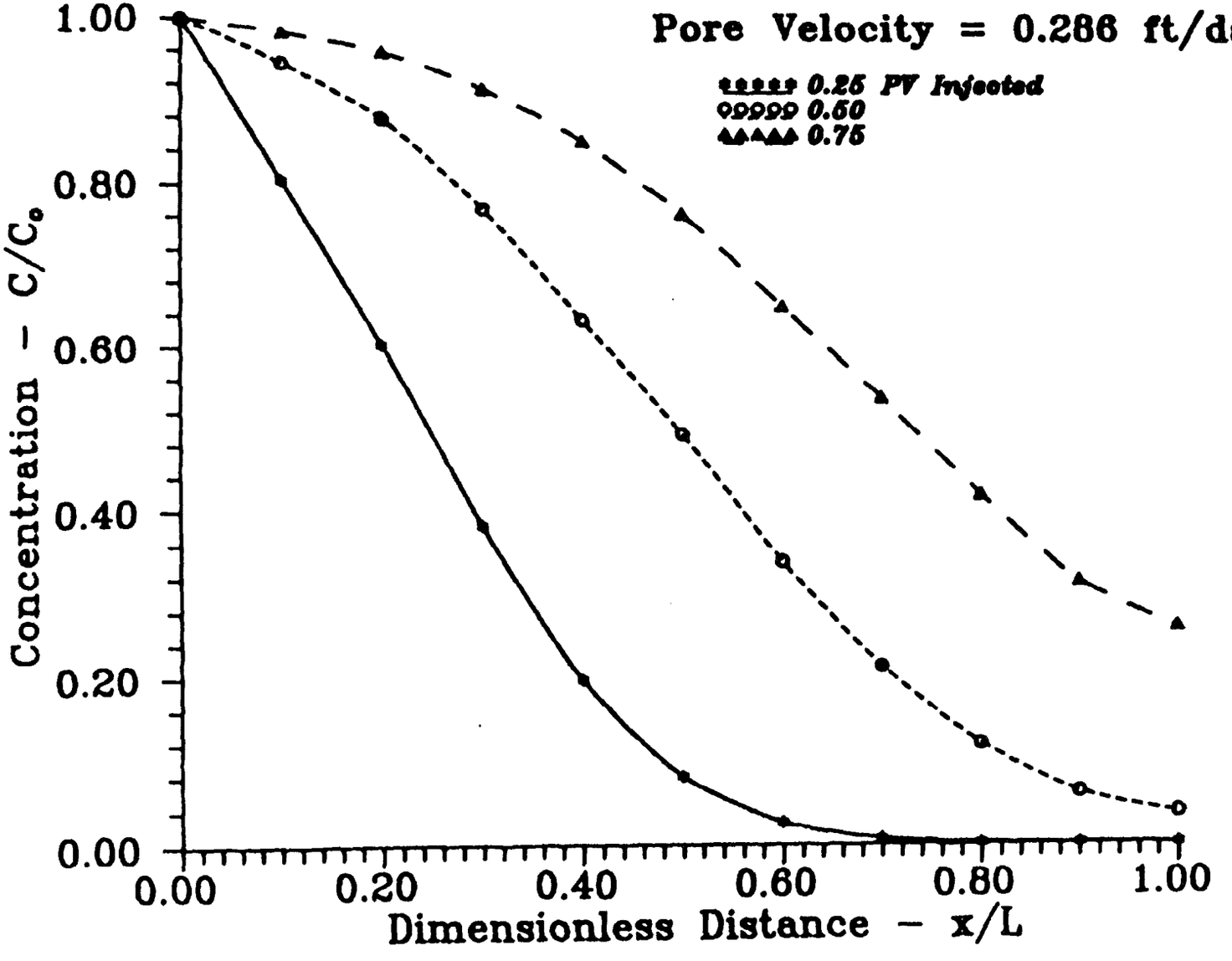

Figure 4
Concentration Profile Versus Injection Rate

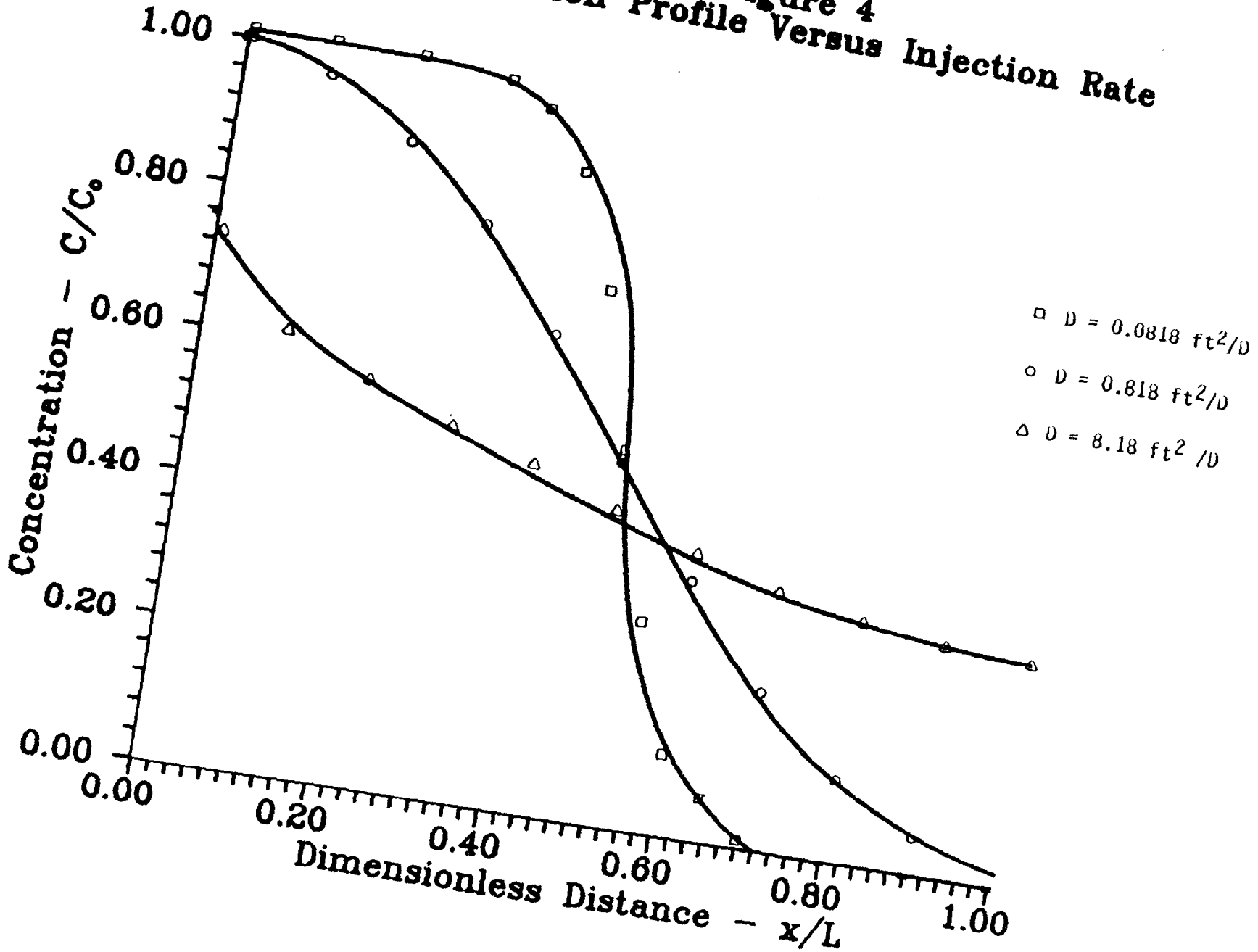

Figure 5
Concentration Profile Versus Pore Volume

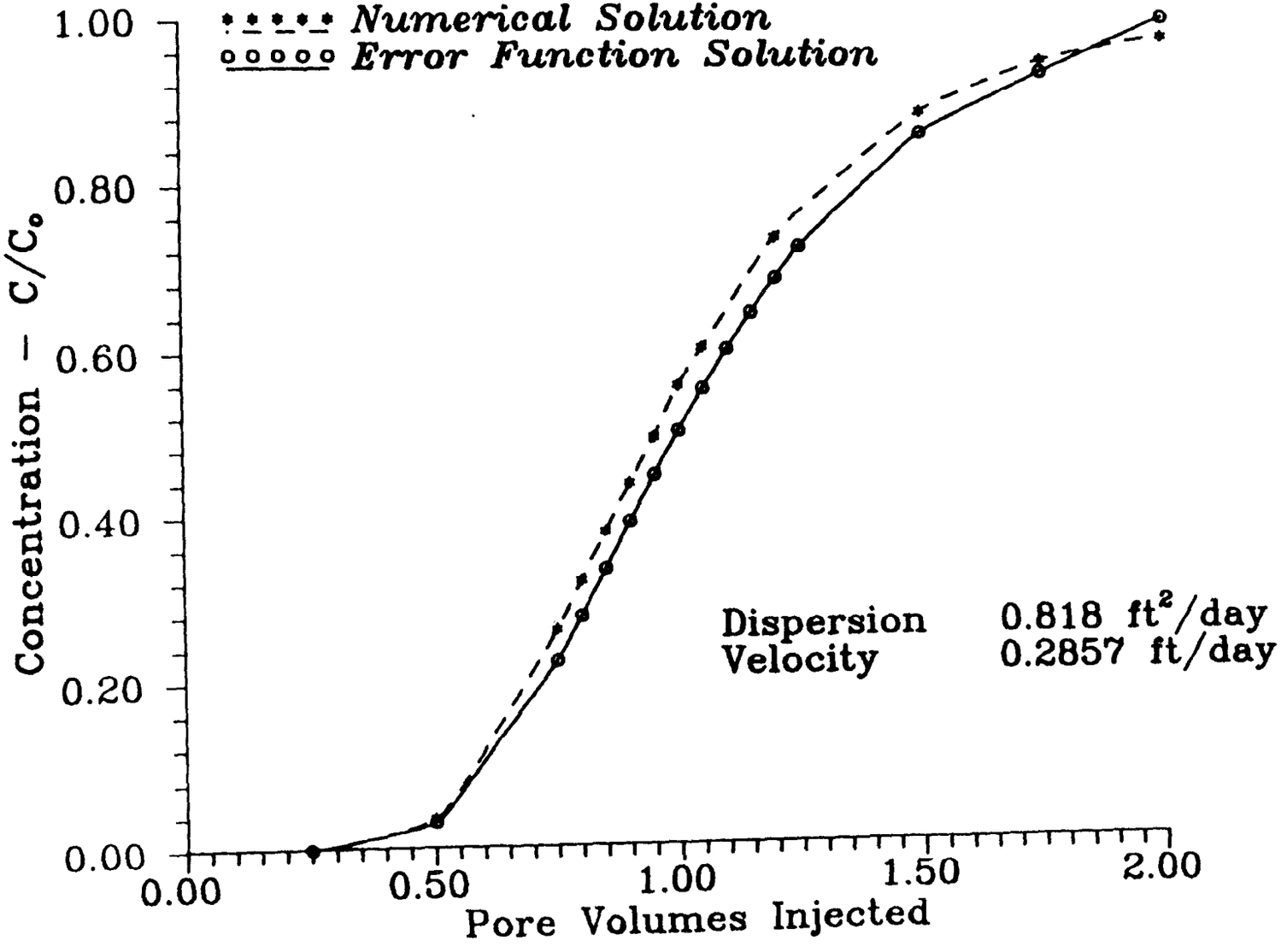

Figure 6
Concentration Profile Versus Injection Rate

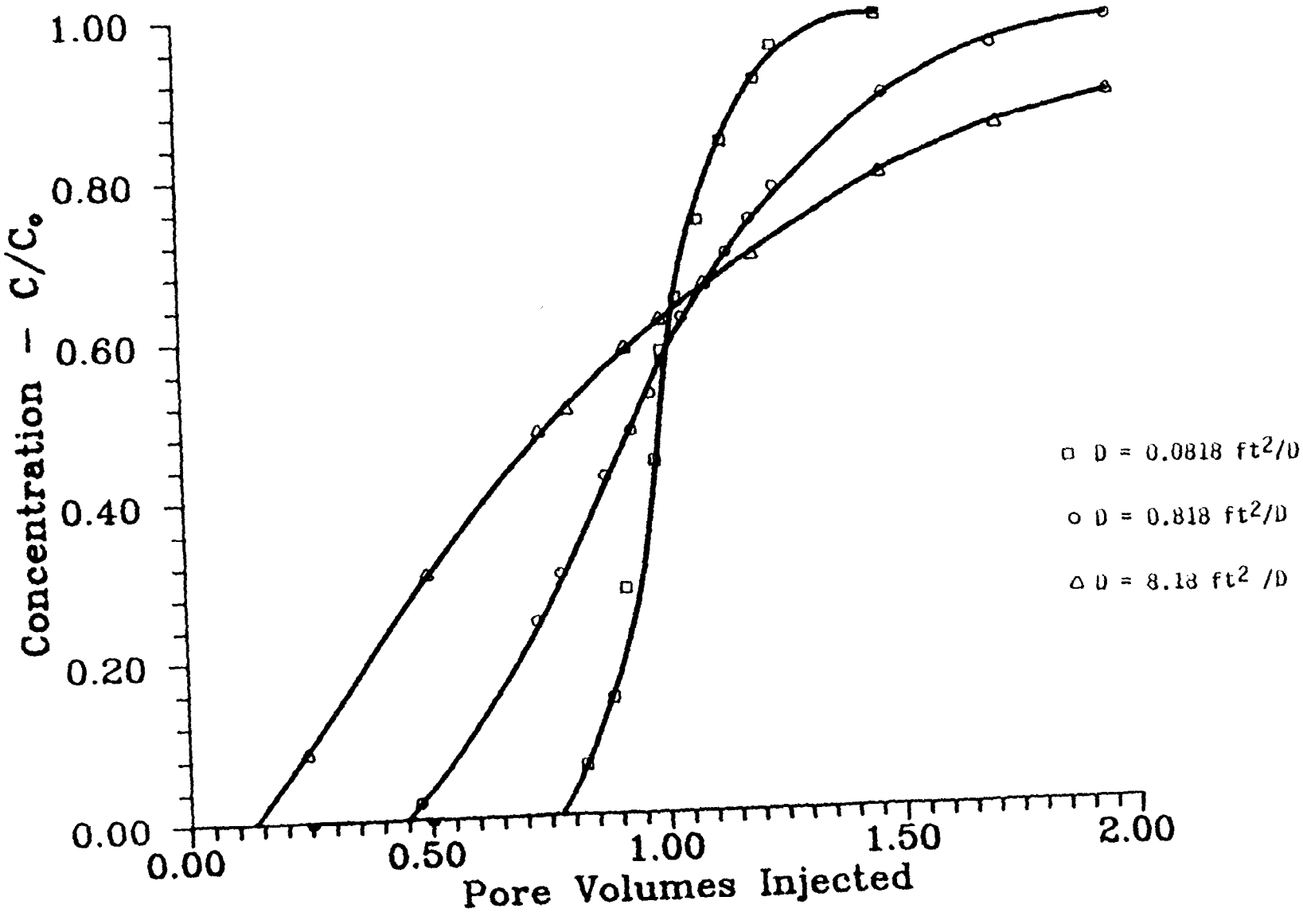

The following problem, 2A, has been contributed by Talib Syed and Ghulam Iqbal of Engineering Enterprises. This contribution is gratefully acknowledged by Scientific Software-Intercomp, Inc.

PROBLEM 2A

SOLUTE MOVEMENT IN DEEP WELL INJECTION

1. Objective

The objective of this section is to study the phenomena of diffusion and dispersion associated with the movement of solute (waste material) into an aquifer during deep well injection operations and to discuss the governing equations along with their solutions for relatively simple cases. Two problems related to linear and radial movement of solute have been worked out to demonstrate various aspects of the process. The complexities that may arise in certain field cases are also briefly mentioned to make the reader aware of the usual problems encountered in this type of study.

2. Introduction

When a solute is introduced into a subsurface porous medium (aquifer) by injection through a deep well, the concentration profile of the solute at any point in time and location is of prime importance from the containment point of view. Due to dispersion, the leading edge of a solute concentration profile may be found far ahead of that traced by bulk movement of an immiscible fluid. Solute concentration is known to be dependent on three important phenomena. These are advection, diffusion and mechanical mixing (or mechanical dispersion).

3. Mechanisms of advection, diffusion and dispersion

Advection, also referred as convection, results in the change of solute

concentration at a particular point in the aquifer as the solute is carried past that point by water (solvent). The rate of displacement is equal to the average velocity of water in pores. During injection of solute, motion of water in the porous media is created by an injection pressure which is higher than the initial average pressure of the aquifer.

When a solute concentration gradient exists between two adjacent regions of an aquifer, diffusion of solute material takes place, with the net effect of an uniform concentration throughout the system. However, diffusion is known to be a relatively slow process, and its contribution in changing solute concentration at a particular point may not be significant when a high fluid velocity is present during injection.

Mechanical dispersion, or mixing, is mainly caused by microscopic heterogeneties present in porous media and the net result is the spreading out of the injected solute from the path predicted by advective hydraulics. Tortuosity and size variation of pore channels along with the drag force exerted on fluid flowing close to the pore walls contribute to the phenomenon.

4. Dispersion Coefficient

Diffusion and mechanical dispersion are commonly lumped together and referred to as hydrodynamic dispersion and the effective dispersion coefficient is defined as (Freeze and Cherry, 1979, and Javandel, et al, 1984)

$$D_e = \bar{D} + \alpha v^m \qquad (1)$$

in which D_e is the effective dispersion coefficient (L^2/T), $\bar{D}$ is the effective diffusion coefficient (L^2/T), α is dispersivity (L), v is the average fluid velocity in pores (L/T), and m is an exponent with values ranging between 1 and 1.5. L and

T denote consistent units in length and time, respectively.

The interstitial pore velocity term appearing in Eq. (1) can be obtained from Darcy velocity (bulk velocity) by noting that v = Darcy velocity / porosity. The effective value of diffusion coefficient is determined from known value by noting that $\overline{D} = wD^*$, where w ranges between 0.67 and 0.707 depending on tortuosity of porous medium and D^* is the diffusion coefficient (Perkins and Johnston, 1963). Values of m, $\overline{D}$ and α are obtained from field or laboratory studies.

It is also necessary to distinguish between longitudinal and transverse dispersion. While the former occurs in the principal direction of flow, the latter takes place at right angles to flow. Subscripts L and T are often assigned to the dispersion coefficients accordingly. Longitudinal dispersion coefficients are known to have values one or more orders of magnitude higher than the transverse dispersion coefficients when an appreciable fluid velocity is present.

5. Governing equations, boundary conditions and assumptions

Solute movement in an aquifer as traced by its concentration profile with respect to time and distance is represented by a partial differential equation based on mass balance considerations of the injected material. The law of mass conservation dictates that, in the absence of chemical reaction or adsorbtion, the rate of mass input in a control volume located in the flow regime must be accounted for by the rate of mass output and the rate of change of solute concentration within the control volume.

[Rate of change in solute conc.] = [Rate of output] - [Rate of input]

The details of derivation can be found in literature (Freeze and Cherry, 1979), and

the resulting equation takes the form, in one dimension:

$$D_e \frac{\partial^2 C}{\partial x^2} - v \frac{\partial C}{\partial x} = \frac{\partial C}{\partial t} \qquad (2)$$

where C is the solute concentration, x is the distance in the direction of flow (L) and t is time of injection (T). The equation is frequently referred to as the *advection-dispersion equation* in literature. The first term in Eq. (2) represents the change in solute concentration due to hydrodynamic dispersion at a point in a one-dimensional flow regime, and the second term accounts for the change in concentration due to bulk movement of fluid past that point. A homogeneous isotropic porous medium is assumed in deriving the equation.

Eq. (2) can be solved either numerically or analytically under appropriate boundary conditions. Each method has its own advantages and limitations (Javandel, 1984). An approximate analytical solution (Ogata, 1970) of Eq. (2), subject to the following boundary conditions

$$C(x,0) = 0, \qquad x \geq 0 \qquad (3)$$

$$C(0,t) = C_0, \qquad t \geq 0 \qquad (4)$$

$$\lim_{x \to \infty} C(x,t) = 0, \qquad t \geq 0 \qquad (5)$$

can be written as

$$\frac{C}{C_o} = \tfrac{1}{2} \left[1 - \text{erf} \left(\frac{x - v\,t}{2\sqrt{D_e\,t}} \right) \right] \qquad (6)$$

where erf is the *error function.* Values of the function are available in mathematical handbooks and other literature (Javandel, 1984). The function can also be computed quickly by hand-held computer with the help of the following polynomial (Spiegel, 1968):

$$\text{erf}(z) = \frac{2}{\sqrt{\pi}}\left(z - \frac{z^3}{3.1!} + \frac{z^5}{5.2!} - \frac{z^7}{7.3!} + \ldots\ldots\right) \tag{7}$$

It should be noted that Eq. (6) may also be written in terms of *complementary error function* as

$$\frac{C}{C_o} = \tfrac{1}{2}\left[\text{erfc}\left(\frac{x - v\,t}{2\sqrt{D_e\,t}}\right)\right] \tag{6a}$$

where, erfc(z) = 1 - erf(z).

The boundary conditions given in Eqs. (3) through (5) describe an aquifer where the solute concentration is initially at zero. Injection of solute with a concentration of C_0 is then commenced. The boundaries of the aquifer are at sufficient distance away from the injection well so that the solute concentration can be assumed to be zero at the outer limits during the period of injection.

For the case of underground disposal of waste material through deep wells, fluid flow geometry around the injection point is predominantly radial. Hence, it is more realistic to cast the advection-dispersion equation in radial coordinates. The radial form of advection-dispersion equation (Javandel, 1984),

$$\alpha_L v \frac{\partial^2 C}{\partial r^2} - v \frac{\partial C}{\partial r} + \frac{\bar{D}}{r}\frac{\partial}{\partial r}\left(r\frac{\partial C}{\partial r}\right) = \frac{\partial C}{\partial t} \tag{8}$$

may be solved subject to the following boundary conditions,

$$C(r,0) = 0, \qquad r \geq 0 \tag{9}$$

$$C(0,t) = C_o, \qquad t \geq 0 \tag{10}$$

$$\lim_{r \to \infty} C(r,t) = 0, \qquad t \geq 0 \tag{11}$$

$$\frac{\partial C(r,0)}{\partial t} = 0\ , \qquad r \geq 0 \tag{12}^*$$

to yield an approximate analytical solution (Hoopes and Harleman, 1967) as in the

*This boundary condition applies everywhere in the aquifer except at the injection point.

Based on Eq. (15), the pore velocity in radial case can be computed as

$$v = \frac{Q}{2\pi\, r\, h\, n} \tag{16}$$

It is evident from the above equation that v decreases as the radial distance from the injection point, r, increases in magnitude. Eq. (14) can be written, noting that $\overline{D} = 0$, as

$$z = \frac{r^2/2 - Qt\,/\,(2\pi\, h\, n)}{\sqrt{\frac{4}{3}\,\alpha\, r^3}} \tag{17}$$

Inspection of the above equation shows that z = 0 at

$$r^2/2 = \frac{Q\,t}{(2\,\pi\,h\,n)} \tag{18}$$

Again, when z = 0, erf(z) is also zero, and the value of C/C_o in Eq. (13) becomes 1/2. Thus the point where solute concentration is half the input concentration can be calculated readily from Eq. (18). In the present example, that point is

$$\begin{aligned} r_{C/C_o=0.5} &= \sqrt{Q\,t\,/\,(\pi\,h\,n)} \\ &= \sqrt{(20 m^3/hr)(10*365*24 hr)/(\pi * 10\ m * 0.2)} \\ &= 528\ m \end{aligned} \tag{19}$$

Hence, it is found that, after 10 years of continuous injection, solute concentration has increased from zero to 1000 ppm at 528 meters (1732 ft) away from the well. We can also determine the solute concentration at, say, r = 550 m. From Eq. (17), we find the value of z as

entire concentration profile is plotted in Fig. 2.

However, it is seen that the injected material has moved with a sharp front without much spreading out of solute into the aquifer. The reason for above is the relatively low value of effective dispersion coefficient used in the problem. However, when the value of the effective dispersion coefficient is increased by one and two orders of magnitude (D_e = 0.818 and 8.18 ft^2/day, respectively), solute concentration profile does begin to flatten out as evident from Fig. 3. In other words, solute is dispersed far ahead and deep into the aquifer when the dispersion coefficient is relatively high. A detailed discussion of solute behavior for the radial dispersion case is presented below.

7. The radial dispersion problem

We now present a simplified version of a typical deep well injection problem where the objective is to find the solute (waste) concentration profile in an aquifer at different time intervals of injection. The computations are based on Eq. (13). Data for the problem is taken from published literature (Javandel, 1984) and given below:

Initial solute conc., C_o = 2000 ppm

Rate of injection, Q = 20 m^3/hr

Injection period, t = 10 yrs

Aquifer thickness, h = 10 m

Aquifer porosity, n = 0.2

Longitudinal dispersivity, α_L = 0.1 m

Effective diffusion coefficient, $\overline{D}$ = 0

Exponent in Eq. (1), m = 1

following:

$$\frac{C}{C_o} = \frac{1}{2}\,[\,1 - \mathrm{erf}(z)\,] \tag{13}$$

where,

$$z = \frac{r^2/2 - r\,v\,t}{\sqrt{\left(\frac{4}{3}\,\alpha_L\,\overline{r^3} + \frac{\overline{D}}{v}\,\overline{r^3}\right)}} \tag{14}$$

and r is the radial distance of a point from the injection well (L). The boundary conditions stipulated in radial flow are similar to those found in linear one-dimensional case. Once the values of v, α_L and $\overline{D}$ are either known or estimated, Eqs. (13) and (14) can be used to compute the concentration of injected solute as a function of r and t.

6. The 1-D linear problem

We first consider one-dimensional movement of solute and its concentration profile in a linear finite strip (Fig. 1) which is 2000 ft long, 50 ft wide and 10 ft thick. The data for this problem are provided by Scientific Software Intercomp and given in the following:

Aquifer porosity, n = 0.2

Effective dispersion coefficient, $D_e = 0.0818$ ft^2/day

Injection rate, Q = 5 bbl/day

Solute is continuously introduced into the system at a concentration of C_o and its concentration profile will be computed analytically based on Eq. (6).

As a first step, we calculate the pore velocity of fluid as

$$v = \frac{\text{Volumetric flowrate}}{\text{cross–sectional flow area} * \text{porosity}} \qquad (15)$$

$$= \frac{(5 \text{ bbl/day}) * (5.615 \text{ cft/bbl})}{(50 * 10 \text{ sqft}) * (0.2)}$$

$$= 0.2807 \text{ ft/day}$$

The 'pore volume' of the strip considered here can be calculated by multiplying its bulk volume and porosity. The value is found to be 2000*50*10*0.2 = 200,000 cubic ft.

Now, let us compute the solute concentration profile following injection of a specific volume of fluid containing the waste material. With an injection rate of 5 bbl/day, the time to inject, say, half the pore volume is

$$t = \frac{½ (200{,}000 \text{ cft})}{5 * 5.615 \text{ cft/day}}$$

$$= 3562 \text{ days or } 9.76 \text{ years.}$$

Based on bulk flow considerations alone, with no solute present, the injected fluid is expected to advance half the length of strip (=1000 ft) when total injected volume is half the pore volume. Our *objective* is to find the concentration of solute ahead of the half-way point in presence of hydrodynamic dispersion.

For an example, let us compute the solute concentration (expressed as C/C_o, the fraction of the input concentration), at 1050 feet from the injection point. Using Eq. (6),

$$\frac{C}{C_o} = ½ \left[1 - \text{erf} \left(\frac{1050 - 0.2807 * 3562}{2 \sqrt{0.0818 * 3562}} \right) \right]$$

$$= ½ [1 - \text{erf} (1.4688)] = 0.0188 \text{ or } 1.88 \%$$

The above result shows that the solute has travelled beyond the half-way point, and has a detectable concentration (about 2% of initial value) at 1050 feet. The

$$z = \frac{550^2/2 - 20 * 10 * 365 * 24 / (2\pi * 10 * 0.2)}{\sqrt{\frac{4}{3} * 0.1 * 550^3}}$$

$$= 2.51$$

The solute concentration is now computed from Eq. (13) as, $C = \frac{1}{2} C_o [1 - \text{erf} (2.51)] = 0.39$ ppm. The entire profile for the radial case (C as a function of r after 10 years) is presented in Figure 4. The effects of various parameters on solute concentration are now investigated.

7.1 Period of injection

Fig. 5 shows the frontal advance of injected solute after 10, 20 and 30 years of continuous injection operation. It is evident that solute travels farther and farther into the aquifer away from the well bore with longer injection time intervals. After 30 years, the point where C = 1000 ppm is located at r = 915 m compared to 528 m calculated for 10 years of injection. The computation is based on Eq. (19), and reflects an advance of 387 m (1270 ft) in 20 more years. Inspection of Eq. (19) suggests that, when $\overline{D}$ is negligible, the point where the solute concentration is half the input concentration is proportional to the square root of the length of injection period when other parameters remain the same.

7.2 Dispersion coefficient

A very important aspect of the waste injection problem is to investigate the role of the dispersion coefficient on the solute concentration profile. For the sake of demonstration, the value of α_L is increased by one and two orders of magnitude (α_L = 1 and 10 m, respectively). Concentration profiles calculated with the new values of α_L are plotted in Figure 6 and the results are presented in Table 1. For a low value of dispersivity (α_L = 0.1 m), the concentration profile is relatively

sharp. However, with increase in dispersivity, solute is considerably spread out in the aquifer and the leading edge of the concentration profile travels far ahead of the bulk flow.

For example, when α_L = 10 m, let us calculate the point where the solute concentration is 0.39 ppm in the aquifer. From Eq. (13), the value of Z can be calculated as 2.51 for a C = 0.39 ppm. The value of r can now be calculated as 861 m from Eq. (17), which is 311 m (1020 ft) farther away from the injection well compared to r = 550 m obtained with a relatively low dispersivity of α_L = 0.1 m.

It is also of interest to calculate the value of solute concentration at r = 550 m with α_L = 10 m. Based on Eqs. (13) and (17), C is calculated to be 722 ppm, which is an increment by three orders of magnitude from C = 0.39 ppm calculated with α_L = 0.1 m.

8. Practical considerations

Analytic solutions are based on the assumption that all equation coefficients such as α and $\overline{D}$ are nonvariant throughout the solution domain. This implies a rather ideal condition where the porous medium is assumed to be homogeneous in nature. However, in order to make meaningful analysis, reservoir heterogeneities inherent in most field cases must be incorporated in the framework of the solution scheme.

A widely used approach to include variations in reservoir properties in the analysis is based on a numerical approach, where the region of interest is divided into a predetermined number of subregions (grid blocks), and each block is assigned different reservoir properties. In certain cases, appropriate averaging of reservoir properties and incorporation of the average values in analytic solutions

may also be accomplished for initial estimates.

The approximate analytic solutions presented here is valid for a 'semi-infinite' aquifer where no appreciable solute concentration remains zero at the outer limits during the period of injection. For small aquifers with nearby boundaries, use of the analytical methods presented here may lead to an erroneous solution for long injection periods. However, numerical methods permit the incorporation of complex boundary conditions in solute movement studies.

The concentration profile obtained by the analytic solution in radial geometry is based on the assumption that the concentration profile is symmetric around the point of injection. In the case of anisotropic formations where directional permeability (hydraulic conductivity) is predominant, the analysis is not valid. Solution of the above problem may be obtained by numerical methods based on a two-dimensional advection-dispersion equation where the numerical grids are aligned to the principal direction of flow.

Realistic values of dispersion coefficients may not be readily available for use in simulation. Values of the coefficient obtained by using core samples in laboratory studies may be one or more orders of magnitude less than the actual field value (Lake and Hirasaki, 1981). The reason lies in the fact that small core samples obtained from the vicinity of a drilled well cannot represent the field scale heterogeneities present in the entire flow region.

Since typical field practice includes downtime for trouble-shooting and maintenance of operating equipment, the injection of waste material may not be continuous as assumed in the simplified problems presented above.

REFERENCES

Freeze, R.A., and Cherry, J.A., 1979, *Groundwater*, Prentice-Hall, New Jersey.

Hoopes, J.A., and Harleman, D.R.F., 1967, 'Dispersion in Radial Flow from A Recharging Well', J. Geophys. Res., 72(14).

Javandel, I., et al, 1984, *Groundwater Transport: Handbook of Mathematical Models*, Am. Geophys. Union, Washington.

Lake, L.W., and Hirasaki, G. J., 1981, 'Taylor's Dispersion in Porous Media', Soc. Pet. Eng. J., August issue.

Ogata, A., 1970, 'Theory of Dispersion in A Granular Medium', U.S. Geol. Surv. Prof. Paper 411-I.

Perkins, T.K., and Johnston, O.C., 1963, 'A Review of Diffusion and Dispersion in Porous Media', Soc. Pet. Eng. J., Vol. 3.

Spiegel, M.R., 1968, *Mathematical Handbook*, McGraw-Hill, New York.

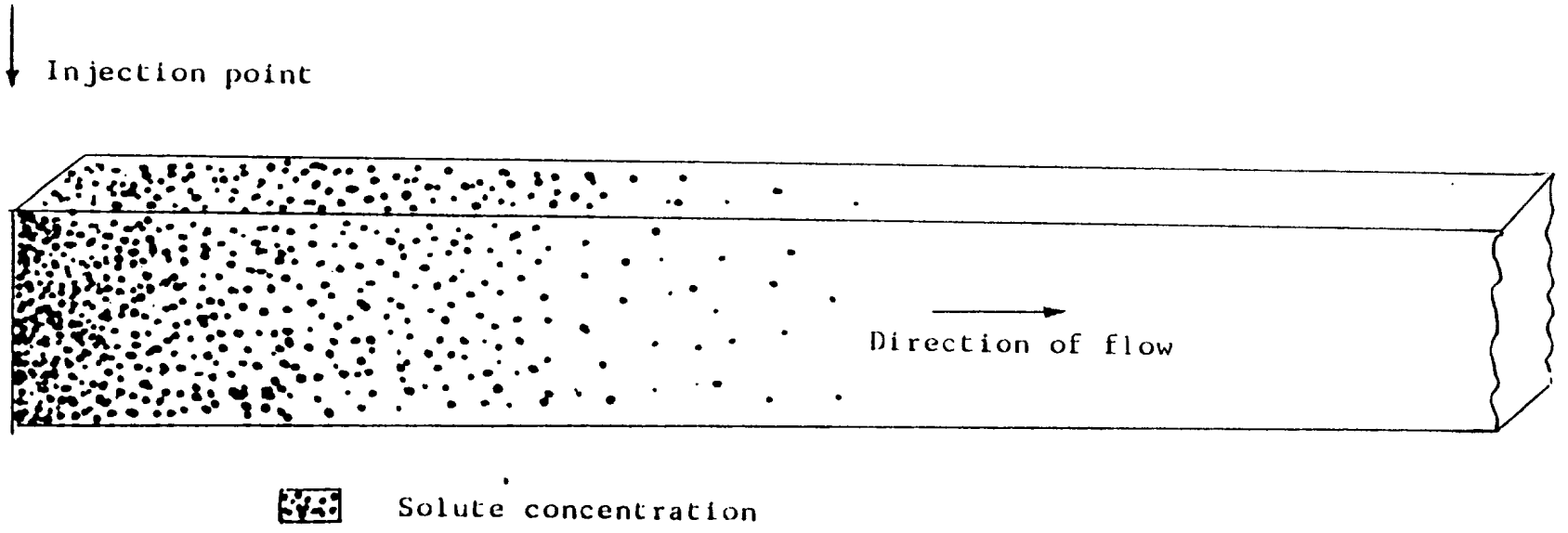

Figure 1 : Solute movement in a linear strip visualized in 1-D problem.

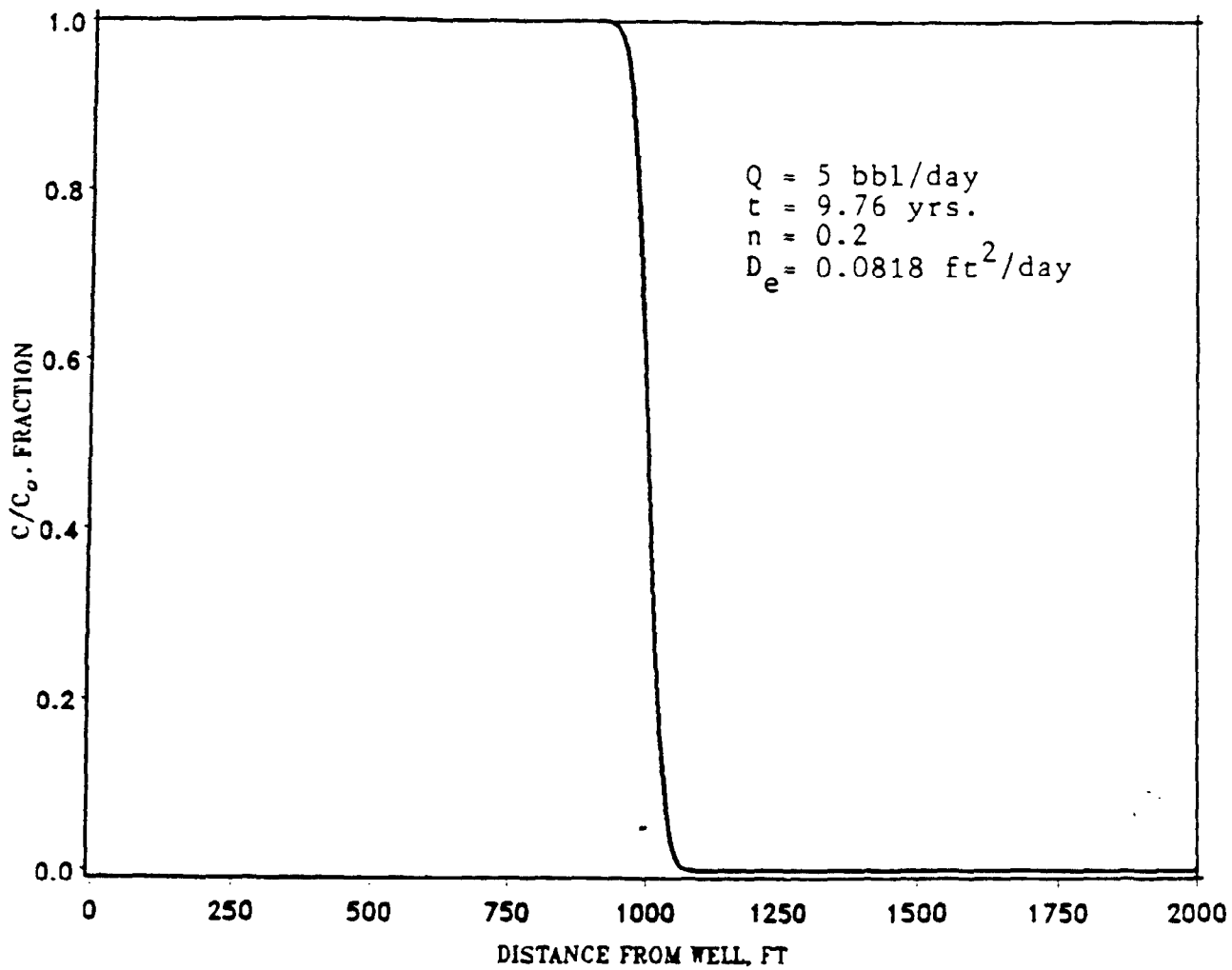

FIG 2 : SOLUTE CONCENTRATION PROFILE IN 1-D PROBLEM

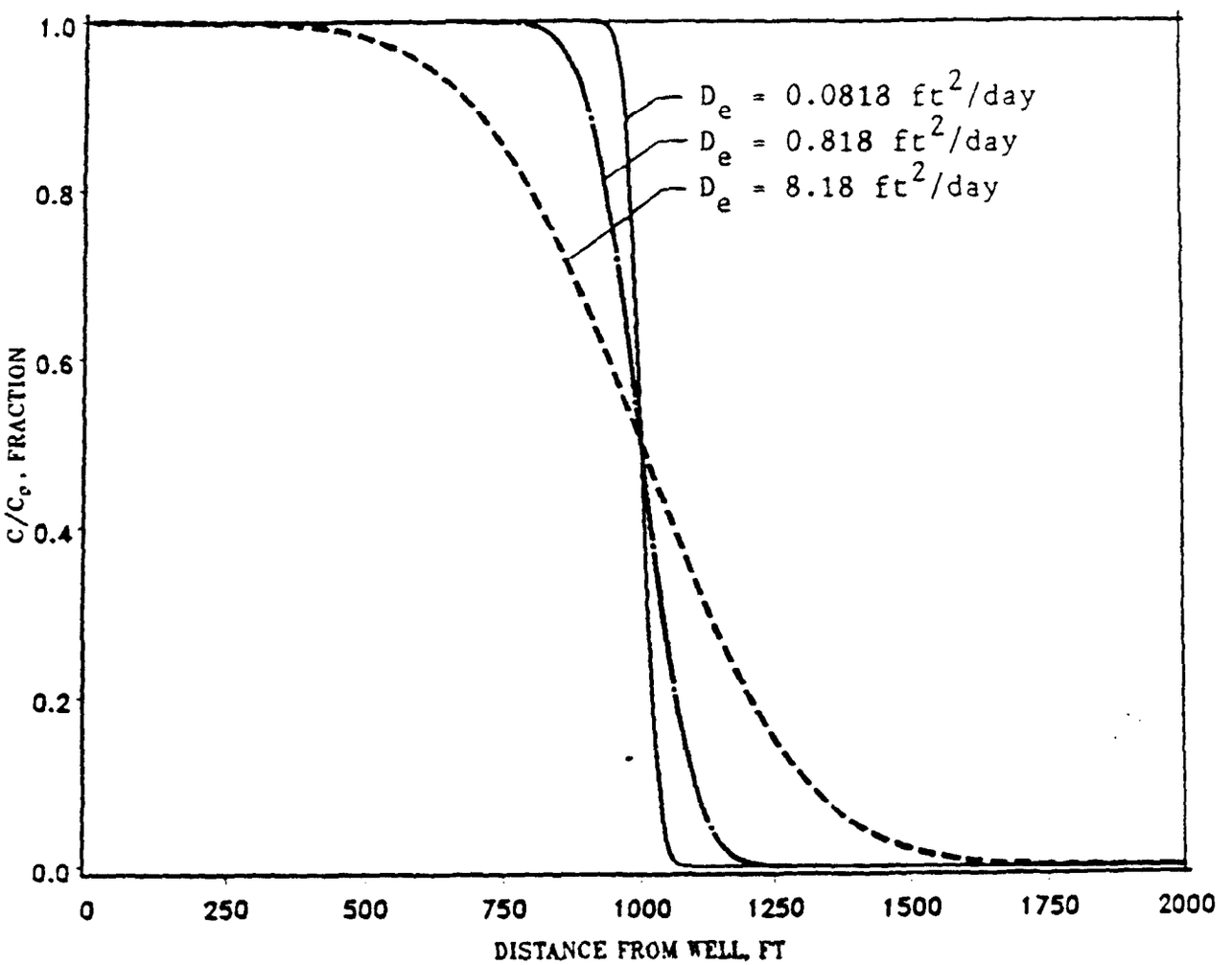

FIG 3 : EFFECT OF DISPERSION COEFFICIENT ON CONC. PROFILE

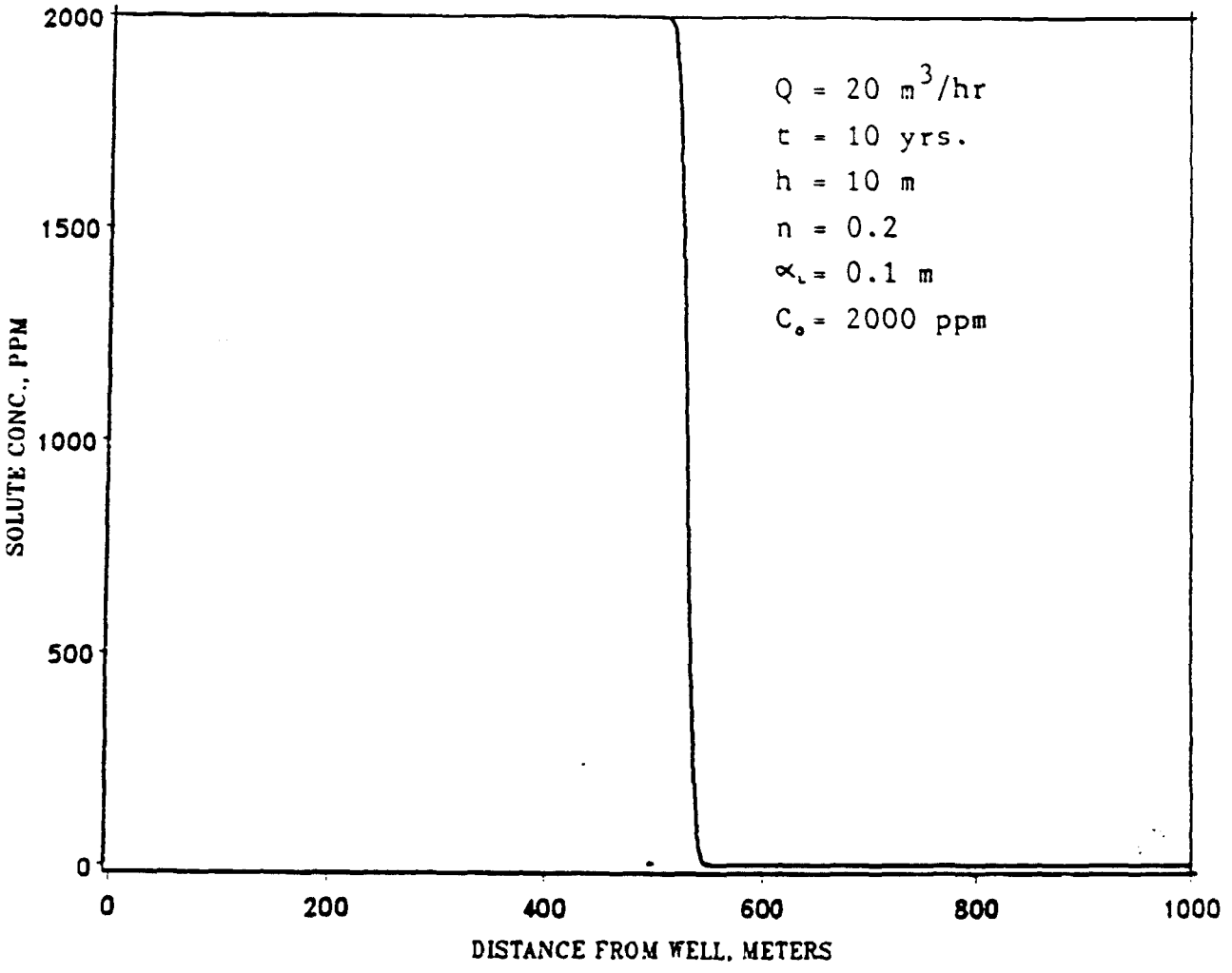

FIG 4 : SOLUTE CONC. PROFILE IN RADIAL CASE

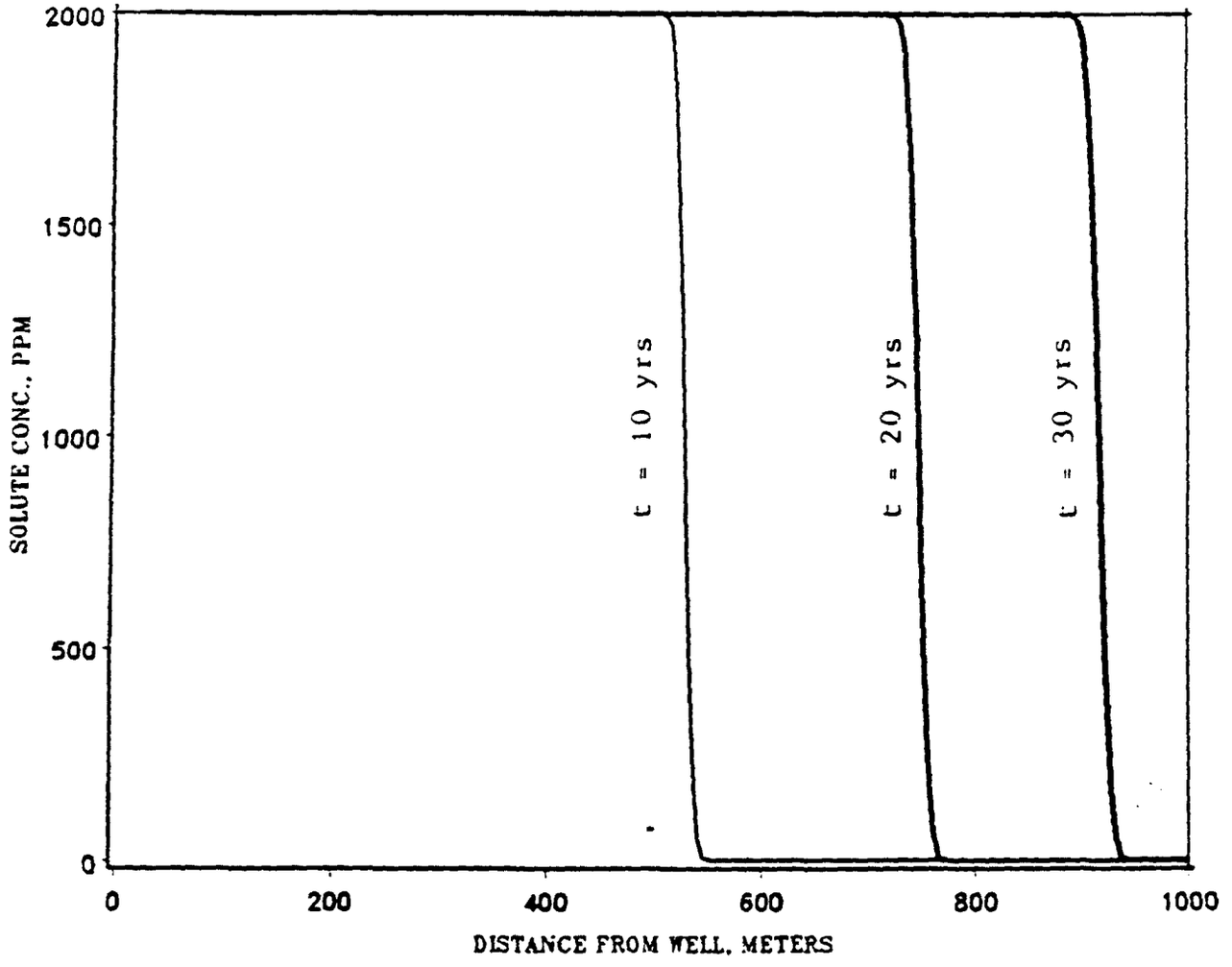

FIG 5 : SOLUTE MOVEMENT WITH YEARS OF INJECTION

TABLE I

SOLUTE CONCENTRATION PROFILE IN RADIAL CASE

r, m	Dispersivity, m		
	.1	1.0	10.0
2.5	100.00	100.00	100.00
3.0	100.00	100.00	100.00
3.5	100.00	100.00	100.00
4.0	100.00	100.00	100.00
4.5	100.00	100.00	100.00
5.0	100.00	100.00	100.00
5.5	100.00	100.00	100.00
6.0	100.00	100.00	100.00
6.5	100.00	100.00	100.00
7.0	100.00	100.00	100.00
7.5	100.00	100.00	100.00
8.0	100.00	100.00	100.00
8.5	100.00	100.00	100.00
9.0	100.00	100.00	100.00
9.5	100.00	100.00	100.00
10.0	100.00	100.00	100.00
10.5	100.00	100.00	100.00
11.0	100.00	100.00	100.00
11.5	100.00	100.00	100.00
12.0	100.00	100.00	100.00
12.5	100.00	100.00	100.00
13.0	100.00	100.00	100.00
13.5	100.00	100.00	100.00
14.0	100.00	100.00	100.00
14.5	100.00	100.00	100.00
15.0	100.00	100.00	100.00
15.5	100.00	100.00	100.00
16.0	100.00	100.00	100.00
16.5	100.00	100.00	100.00
17.0	100.00	100.00	100.00
17.5	100.00	100.00	100.00
18.0	100.00	100.00	100.00
18.5	100.00	100.00	100.00
19.0	100.00	100.00	100.00
19.5	100.00	100.00	100.00
20.0	100.00	100.00	100.00
20.5	100.00	100.00	100.00
21.0	100.00	100.00	100.00
21.5	100.00	100.00	100.00
22.0	100.00	100.00	100.00
22.5	100.00	100.00	100.00
23.0	100.00	100.00	100.00
23.5	100.00	100.00	100.00
24.0	100.00	100.00	100.00
24.5	100.00	100.00	100.00
25.0	100.00	100.00	100.00
25.5	100.00	100.00	100.00
26.0	100.00	100.00	100.00
26.5	100.00	100.00	100.00
27.0	100.00	100.00	100.00
27.5	100.00	100.00	100.00
28.0	100.00	100.00	100.00
28.5	100.00	100.00	100.00
29.0	100.00	100.00	100.00
29.5	100.00	100.00	100.00
30.0	100.00	100.00	100.00
30.5	100.00	100.00	100.00
31.0	100.00	100.00	100.00
31.5	100.00	100.00	100.00
32.0	100.00	100.00	100.00
32.5	100.00	100.00	100.00
33.0	100.00	100.00	100.00
33.5	100.00	100.00	100.00
34.0	100.00	100.00	100.00
34.5	100.00	100.00	100.00
35.0	100.00	100.00	100.00
35.5	100.00	100.00	100.00
36.0	100.00	100.00	100.00
36.5	100.00	100.00	100.00
37.0	100.00	100.00	100.00
37.5	100.00	100.00	100.00
38.0	100.00	100.00	100.00
38.5	100.00	100.00	100.00
39.0	100.00	100.00	100.00
39.5	100.00	100.00	100.00
40.0	100.00	100.00	100.00
40.5	100.00	100.00	100.00
41.0	100.00	100.00	100.00
41.5	100.00	100.00	100.00
42.0	100.00	100.00	100.00
42.5	100.00	100.00	100.00
43.0	100.00	100.00	100.00
43.5	100.00	100.00	100.00
44.0	100.00	100.00	100.00
44.5	100.00	100.00	100.00
45.0	100.00	100.00	100.00
45.5	100.00	100.00	100.00
46.0	100.00	100.00	100.00
46.5	100.00	100.00	100.00
47.0	100.00	100.00	100.00
47.5	100.00	100.00	100.00
48.0	100.00	100.00	100.00
48.5	100.00	100.00	100.00
49.0	100.00	100.00	100.00
49.5	100.00	100.00	100.00
50.0	100.00	100.00	100.00
50.5	100.00	100.00	100.00
51.0	100.00	100.00	100.00
51.5	100.00	100.00	100.00
52.0	100.00	100.00	100.00
52.5	100.00	100.00	100.00
53.0	100.00	100.00	100.00
53.5	100.00	100.00	100.00
54.0	100.00	100.00	100.00
54.5	100.00	100.00	100.00
55.0	100.00	100.00	100.00
55.5	100.00	100.00	100.00
56.0	100.00	100.00	100.00
56.5	100.00	100.00	100.00
57.0	100.00	100.00	100.00
57.5	100.00	100.00	100.00
58.0	100.00	100.00	100.00
58.5	100.00	100.00	100.00
59.0	100.00	100.00	100.00
59.5	100.00	100.00	100.00
60.0	100.00	100.00	100.00
60.5	100.00	100.00	100.00
61.0	100.00	100.00	100.00
61.5	100.00	100.00	100.00
62.0	100.00	100.00	100.00
62.5	100.00	100.00	100.00
63.0	100.00	100.00	100.00
63.5	100.00	100.00	100.00
64.0	100.00	100.00	100.00
64.5	100.00	100.00	100.00
65.0	100.00	100.00	100.00
65.5	100.00	100.00	100.00
66.0	100.00	100.00	100.00
66.5	100.00	100.00	100.00
67.0	100.00	100.00	100.00
67.5	100.00	100.00	100.00
68.0	100.00	100.00	100.00
68.5	100.00	100.00	100.00
69.0	100.00	100.00	100.00
69.5	100.00	100.00	100.00
70.0	100.00	100.00	100.00
70.5	100.00	100.00	100.00
71.0	100.00	100.00	100.00
71.5	100.00	100.00	100.00
72.0	100.00	100.00	100.00
72.5	100.00	100.00	100.00
73.0	100.00	100.00	100.00
73.5	100.00	100.00	100.00
74.0	100.00	100.00	100.00
74.5	100.00	100.00	100.00
75.0	100.00	100.00	100.00
75.5	100.00	100.00	100.00
76.0	100.00	100.00	100.00
76.5	100.00	100.00	100.00
77.0	100.00	100.00	100.00
77.5	100.00	100.00	100.00
78.0	100.00	100.00	100.00
78.5	100.00	100.00	100.00
79.0	100.00	100.00	100.00
79.5	100.00	100.00	100.00
80.0	100.00	100.00	100.00
80.5	100.00	100.00	100.00
81.0	100.00	100.00	100.00
81.5	100.00	100.00	100.00
82.0	100.00	100.00	100.00
82.5	100.00	100.00	100.00
83.0	100.00	100.00	100.00
83.5	100.00	100.00	100.00
84.0	100.00	100.00	100.00
84.5	100.00	100.00	100.00
85.0	100.00	100.00	100.00
85.5	100.00	100.00	100.00
86.0	100.00	100.00	100.00
86.5	100.00	100.00	100.00
87.0	100.00	100.00	100.00
87.5	100.00	100.00	100.00
88.0	100.00	100.00	100.00
88.5	100.00	100.00	100.00
89.0	100.00	100.00	100.00
89.5	100.00	100.00	100.00
90.0	100.00	100.00	100.00
90.5	100.00	100.00	100.00
91.0	100.00	100.00	100.00
91.5	100.00	100.00	100.00
92.0	100.00	100.00	100.00
92.5	100.00	100.00	100.00
93.0	100.00	100.00	100.00
93.5	100.00	100.00	100.00
94.0	100.00	100.00	100.00
94.5	100.00	100.00	100.00
95.0	100.00	100.00	100.00
95.5	100.00	100.00	100.00
96.0	100.00	100.00	100.00
96.5	100.00	100.00	100.00
97.0	100.00	100.00	100.00
97.5	100.00	100.00	100.00
98.0	100.00	100.00	100.00
98.5	100.00	100.00	100.00
99.0	100.00	100.00	100.00
99.5	100.00	100.00	100.00
100.0	100.00	100.00	100.00

*Solute conc. in ppm.

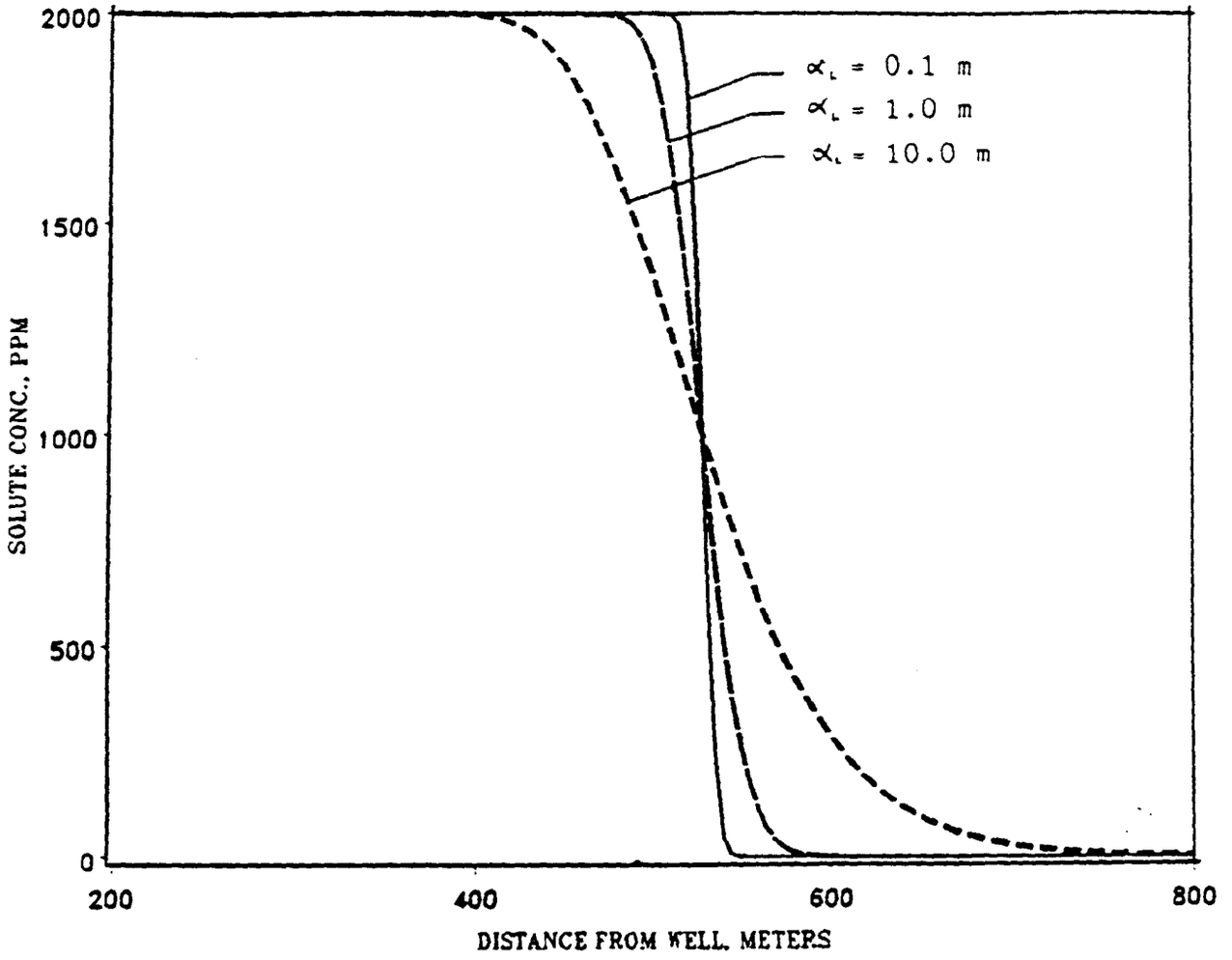

FIG 6 : EFFECT OF DISPERSION COEFFICIENT ON CONC. PROFILE

PROBLEM 3 - ADSORPTION (RETARDATION)

Introduction

In addition to the spread of injected waste due to dispersion there are other physical and modeling phenomena which impact our understanding of deep well disposal.

Chemical constituents in the waste can react in various ways with the rock fabric or with ions in the resident aquifer. Reactions may include precipitation and/or adsorption of waste components upon the inner surfaces of the pore space. There are many complex chemical reactions which accompany these general phenomena; it is not our purpose here to elaborate further, rather we wish to investigate the overall effects of these reactions in terms of the behavior of convective, dispersed fluid flow.

Background on Adsorption (Retardation)

In oilfield simulations the problems of dispersion and adsorption are associated with enhanced oil recovery (EOR) technology. One particular area of EOR concentrates on the lowering of interfacial tension between oil and water so that residual amounts of oil left behind in a waterflooding operation can be mobilized and recovered. In order to effect this mobilization small amounts of surfactant (soap) are injected to lower the interfacial tension between oil and water. Due

to the high cost of surfactant chemicals they are normally injected in small slugs and propelled by polymer thickened water injected after the surfactant slug is injected. In order to remain effective, the surfactant slug (normally 3-10% pore volume) must be maintained in a continuous unbroken band at the front of the polymer bank. This situation calls for a high degree of understanding regarding dispersion and/or adsorption because both phenomena cause deterioration of the surfactant band. Further complications, not addressed here, involve partitioning of the surfactants between the oleic and aqueous phases in this highly complex, multiphase problem.

Adsorption of many chemicals follow a Langmuir type isotherm. In some systems adsorption is purely physical and in other systems a chemical bond is actually formed. In many complex systems the adsorption type is not known so it is referred to as physico-chemical adsorption. In general, the concentration of the adsorbing species in the flowing solution is higher than its concentration on the surface of the "rock." "Rock," as we refer to it here, is the conglomeration of feldspars, cements, clays, minerals, quartz (sand grains) and others that constitute the rock fabric. In and of itself, clay is a generic term since many types exist; montmorillonite, illite, kaolinite, and chlorite are the major types. Due to the platelet type structure of clay the surface area of the rock fabric can be greatly extended by a small (5-10%) percent by weight of clay being present. The surface area of the rock is of major importance since adsorption generally occurs as a molecular monolayer of species on the available surface.

With pure substances the surface area is known; i.e. in laboratory experiments pure substances are often utilized in investigating adsorption. Figure 1 provides such an example; this figure is the adsorption isotherm for cetyltrimethyl ammonium bromide (CTAB) on tricalciumphosphate and calcium carbonate. Note that the adsorption density is expressed in micromoles per square meter of surface area. The independent variable is the equilibrium concentration in solution, millimoles per liter. This isotherm is typical of the Langmuir shape; however since in most natural rock systems we do not know the surface area for the adsorbate we express the adsorption density as milligrams per gram of rock or in lbm of adsorbate per lbm rock.

Further examination of Figure 1 reveals another important characteristic of adsorption; a constant amount of adsorbate is reached at relatively low concentrations in solution and does not increase at higher solution concentrations. Reasoning for this phenomena suggests that a monolayer occupies the available surface area at low concentrations and there is no more room available for additional adsorption even though there is plenty of material in solution to be adsorbed. This equilibrium is established very quickly in terms of the rate-of-reaction as well. For purposes of modeling we may assume that in many cases the adsorption reaction is instantaneous when compared to the time required for bulk flow to move even a microscopic distance. Because the reaction is fast and the adsorption density is constant the frontal advance of waste will be slowed down, and we may refer to adsorption as a retardation of the advancing waste front. Additional discussion of adsorption/retardation may be found in Narasimhn(198?).

The Model

A linear strip similar to the one used in Problem #2, Figure 1, was again utilized as a basis for demonstrating retardation. These effects are present in two-dimensional and three-dimensional space as well; however, the behavioral effects are much easier to identify and quantify in a one-dimensional problem. In these simulations the strip is 2000 ft. long with the number of x-direction grid blocks equal to 200 with delta-x equal to 10 ft. The cross section is 50 ft. (Δy) by 10 ft. (Δz). The porosity is 0.20 and the permeability is 250 md. The rate of injected waste is 50 Bbl/day (2.8075 ft/day). Three cases were simulated; 1) a case with dispersivity equal to 5.0 ft., 2) a case with retardation of waste equal to 6.7×10^{-6} lbm waste/lbm rock, and 3) a case exhibiting the dispersion and retardation of cases 1) and 2).

Example of Adsorption (Retardation)

If we repeat the experience of Problem #2 and position ourselves at the end of the 2000 ft. slab of reservoir and observe the concentration of dispersed waste emerging. We observe the familiar 'S' shaped curve shown in Figure 2. (Recall that the plug flow case with no dispersion would be illustrated as a vertical line for C/C_0 at exactly one pore volume on Figure 2). The specific curve is the one represented by small triangles labeled "dispersed." The flow rate here is 2.807 ft/day and the waste front emerges at 0.775 pore volume; before

one pore volume has been injected. The curve has a long "tail" due to dispersion and passes through C/C_o = 0.5 at one pore volume injected as we learned to expect from the error function analytic solution in Problem #2.

The curve represented by small circles is labeled "retarded" because a constant adsorption density of 6.7×10^{-6} lbm waste/lbm rock (0.0067 mgm/gm) has been invoked in the simulator. The third curve, represented by asterisks (*), is labeled "retarded and dispersed" and has the same retardation level and in addition has a physical dispersivity of 5.0 ft. in the model. Since the model utilized is a finite difference model there is also some numerical dispersion involved. It is important to note two distinct features of the "retarded" and the "retarded and dispersed" curves; 1) the fronts are quite sharp, and 2) the fronts are delayed, hence "retarded" in terms of their emergence from the reservoir strip. Both features are earmarks of adsorption.

Figure 3 will provide some additional insight. We are now observing the concentration profile on bulk flow as it appears along the length of the strip. Again, note the reverse 'S' shaped curve for dispersion with no retardation. The concentration profile as "seen" by the rock when adsorption is operative is sharpened because the advancing "toe" of this reverse 'S' shaped dispersion curve is clipped off since it is exposed to fresh rock first, and the "fresh" rock has no species adsorbed on it yet. The overall effect, whether or not dispersion is operative, is to satisfy the adsorption requirement, thus sharpening

the fronts as seen in Figure 3. Remember that Figure 3 is a snapshot along the core at one specific time while Figure 2 is a snapshot at distance x/L = 1.0 for all time.

One other comment may be useful. Once $C/C_0 = 1.0$ all along the strip, i.e. in this case after 1.25 pore volumes have been injected, one can theoretically determine the amount adsorbed on the rock which the waste has passed through simply by integrating the difference between the "dispersed" curve and the "dispersed and retarded" curve in Figure 2. This difference is the sum over pore volume injected from 0.775 to 1.25 of $(C/C_0) \times t$. When multiplied by the injected concentration C_0 the amount adsorbed will have the units of the injected waste. By dividing by the weight of the rock the adsorption density (retardation level) can be computed.

Additional Comment

The retardation problems were simulated using CFTE, SSI's Chemical Flood, Ternary Equilibrium, simulator. CFTE is a finite-difference simulator and suffers from numerical dispersion. The reason that this simulator was chosen is that it accurately calculates adsorption for losses of injected surfactant in oilfield EOR problems or any other contaminant for which a graphical representation of adsorption can be described.

In order to investigate the effect of additional numerical dispersion imbedded in this problem we resort to the method of anlaysis included in Perkins and Johnston(1963). When graphed on arithmetic probability paper the error function solution to miscible displacement becomes a straight line over the interval of $0.10 < C/C_o < 0.90$. A variable, , is defined as:

$$\lambda = \frac{V/V_p - 1.0}{\sqrt{V/V_p}}$$

where

V = volume of fluid injected,

V_p = pore volume of linear core,

V/V_p = number of pore volumes injected.

From Figure 2 (from the "dispersed" curve, represented by triangles):

$$\lambda_{10} = (0.884 - 1.0)/\sqrt{0.884} = -0.12338$$

and $\lambda_{90} = (1.12 - 1.0)/\sqrt{1.12} = +0.11339$

where the subscripts 10, 90 refer to the percent injected fluid in the effluent.

The dispersion, D_ℓ^*, from this analysis is defined as:

$$D_\ell^* = UL\,[(\lambda_{90} - \lambda_{10})/3.625]^2$$

where

U = Darcy velocity, ft/day

L = length of core, ft

Substituting λ_{90}, λ_{10} from above and performing the indicated mathematics;

$$D_{\ell}^{*} = UL\ (0.004266)$$

We also know that $D_{\ell}^{*} = \alpha_L (U/\phi)$ and $U = (U/\phi)\phi$. So

$$\alpha_L = L(.004266) = 2000\ (.004266)$$
$$= 8.532 \text{ ft}$$

At constant velocity, numerical and physical dispersion are additive, so $\alpha_{Lnum} = \alpha_{LTOT} - \alpha_{Lphysical}$ or in this problem $\alpha_{Lnum} = 8.532 - 5.0 = 3.532$ ft.

REFERENCES

Narasimhan, T. N., "Recent Trends in Hydrogeology," Special Paper 189 by The Geological Society of America. See especially the chapter "Contaminant Migration in Saturated Unconsolidated Geologic Deposits" by Robert W. Gillham and John A. Cherry.

Shah, D. O., and Scheeter, R. S., Improved Oil Recovery by Surfactant and Polymer Flooding, Academic Press, 1977.

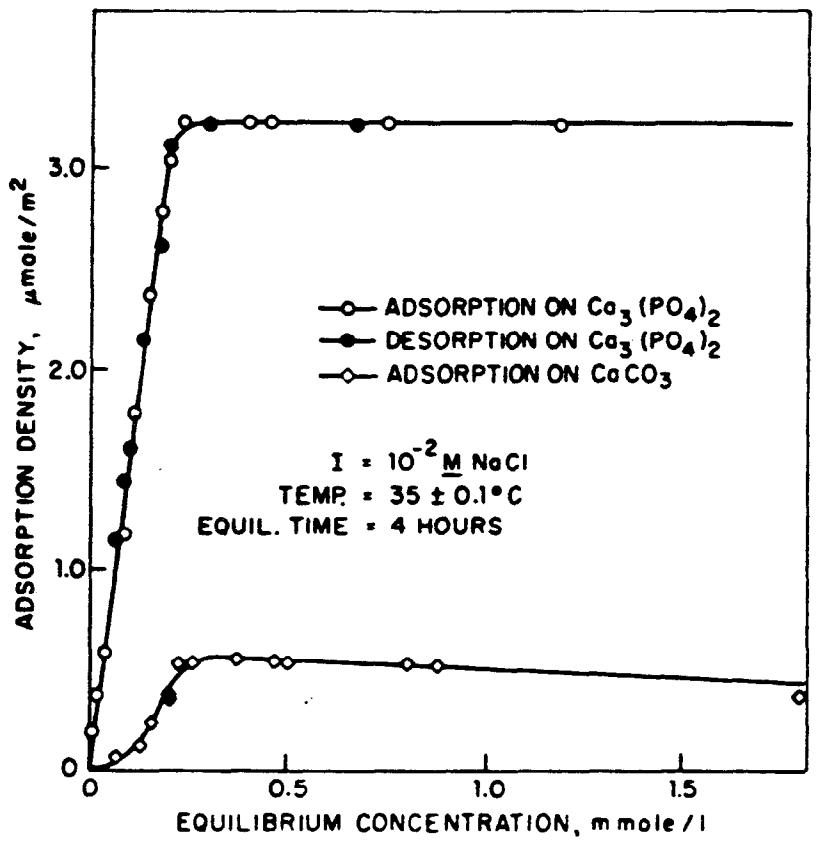

Adsorption isotherm of cetyltrimethylammonium bromide (CTAB) on tricalciumphosphate and calcium carbonate

after Shah and Schechter(1977)

FIGURE 1 ADSORPTION ISOTHERM

FIGURE 2 Frontal Retardation

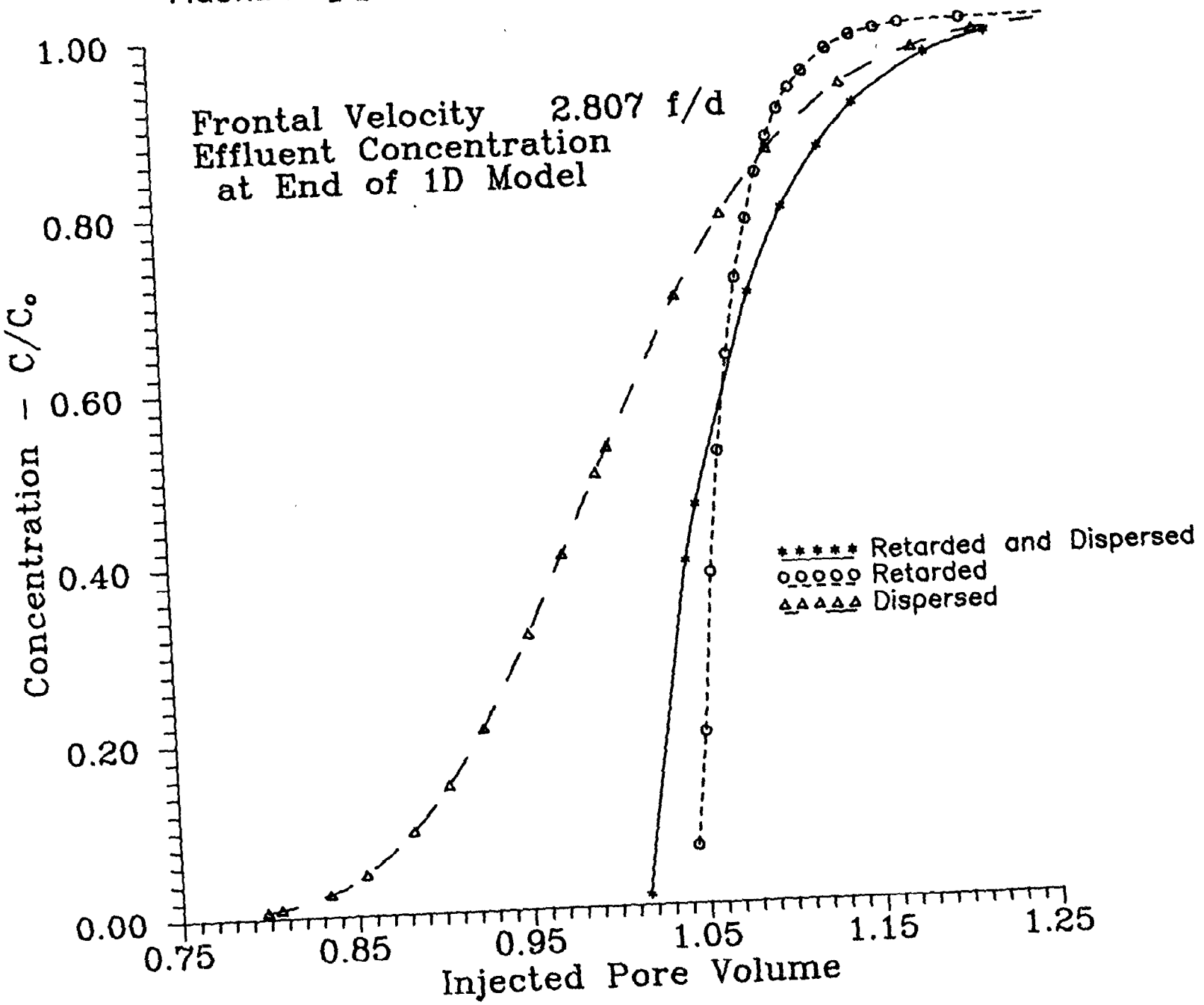

FIGURE 3 Concentration Profile Along 1D Model

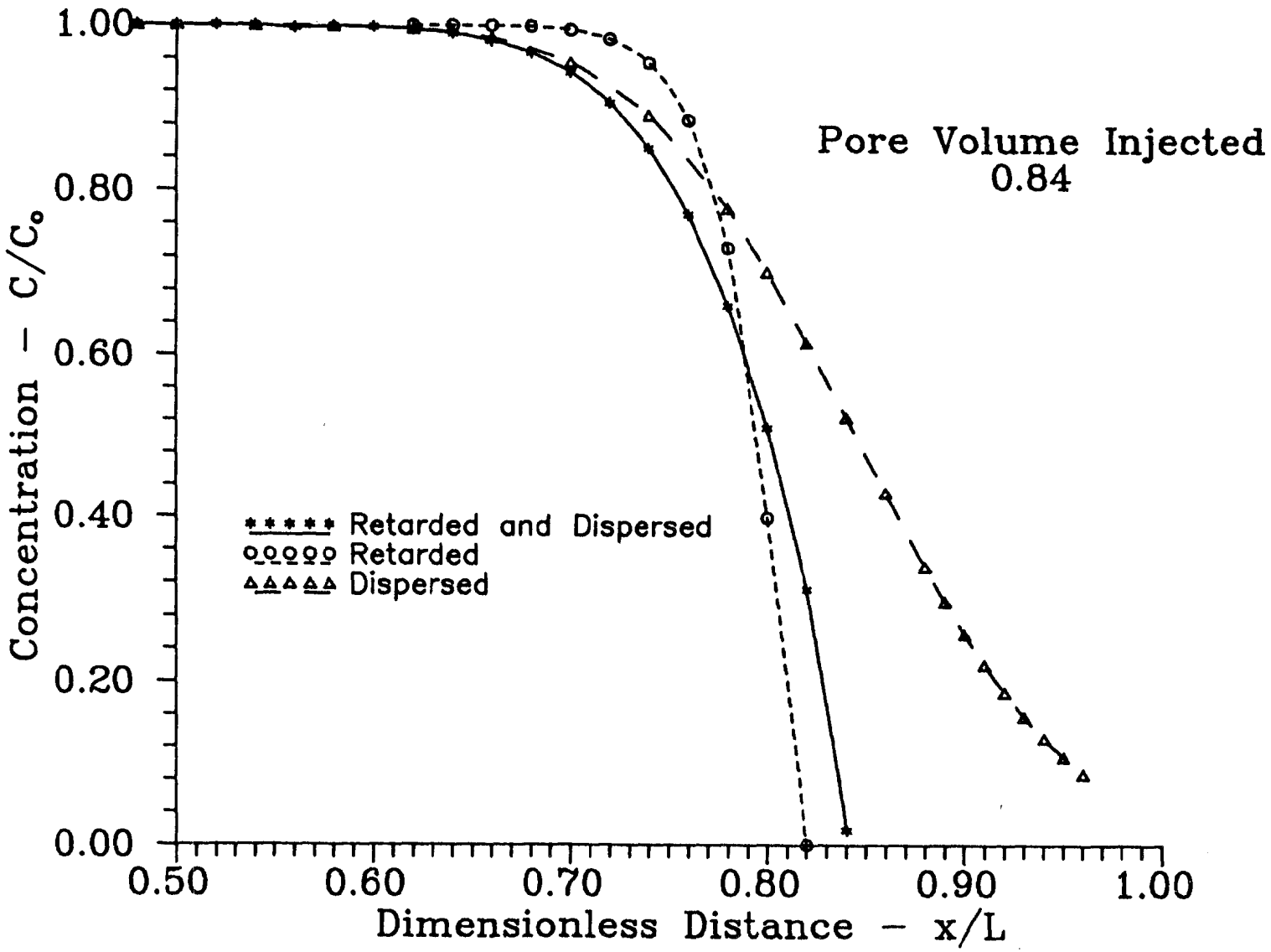

PROBLEM 4 - WELL TESTING EXAMPLES

Introduction

As required by Federal Register, Vol. 52 No. 166, dated August 27, 1987, injection and pressure fall-off testing will be required for all waste disposal wells. The main objectives of well testing will be the monitoring of reservoir injection pressure and the associated reservoir behavior as a result of fluid injection. This report defines and discusses six simulated well test problems which will be used for reference and comparison with actual well tests submitted to the EPA.

Any reservoir can be classified into three main types:

1. Homogeneous
2. Double Porosity
3. Double Permeability

The basic reservoir systems are illustrated in Figure 1-A.

Reservoir type along with the inner and outer boundary conditions control pressure response during a well test. The inner boundary conditions are classified by:

1. Wellbore Storage
2. Skin
3. Fractures
4. Partial Penetration

The outer boundary conditions are classified by:

1. No-Flow Boundary
2. Constant Pressure Boundary

The reservoir model must be determined before a valid analysis of any well test can be performed, Earlougher(1977). The reservoir model applicable to a particular well test can be determined by examining a diagnostic plot of pressure response as a function of test time, Gringarten(1986). A very effective diagnostic plot is defined by a log-log representation of dimensionless pressure(p_D) versus dimensionless time (t_D) in addition to derivative of p_D versus t_D, where p_D and t_D are defined as follows:

$$p_D = \frac{kh}{141.2\ qB\mu}\ \Delta p \tag{1}$$

Where:

$$\Delta p = \frac{p_D}{p_m} \tag{2}$$

$$t_D = \frac{0.000264k}{\phi \mu c_t r_w^2}\ \Delta t \tag{3}$$

Where:

$$\Delta t = \frac{(t_D/C_D)}{t_m} \tag{4}$$

The parameters t_m and p_m are defined as the time match and the pressure match respectively and are constant values that are used to force the well test data to match the generated type curve plotted on the diagnostic plot. The pressure match(p_m) is used to calculate the reservoir conductivity(kh) and the time match(t_m) is used to calculate wellbore storage and skin.

The examination of the derivative is a very effective method of determining reservoir type along with the applicable boundary conditions. The only disadvantage of using the derivative to analyze reservoir geometry is the amount of tedious calculation necessary to generate the plot. It is therefore imperative that a computer be employed to make such calculations based on the well test data; Gringarten(1986).

Description and Discussion of Example Well Tests

Six well tests were simulated using INTERPRET, a licensed product of Scientific Software Intercomp (SSI). The well test simulations were created by varying reservoir geometry of a base case. Simulated well tests 1-5 were based on homogeneous reservoir behavior and well test six was based on dual-porosity reservoir behavior.

Two plots were generated for each simulation; the diagnostic type curve plot and a standard Horner plot corrected for multi-rate injection data (Superposition); Matthews and Russell(1967). The Horner plot was appended as it will probably be the most common type of plot

submitted to the EPA. For a single injection rate followed by a single shut-in (fall-off) the superposition rate function is defined by:

$$S\ R\ F = q_{inj} \cdot \log \frac{T_{inj} - \Delta t}{\Delta t} \qquad (5)$$

Where:

S R F = Superposition Rate Function(bbls/day)

q_{inj} = Injection Rate(bbls/day)

T_{inj} = Total Time of Injection(hrs)

Δt = Shut-in Time(hrs)

EXAMPLE WELL TEST 1

Example well test 1, the base case, assumed an infinite acting reservoir which precludes the presence of an outer boundary. The inner boundary conditions included wellbore storage and skin. The values of the input variables that were used to simulate the well test are as follows:

Reservoir Pressure(p)	=	3752 psig
Reservoir Thickness(h)	=	15 ft
Effective Permeability(k)	=	46 md
Skin Factor(S)	=	1.0
Wellbore Storage(C_D)	=	940
Injection rate(q_{inj})	=	700 bbls/day

Porosity(ϕ)	=	0.20
Wellbore Radius(r_w)	=	0.458 ft
Total Compressibility(c_t)	=	1.0x10-4 1/psi
Fluid Viscosity(μ)	=	0.50 cp
Time Match(t_m)	=	41
Pressure Match(p_m)	=	0.014

These input variables were held constant for all well tests. The examples to follow were generated by adding various outer boundary conditions to the base case.

Figures 1 and 1-H, the diagnostic and Horner plot respectively, were generated based on the well test simulation of the base case. The points on the plot are measured pressures based on the simulation, and the solid line is the type curve based on the assumed reservoir model. The measured pressure points and the type curve match perfectly because the type curve was used to generate the well test data.

Referring to Figure 1 wellbore storage and skin effects terminate at point "A". Wellbore storage effects can be easily identified on the diagnostic plot because the measured pressure points must track the unit slope line. The well test reaches the infinite acting period at point "B" which is near the end of the test. The fall-off period was 12 hours which can be calculated by dividing the last measured T_D/C_D value of 500 by the time match of 41.0.:

$$\Delta t = (t_D/C_D)/t_m \tag{6}$$

It should be noted that if this were an actual well test the fall-off test duration should have been extended to not only verify the infinite acting period but to also determine outer boundaries if present. The necessary test time as a function of radius of investigation is defined by:

$$\Delta t = \frac{1192\ r_D^2 \phi \mu c_t}{k} \tag{7a}$$

Where:

t	=	Fall-off Test Duration	(hours)
r_D	=	Radius of Investigation	(ft)
ϕ	=	Formation Porosity	(fraction)
μ	=	Fluid Viscosity	(cp)
c_t	=	Total System Compressibility	(1/psi)
k	=	Effective Permeability	(md)

The Horner plot (Fig. 1-H) illustrates the effects of wellbore storage and skin at early times. The pressure points become linear at later shut in times as theory dictates. The straight line portion of the Horner plot at later times can be used to determine the effective kh if outer boundary effects are not present. The lack or presence of outer boundaries can be verified by examining the derivative on the diagnostic plot. Since this is a simulation of an infinite acting reservoir the straight line of the Horner plot can be extrapolated to

average the reservoir pressure of 3752 psig at a superposition value of zero which is equivalent to an infinite shut-in time.

EXAMPLE WELL TEST 2

Simulated well test number 2 is identical to the base case with the addition of a sealing fault located 600 ft from the wellbore. The effects of the fault can be seen on Figure 2 by examining the derivative starting at point "A". The derivative begins to stabilize to a p_D value of 0.50 but then the effects of the sealing fault begin to affect the pressure response. The derivative starts to increase and stabilizes to a new level of 1.0, twice the original stabilization level. The diagnostic plot is very useful in determining sealing barriers such as intersecting fault planes.

The same phenomenon can be seen on the Horner plot (Fig. 2-H) as a change in slope at point "B". The slope of the Horner plot after the pressure response of the fault has been fully developed will be exactly twice the slope of pressure response of the infinite acting period, Earlougher(1980). The intersection of these two straight lines may be used to calculate the distance of the fault to the wellbore by using the following equation:

$$L = 0.01217 \frac{k \Delta t_x}{\phi \mu c_t} \qquad (7)$$

Where:

L = Distance to the fault line (ft)

Δt_x = Test time at the intersection of the two straight line extrapolations

The value of the superposition rate function at the intersection of the two straight lines is 370 bbls/day. Using the injection rate of 700 bbls/day and an injection time of 200 hours the test time(Δt_x) was calculated to be 84 hours by rearranging Equation 5. Using Equation 7, the distance to the fault line was calculated to be 590 ft which agrees closely to the simulated model input of 600 ft. Equation 7 would not be used to calculate the distance to the fault when interactive computer modelling is used to match test data, as the fault distance is an input variable to the reservoir model type curve. The distance to the fault is varied by trial and error to effect a match of measured pressure data.

The reservoir conductivity (kh) is obtained from the slope of the infinite acting period (Line 1) and the average reservoir pressure is obtained from the extrapolation of Line 2 after the effects of the fault have been fully developed which is determined from the diagnostic plot.

EXAMPLE WELL TEST 3

A fracture intersecting the wellbore was added to the base case to simulate well test number 3. This is very important case to consider

for an injection well. The near wellbore area will be artificially fractured if the injection pressure exceeds the fracture gradient of the reservoir therefore the containment of injected fluids is not guaranteed.

Fracture gradients vary widely depending on reservoir type, sedimentary process and post tectonic upheavals. Typical fracture gradients can be as low as 0.70 psi/ft and as high as 0.90 psi/ft. There are correlations for calculating the fracture gradient for a continuous sedimentary basin such as the Gulf Coast region. These correlations do not apply to older areas where severe folding and faulting may have lowered the fracture gradient substantially. One method of determining the fracture gradient for a particular area is to perform a leak-off test. The leak-off test is performed by pumping fluid, in increments, into the reservoir and plotting the pressure increase versus volume of fluid pumped. As fluid is pumped the surface pressure will increase until the threshold pressure of the formation is reached; at which time an instantaneous pressure drop will be observed. The decrease in pressure is due to having created a "mini-fracture" in the formation. The pressure will then stabilize to a pump in pressure for a given injection rate. Drilling mud must be used to perform the leak-off test to maintain a filter cake while pumping.

The injection pressure is a function of both injection rate and average reservoir pressure. Since injection pressure is a function of

rate all well testing should be performed at the highest injection rate expected during the life of the disposal project. Once a maximum injection rate has been established the rate should not be exceeded without further well testing to verify that fractures are not being propagated.

Figures 3 and 3-H illustrate the simulated well test 3. At early times the slope of the diagnostic curve is 1/2 which is characteristic of linear or channel flow . The derivative stabilizes very quickly, indicating that infinite acting period has been reached after only 15 minutes of shut in time. Referring to the Horner plot (Fig. 3-H) the straight line and slope of the curve is again defined at a very early shut in time. The 1/2 slope of the diagnostic plot and the early stabilization make the fractured model case easily recognizable. Analysis of the pressure reponse for kh is valid only after fracture reponse has dissipated. Again, the proper region to be used to analyze kh can be obtained from the derivative plotted on the diagnostic plot. The derivative must be stabilized to a value of 0.50 for the analysis to be valid.

EXAMPLE WELL TEST 4

This example was based on an injection test rather than a fall-off test. The injection rate was 700 BOPD for a period of 240 hours. External boundaries are defined better during flow testing. Well test example 4 was simulated based on a closed 160 acre square drainage

area with the well placed in the center of the square. The diagnostic plot (Fig. 4) traces the type curve for the infinite acting case until the external boundaries are felt. Had the test been terminated at 3 hours(T_D/C_D=123) the pressure point match would have indicated a typical infinite acting homogeneous reservoir. The pressure change and derivative of the pressure change will increase indefinitely once the pressure boundaries start to influence the pressure response at the well. This pressure response is analogous to the early time wellbore storage effects and is dependent on fluid compressibility. The derivative of pressure response caused by the single sealing fault (Example 2) will stabilize at a level exactly double that of the infinite acting period; therefore these two cases cannot be confused, unless the test time is too short to verify the second stabilization level.

The average reservoir pressure for this case is indirectly related to the extrapolated pressure obtained from the Horner plot (Fig. 4-H). The actual average reservoir pressure can be estimated by adjusting the extrapolated Horner pressure based on the shape of drainage area and the wellbore's orientation inside the drainage area; Matthews (1967). The total drainage area of a closed system can be estimated by type curve matching the diagnostic plot, but the shape of the drainage area is very difficult to determine. Since the shape of a closed drainage area and orientation to the wellbore is usually unknown, the actual average reservoir pressure is also unknown.

Since waste disposal products and the in situ fluids in deep water aquifers have low compressibilities caution should be taken when injecting into a closed system. The injection pressures should be monitored very closely so as not to fracture the formation around the wellbore. Should the well be artificially fractured the resulting well test will be similar to example 3.

EXAMPLE WELL TEST 5

Well test example 5 was simulated based on a partially closed 320 acre rectangular drainage area. Again, the pressure analysis was based on an injection test. The well was located 530 ft from the nearest sealing boundary and 4750 ft from a constant pressure boundary. The diagnostic plot traces the type curve for the infinite acting case until the pressure response of the nearest sealing boundary is observed. Again, had the test been terminated prematurely, the pressure point match would have indicated a typical infinite acting homogeneous reservoir.

The first sealing boundary becomes evident after 20 hours of testing time (T_D/C_D=820). The constant pressure boundary, which is indicated by a turn down of the derivative, is observed after 100 days of testing time. Constant pressure boundaries will not be observed on standard well tests because of the extremely long test times required to observe the required pressure behavior.

EXAMPLE WELL TEST 6

The last well testing example is based on a dual-porosity reservoir model with wellbore storage and skin. A dual-porosity reservoir consists of two porous media regions: primary and secondary porosity. The secondary porosity is considered to be uniformly distributed throughout the primary porosity. Primary porosity is the matrix rock whose properties are controlled by sedimentary processes and post-depositional lithification. Secondary porosity, the fracture network, is usually believed to have been developed subsequent to the primary porosity as a result of mechanical deformation, solution or dolomitization of the original matrix. Fluids injected into the formation will be taken by the secondary porosity fractures and ultimately distributed to the primary rock matrix at some distance from the wellbore.

Dual-porosity reservoirs can be defined by using two dimensionless terms; Matthews(1967) and Gringarten(1984):

$$\omega = \text{storativity ratio} = \frac{(\phi c_t)_f}{(\phi c_t)_f + (\phi c_t)_m} \tag{8}$$

$$\lambda = \text{interporosity flow coefficient} = \alpha r_w^2 \frac{k_m}{k_f} \tag{9}$$

Where:

m subscript denotes the rock matrix properties

f subscript denotes the fracture properties

The simulated test for example 6 was based on a storativity ratio(ω) of 0.01 and a interporosity flow coefficient(λ) of $1x10^{-7}$. Figures 6 and 6-H illustrate the pressure response of a dual-porosity reservoir. The entire reservoir system stabilized after 100 days of shut in time (t_D/C_D=106). There will be two straight line regions on the Horner plot, one for the secondary porosity response and one for the total system response. The slope of these two lines will be identical which distinguishes this response from a no-flow boundary case where the slope of the final straight line is double that of the slope in the infinite acting period. Either staight line portion can be anayzed for kh.

DATA COLLECTION

As previously discussed the pressure points were generated from simulation of a given type curve which means the pressure points will overlay the type curve perfectly. Field data obtained from well testing will always have a degree of scatter which will make the analysis of the diagnostic curve much more difficult.

INJECTION RATE INFORMATION

The well test examples were based on one constant injection rate just prior to shutting in the well. Injection rates prior to actual well tests will not be a continuous constant value. Variable injection rates and shut down periods can be easily accounted for assuming the

rate information is available for analysis. It is imperative that all injection rate data including shut down periods be recorded and submitted with the well test analysis.

PRESSURE TRANSIENT INFORMATION

The well test simulated were analyzed using a diagnostic type curve which involves calculating the time rate of change of the pressure response. A sufficient amount of high quality pressure data is necessary to assure a proper examination of the derivative of the pressure response.

The pressure gauges used to perform well tests must be of very high quality, maintained, and used properly to assure the pressure information is usable. Electronic strain gauge equipment is recommended for this application.

REFERENCES

Earlougher, R.C.: "Advances in Well Test Analysis", SPE Monograph Series, SPE, Dallas, 1977.

Earlougher, R.C.: "Practicalities of Detecting Faults from Buildup Testing", JPT Forum JPT, January, 1980.

Gringarten, A.C.: "Interpretation of Tests in Fissured and Multilayered Reservoirs with Double-Porosity Behavior: Theory and Practice", JPT - Distinguished Author Series, April, 1984.

Gringarten, A.C.: "Computer-Aided Well Test Analysis", SPE paper 14099 Presented at the 1986 International Meeting on Petroleum Engineering, Beijing China, March 17, 1986.

Matthews, C.S. and Russell, D.G.: "Pressure Buildup and Flow Tests in Wells" - Chapter 4, SPE Monograph Series, SPE, Dallas, 1967

Matthews, C.S. and Russell, D.G.: "Pressure Buildup and Flow Tests in Wells" - Chapter 6, SPE Monograph Series, SPE, Dallas, 1967

Matthews, C.S. and Russell, D.G.: "Pressure Buildup and Flow Tests in Wells" - Chapter 10, SPE Monograph Series, SPE, Dallas, 1967

Figure 1

Radial Solution with Wellbore Storage and Skin
Infinite Acting Reservoir

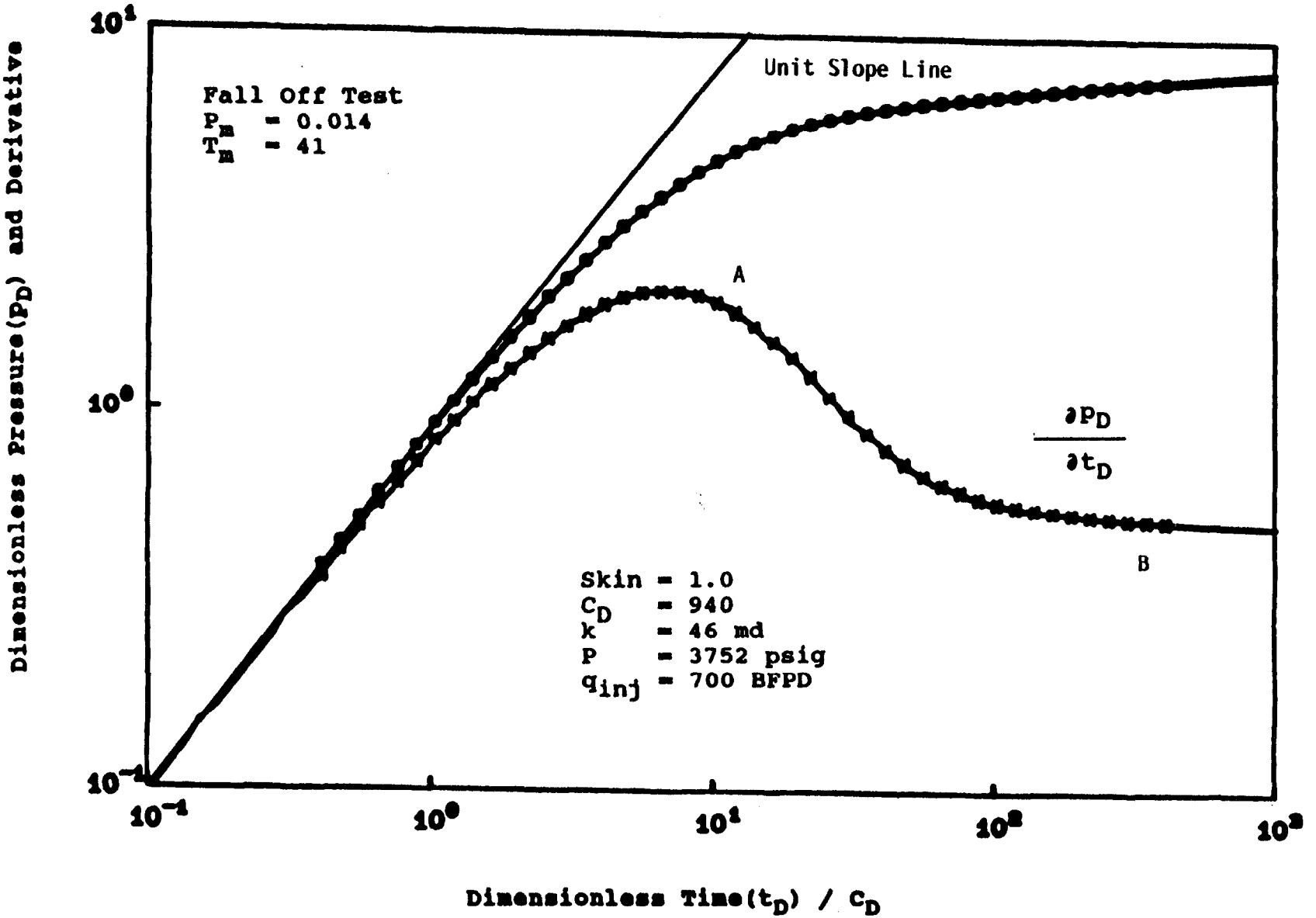

Figure 1-A

Basic Reservoir Systems

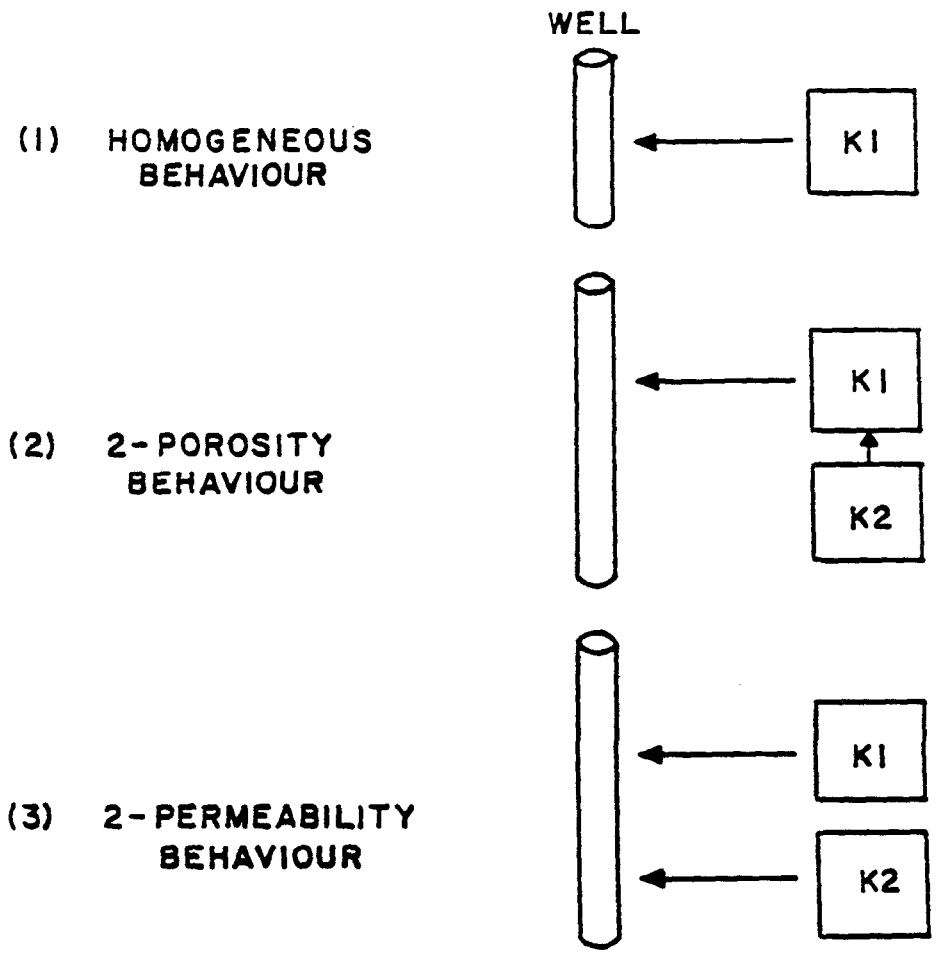

INNER BOUNDARY	RESERVOIR BEHAVIOUR	OUTER BOUNDARY
WELLBORE STORAGE SKIN FRACTURES PARTIAL PENETRATION	HOMOGENEOUS DOUBLE POROSITY DOUBLE PERMEABILITY	SPECIFIED FLOW SPECIFIED PRESSURE

Figure 1-H

Associated Horner Plot

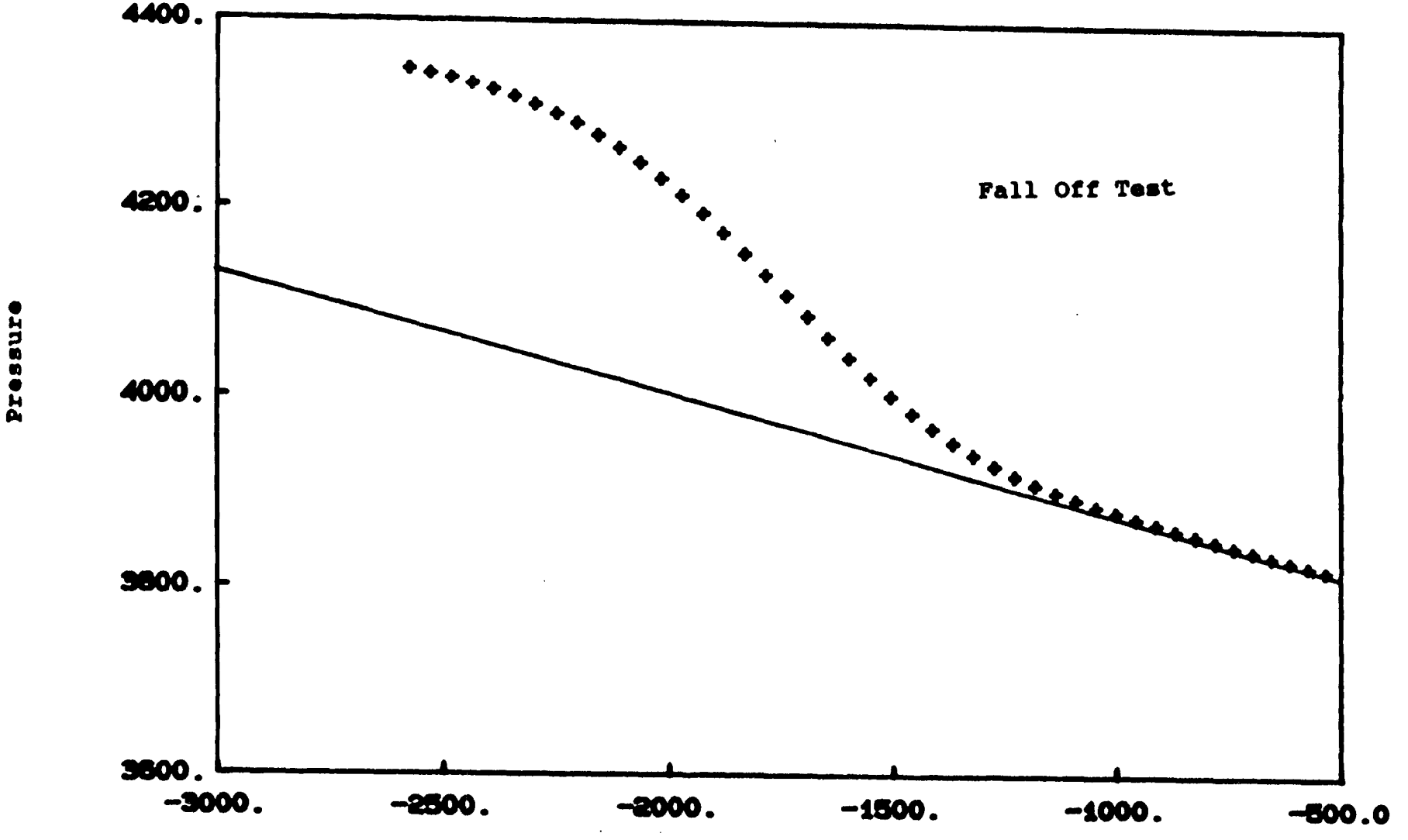

Figure 2

Radial Solution with Wellbore Storage and Skin
Infinite Acting Reservoir with Sealing Fault

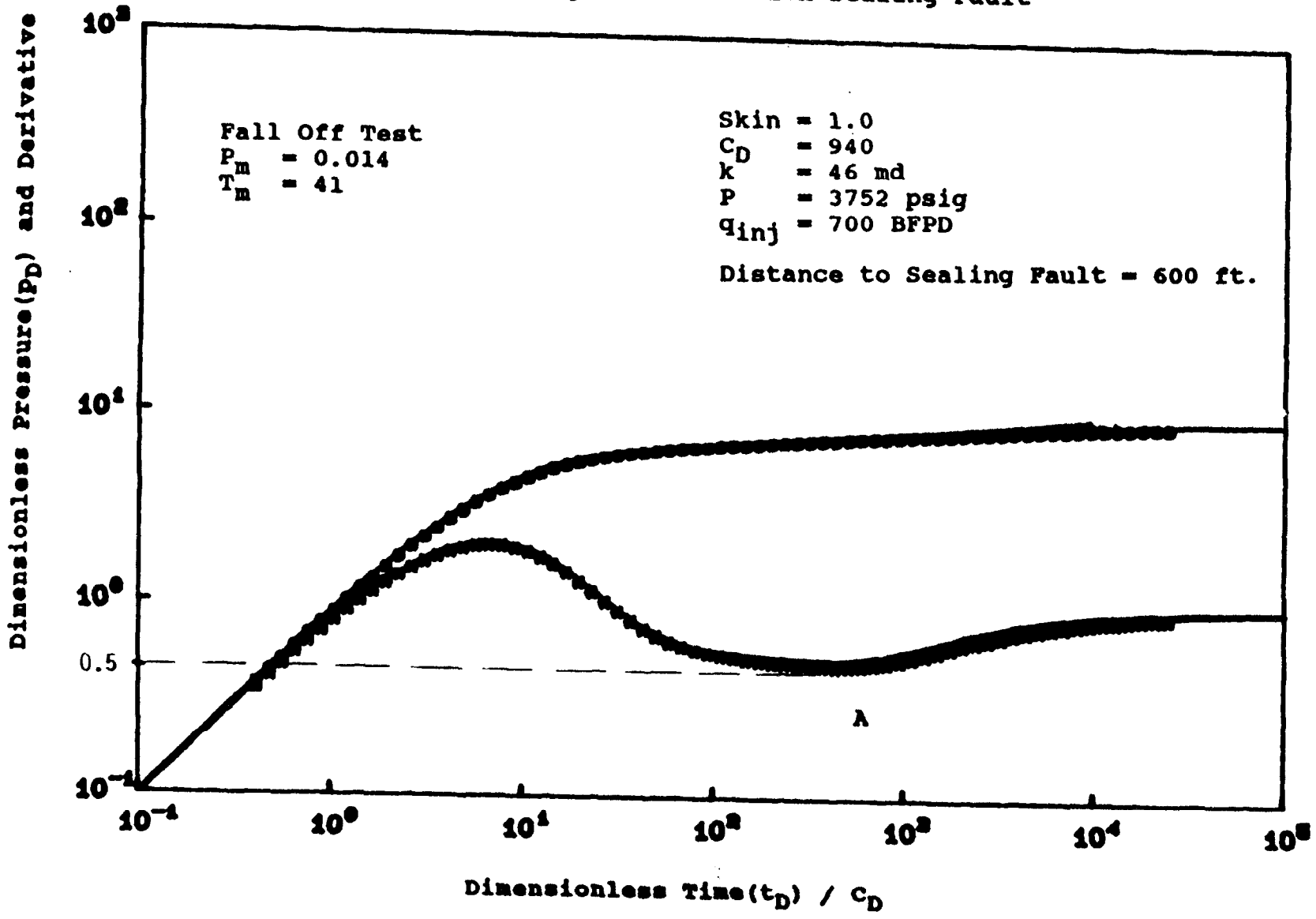

Figure 2-H

Associated Horner Plot

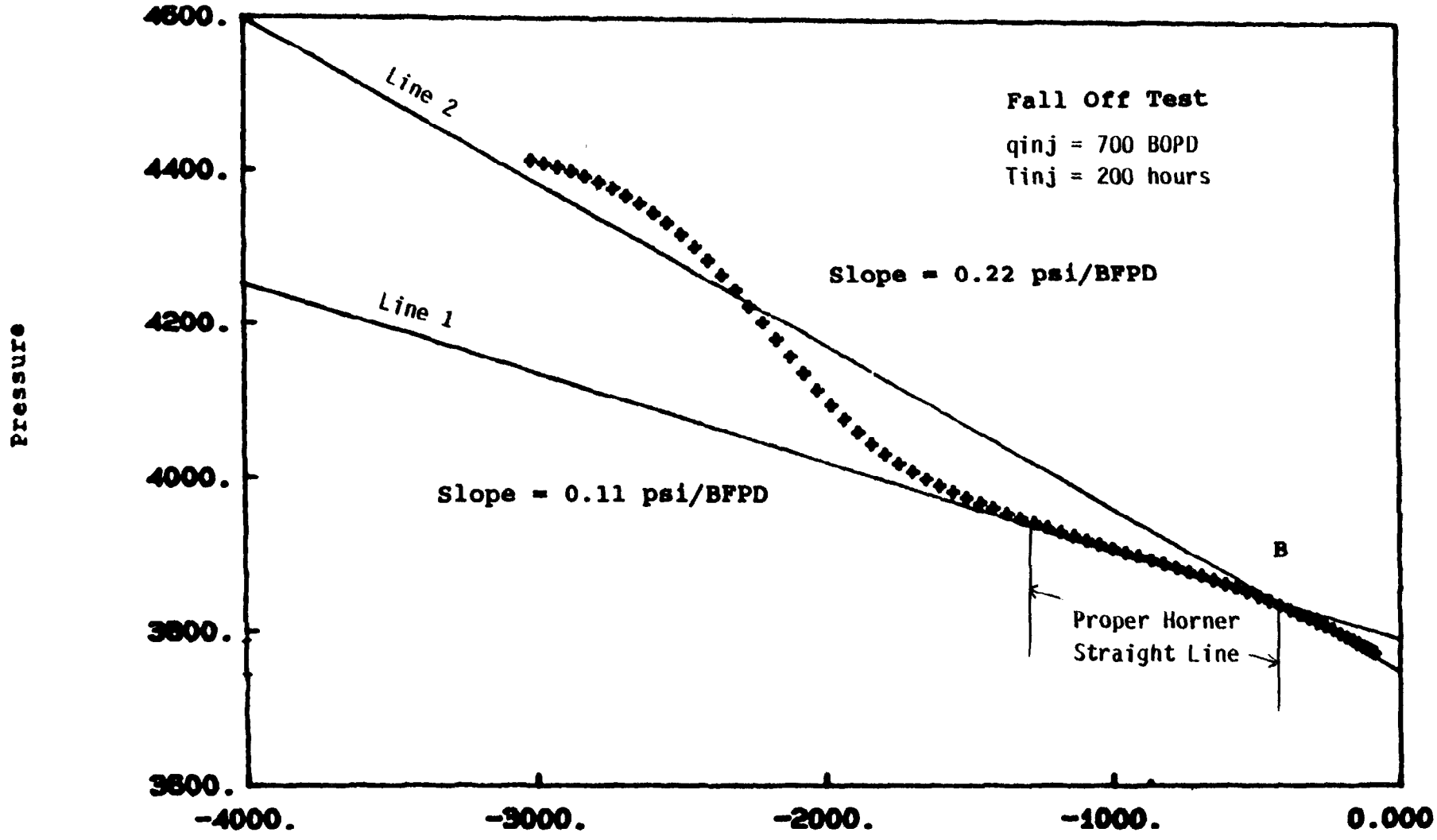

$$q_{inj} \cdot \log\left(\frac{T_{inj-\Delta t}}{\Delta t}\right)$$

Figure 3

Radial Solution with Wellbore Storage and Skin
Infinite Conductivity Fracture
Intersecting the Wellbore

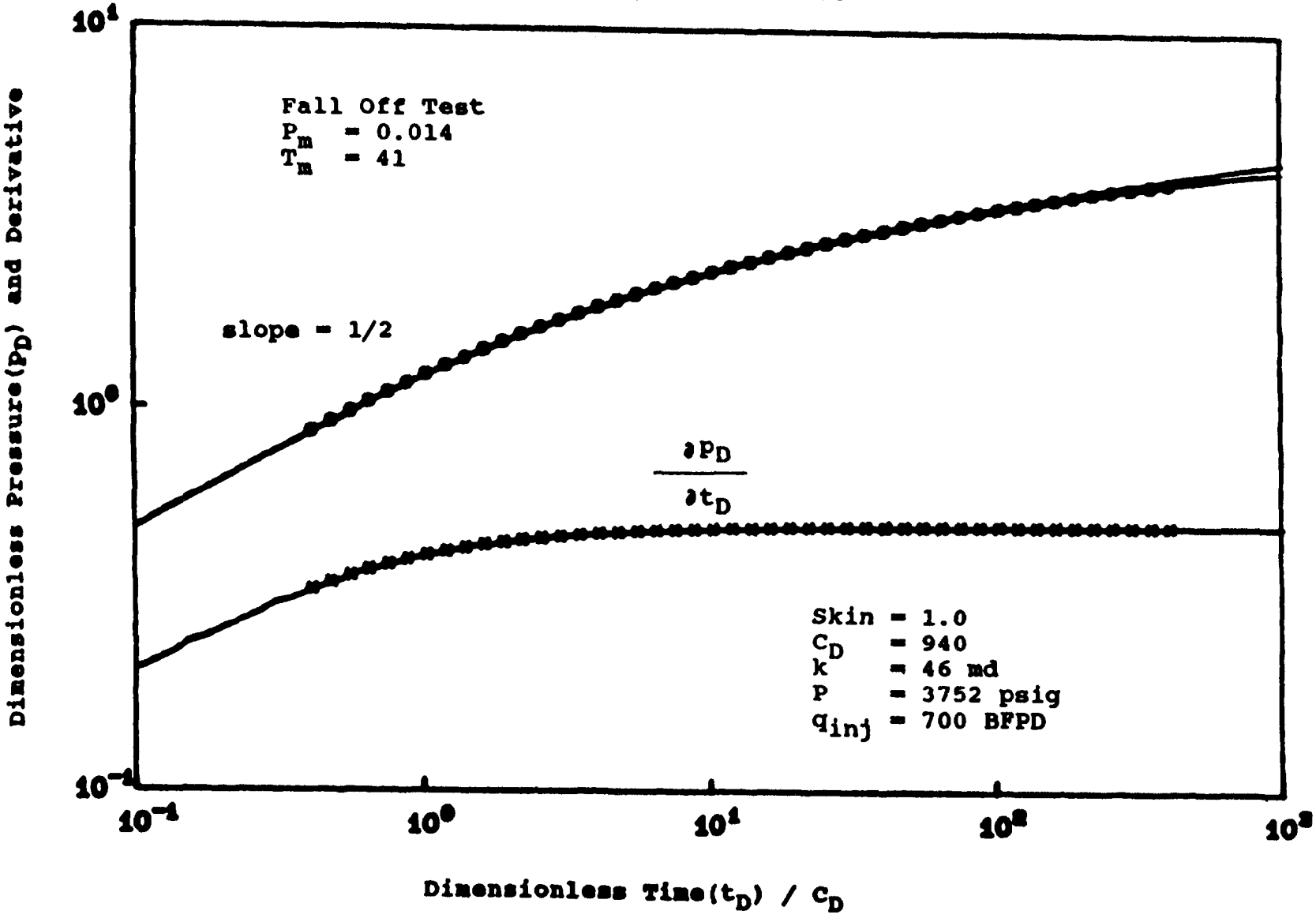

Figure 3-H

Associated Horner Plot

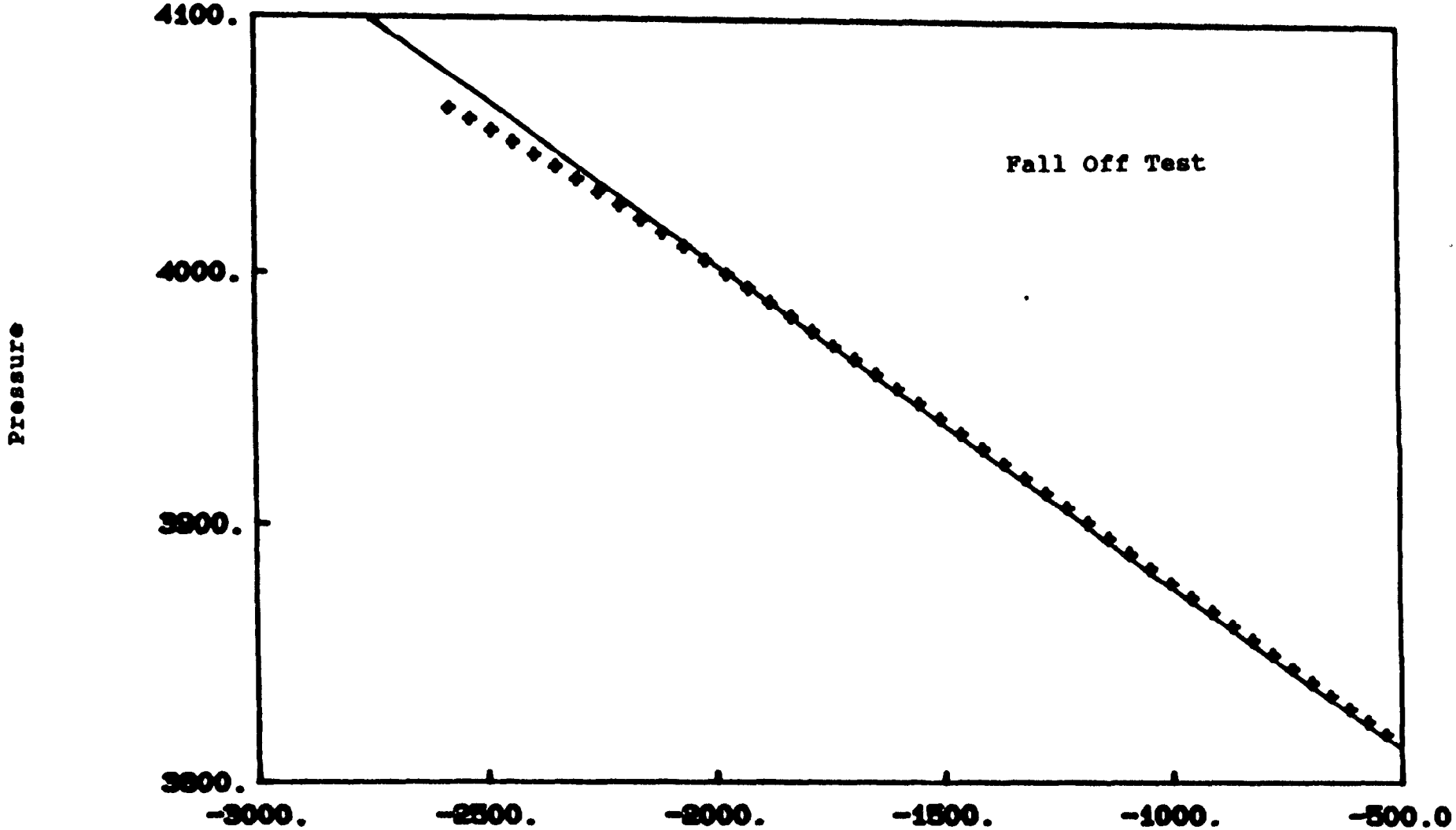

Figure 4

Solution of Square Bounded Reservoir with Wellbore Storage and Skin

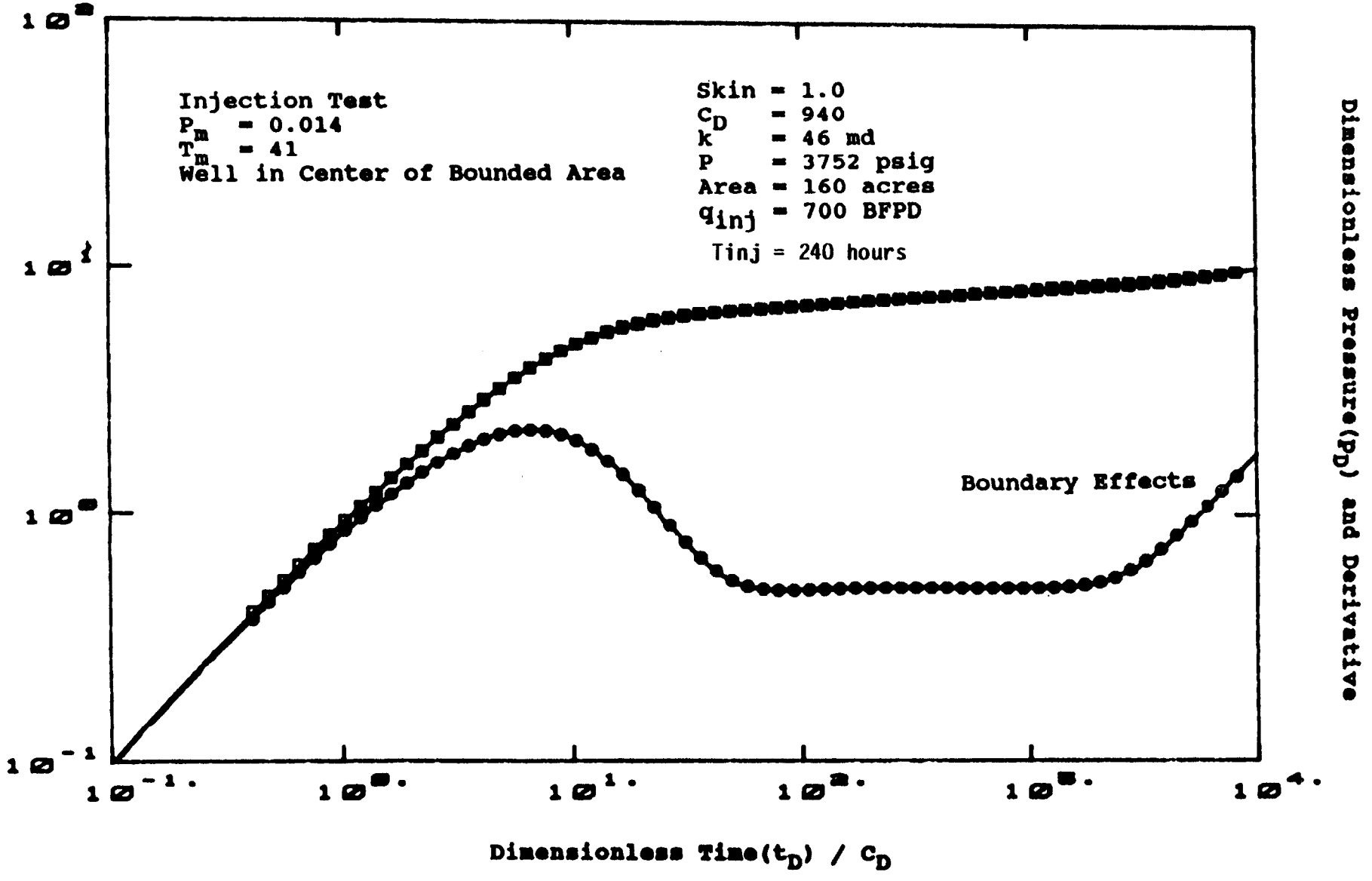

Figure 4-H

Associated Horner Plot

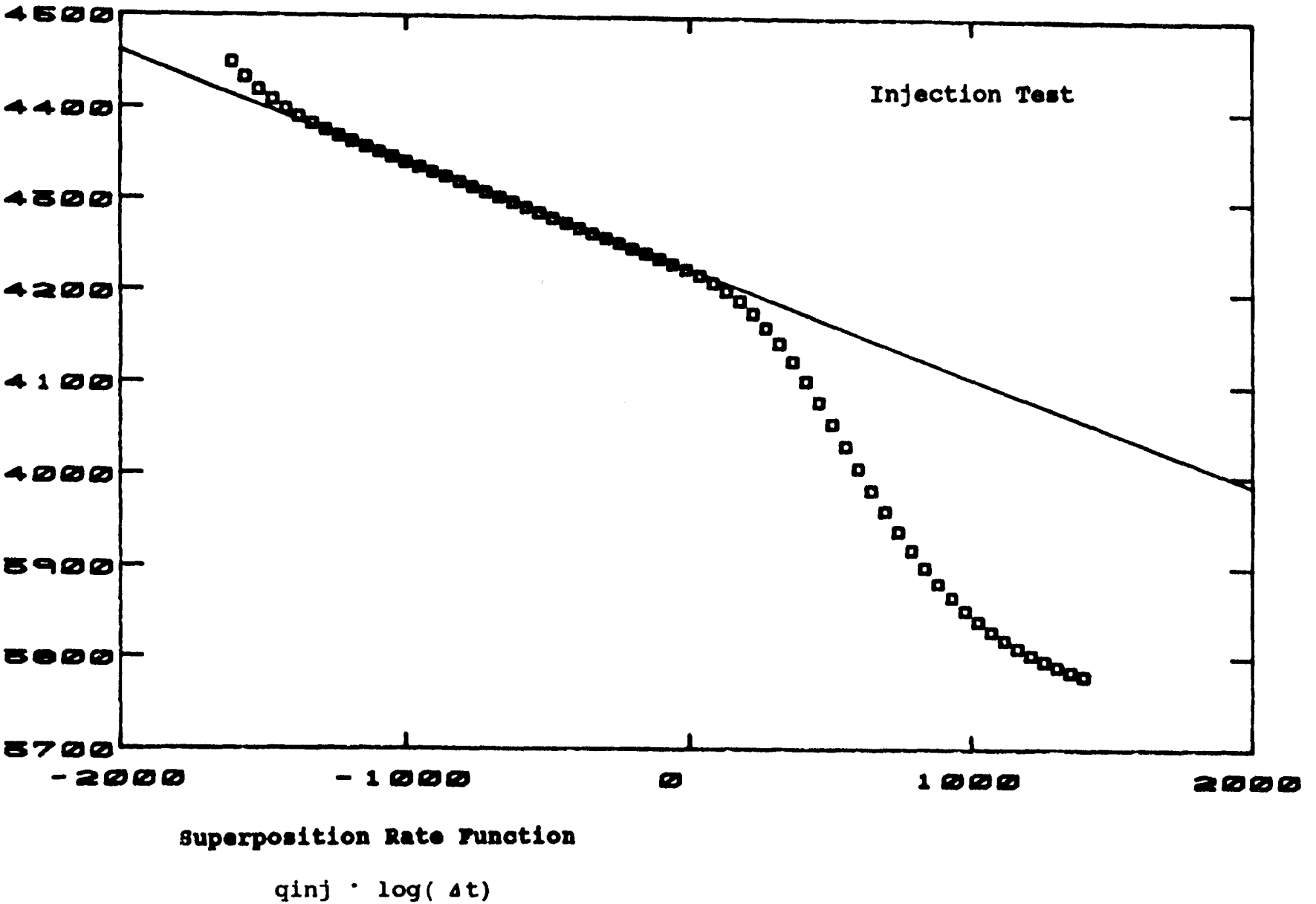

Figure 5

Solution in a Bounded Area with One Side Constant Pressure

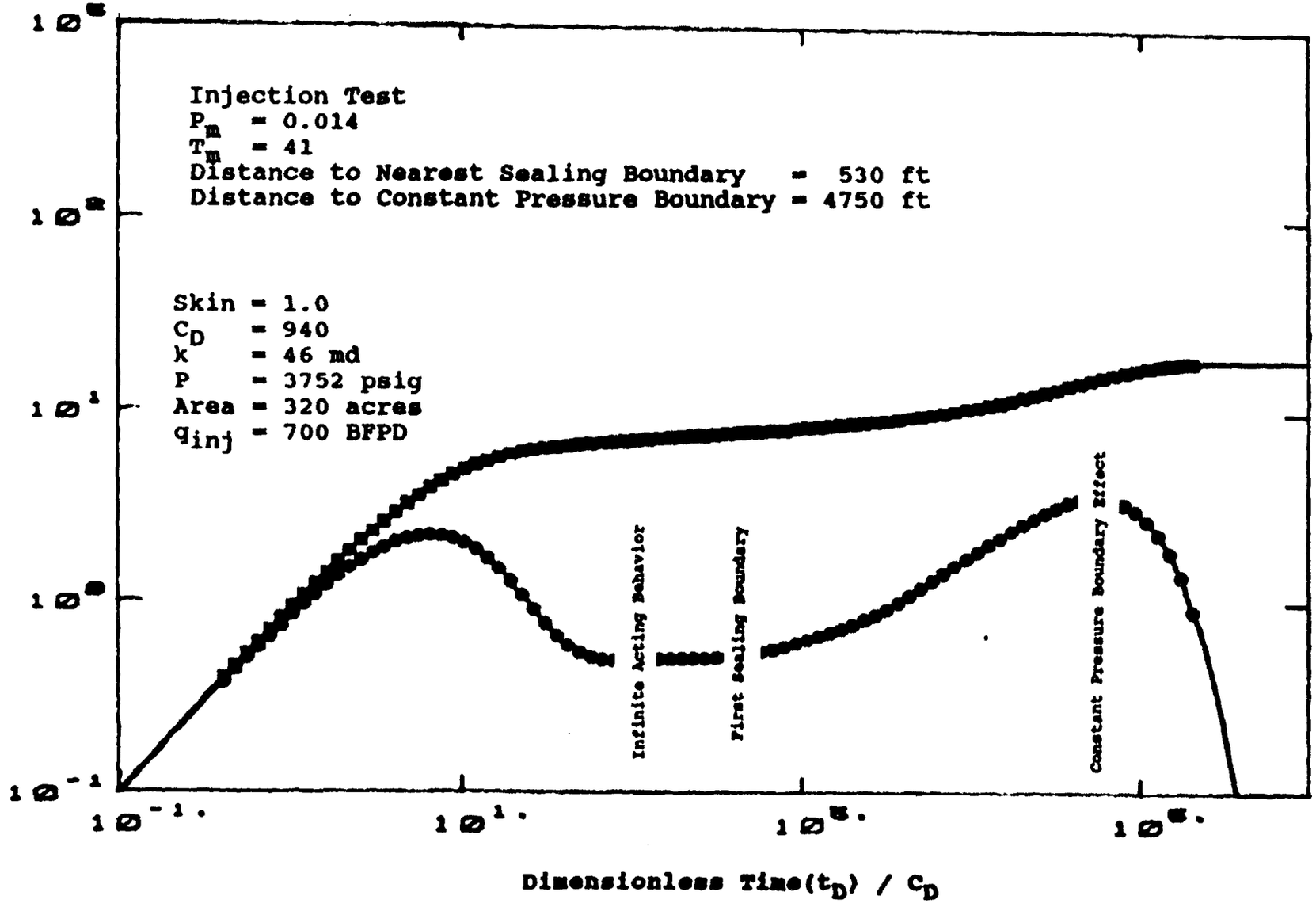

Figure 5-H

Associated Horner Plot

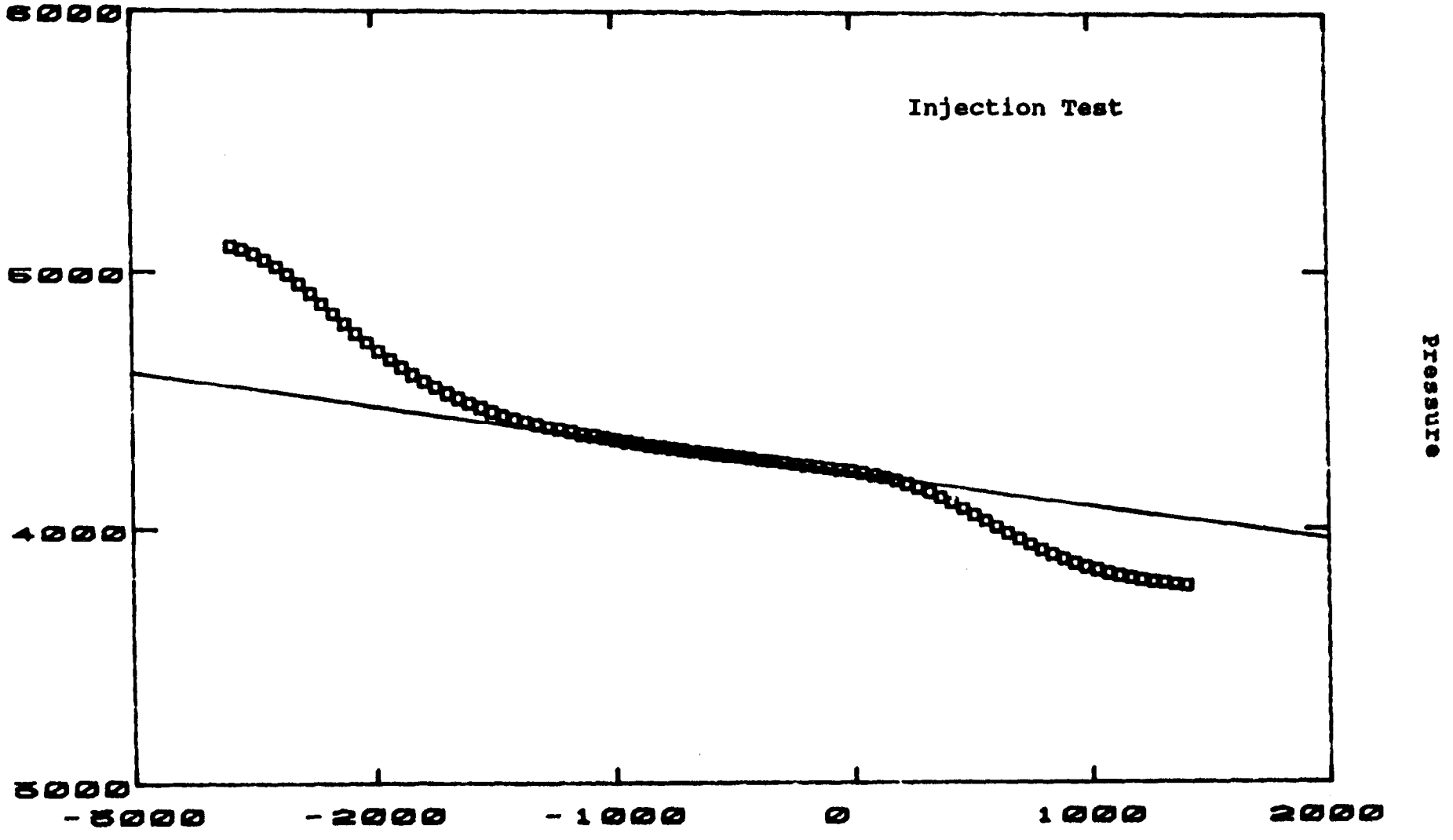

Figure 6

Radial Solution with Wellbore Storage and Skin
Infinite Acting Dual Porosity Reservoir

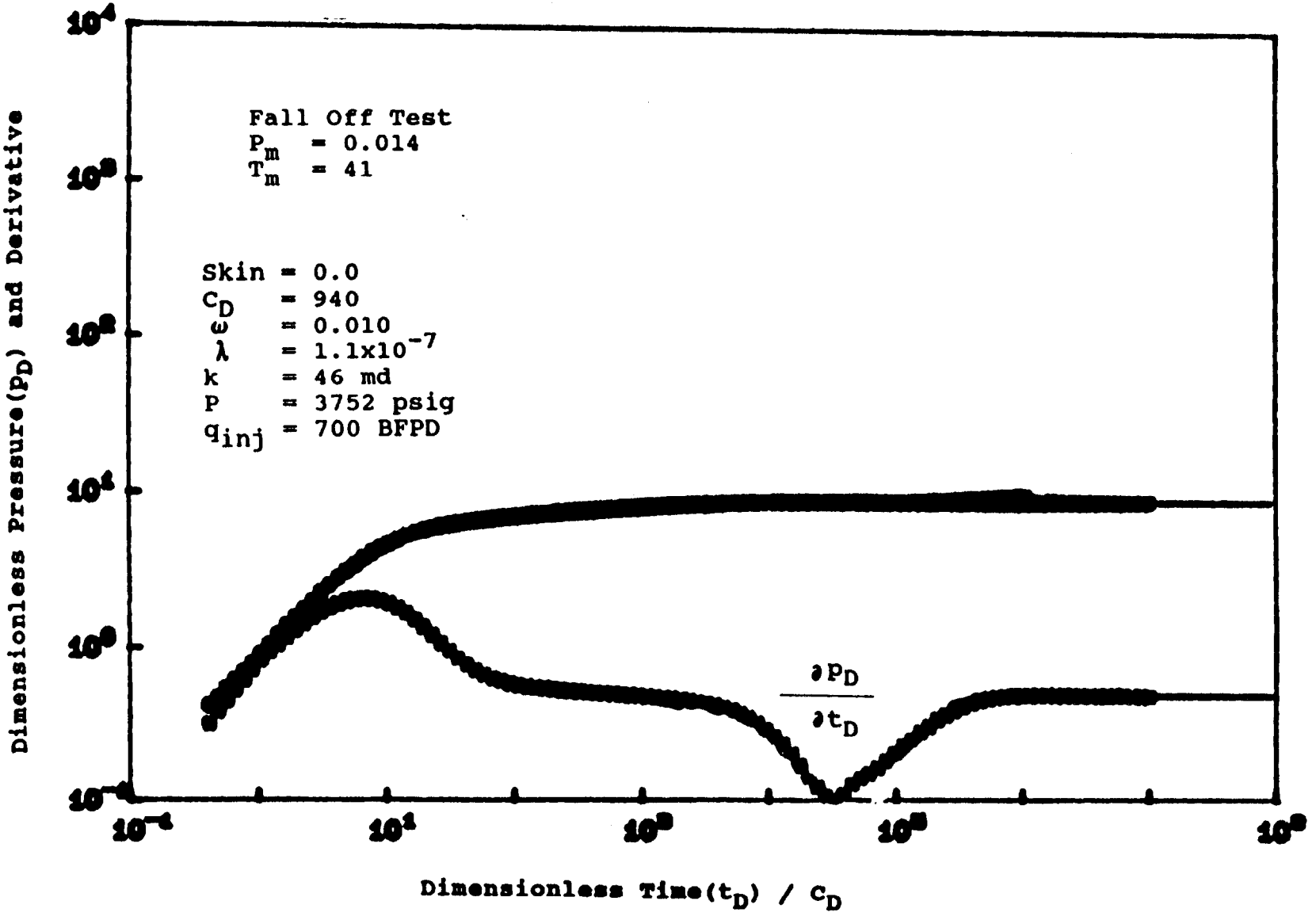

Figure 6-H

Associated Horner Plot

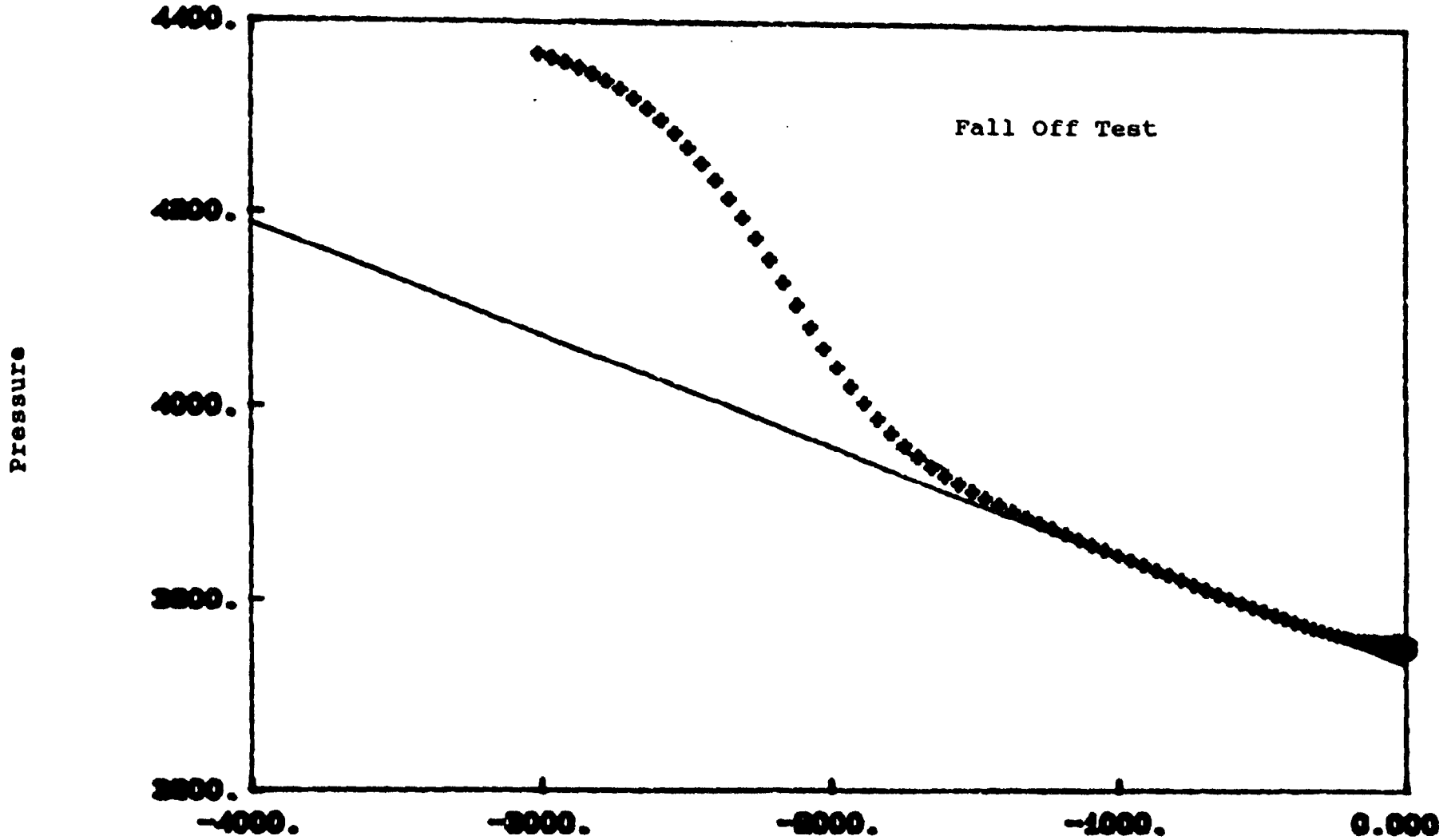

$$q_{inj} \cdot \log\left(\frac{T_{inj}-\Delta t}{\Delta t}\right)$$

PROBLEM 5 - WASTE INJECTION WELL WITH OBSERVATION WELL

WASTECO, a hazardous waste disposal company, is planning to submit a petition to continue its current operation. WASTECO has an injection well, perforated between 2540 and 2570 ft. subsurface, that it has been utilizing for some time. The aquifer pressure is at the prevailing hydrostatic gradient of 0.433 psi/ft. or 1100 psi at the start of injection. WASTECO didn't take any cores when the hole was drilled, but knows that the porosity of the aquifer is around 18-20%. WASTECO has a second well situated about 400 ft. from the current injection well, and the second well is no longer in use as an injector. WASTECO plans to utilize the second well as an observation well for pressure measurements and for downhole sampling. WASTECO believes it can satisfy the petition requirements for containment and decides to construct a reservoir model to demonstrate the containment principle.

WASTECO first runs a pressure fall-off test and determines the average flow capacity of the injection well to be 8500 md-ft. Since the complete 30 ft. injection zone is perforated, this means the average permeability is 283.3 md. WASTECO then seeds the injected waste stream with a tracer and begins sampling downstream at the observation well. The injection rate is 20 bbl/D (35 gallons/hr). Injection and sampling of the tracer is continued for a little over a year, and the observation well sampling results are graphed in Figure 1 as the "actual response" curve.

A numerical model is constructed. It has one homogeneous layer with a permeability of 283.3 md, a thickness of 30 ft., and a porosity of 0.18. A simulation is designed to investigate whether this model can replicate the response of the sampled observation well. The first simulation utilizes no dispersion. The frontal displacement is plug-flow in nature and shown in Figure 2. After several simulation runs in which the dispersivity is increased, a final match is achieved with α_l = 10 ft. (as shown in Figure 2).

As WASTECO begins preliminary discussions with EPA it finds that EPA has additional knowledge about the injection zone in question from another applicant. The second applicant has extensive core and log data and has definitively demonstrated a three-layered reservoir simulation concept. Each layer is 10 ft. in thickness, and each has a uniform 20% porosity. The similarity ends here however, as the second applicant has assigned different permeabilities to the three layers. The top layer is 100 md, the middle layer is 500 md, and the bottom layer is 250 md. A quick computation shows:

$$\bar{k} = \frac{(10 \times 100) + (10 \times 500) + (10 \times 250)}{30} = 283.3 \text{ md}$$

exactly the same average permeability as indicated from the transient test analysis. Earlougher(1977) teaches that layered reservoirs with crossflow between layers behave as a single-layered system of average permeability so the error WASTECO made in assuming a homogeneous 30

ft. zone of 283.3 md is understandable. What isn't so clear; however, is how did WASTECO manage such a good match of the sampled effluent stream with such a model?

Figure 3 shows the three-layered heterogeneous reservoir response to the 20 bbl/day injection rate with no dispersion at all. The shape of the curve, while not exactly like the actual response curve, is similar. The higher permeability layer transports waste the most rapidly followed by the 250 md layer and the 100 md layer (see Figure 4 at 100, 205, and 295 days of injection time respectively). Adding α_l = 4.0 ft. to the heterogeneous model illustrates a perfect match of the actual data. WASTECO utilized an α_l of 10 ft. and a homogeneous, one layer model, to achieve the same end result.

What could go wrong with WASTECO's 30-year operational model? Will WASTECO be doing itself an injustice to continue with the simple model with higher α_l?. Under what conditions is WASTECO's model satisfactory?

Figure 1 - OBSERVATION WELL RESPONSE CURVE

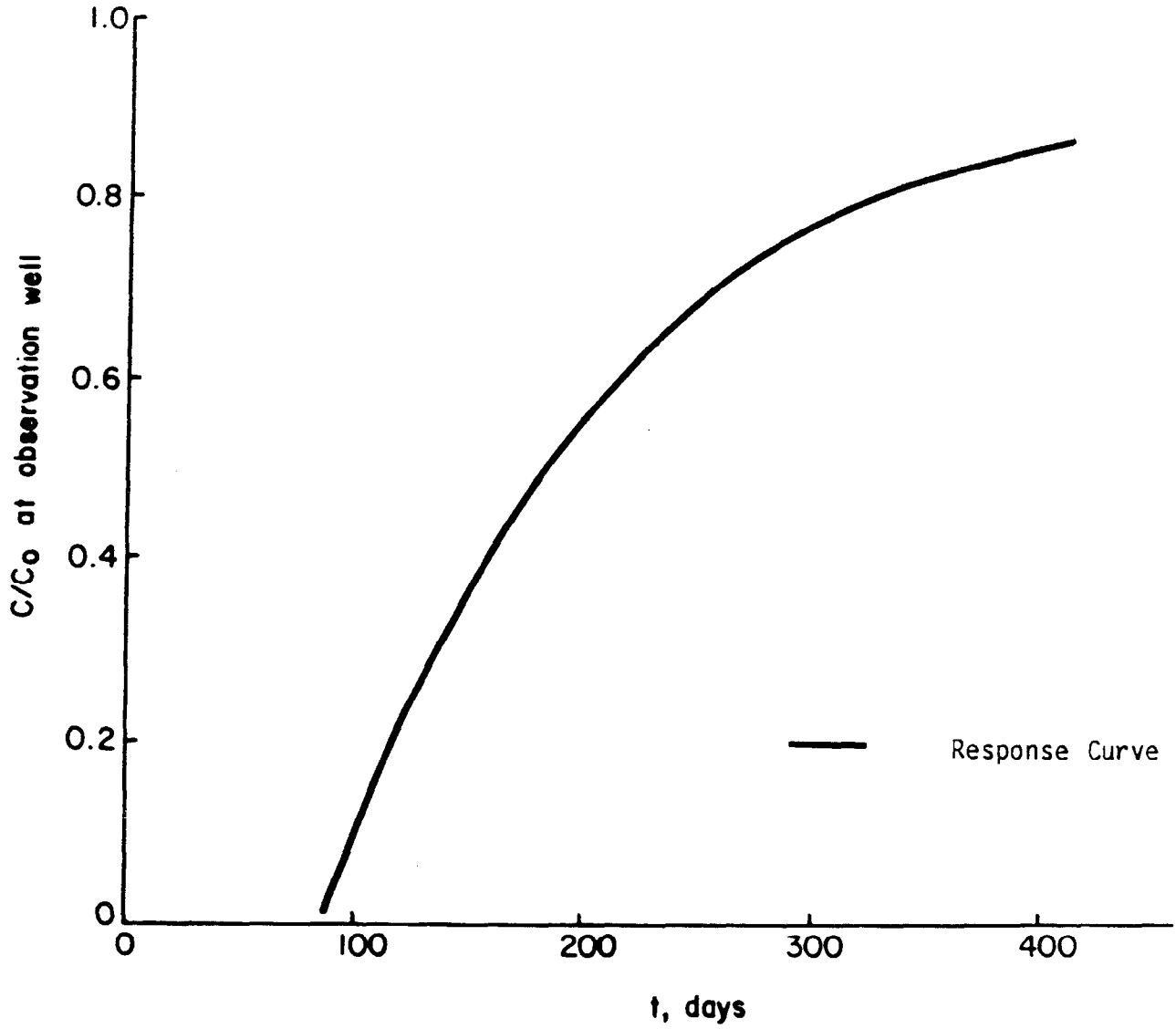

Figure 2 - HOMOGENEOUS SINGLE LAYER MODEL

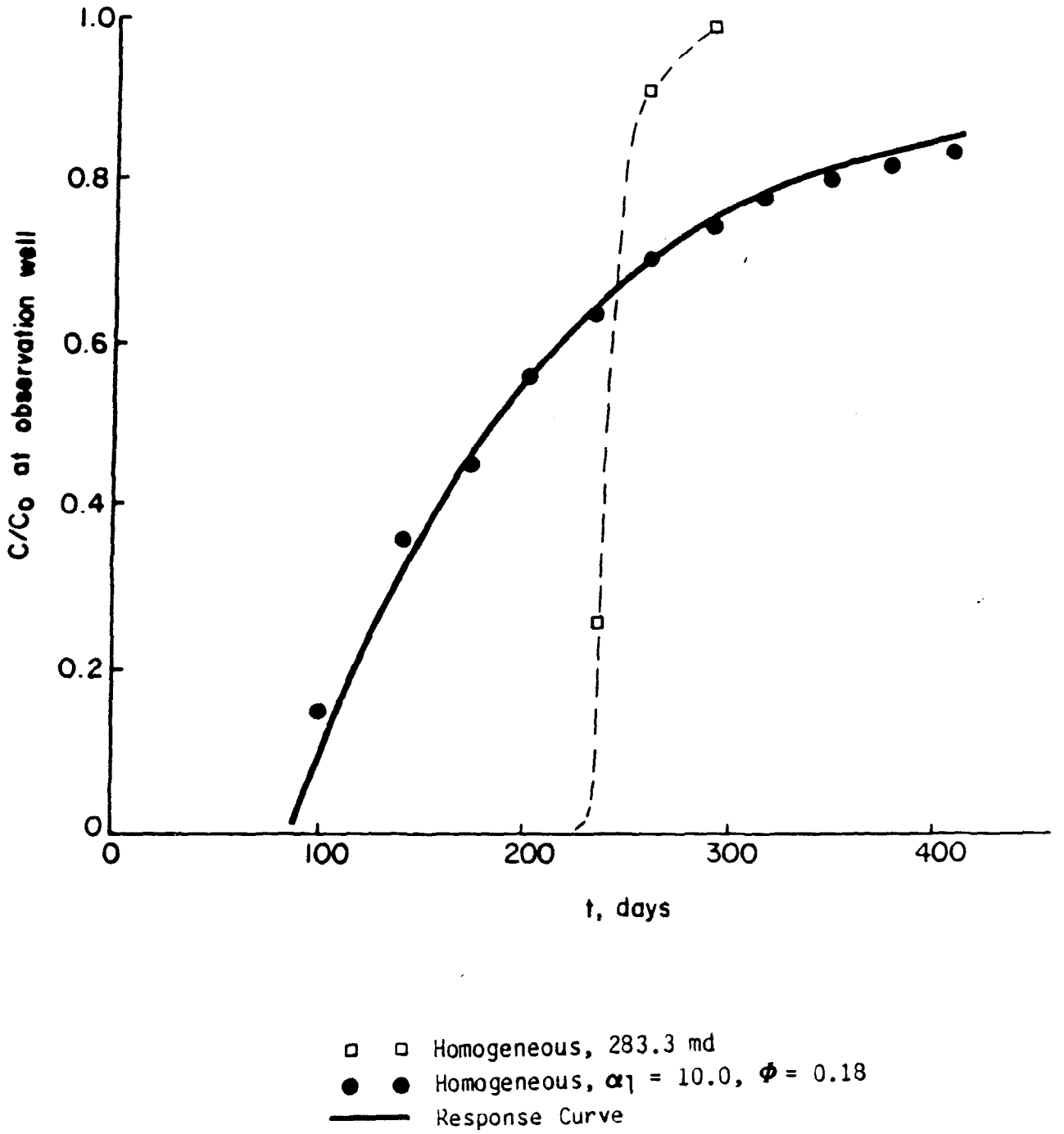

Figure 3 - HETEROGENEOUS, THREE LAYER MODEL

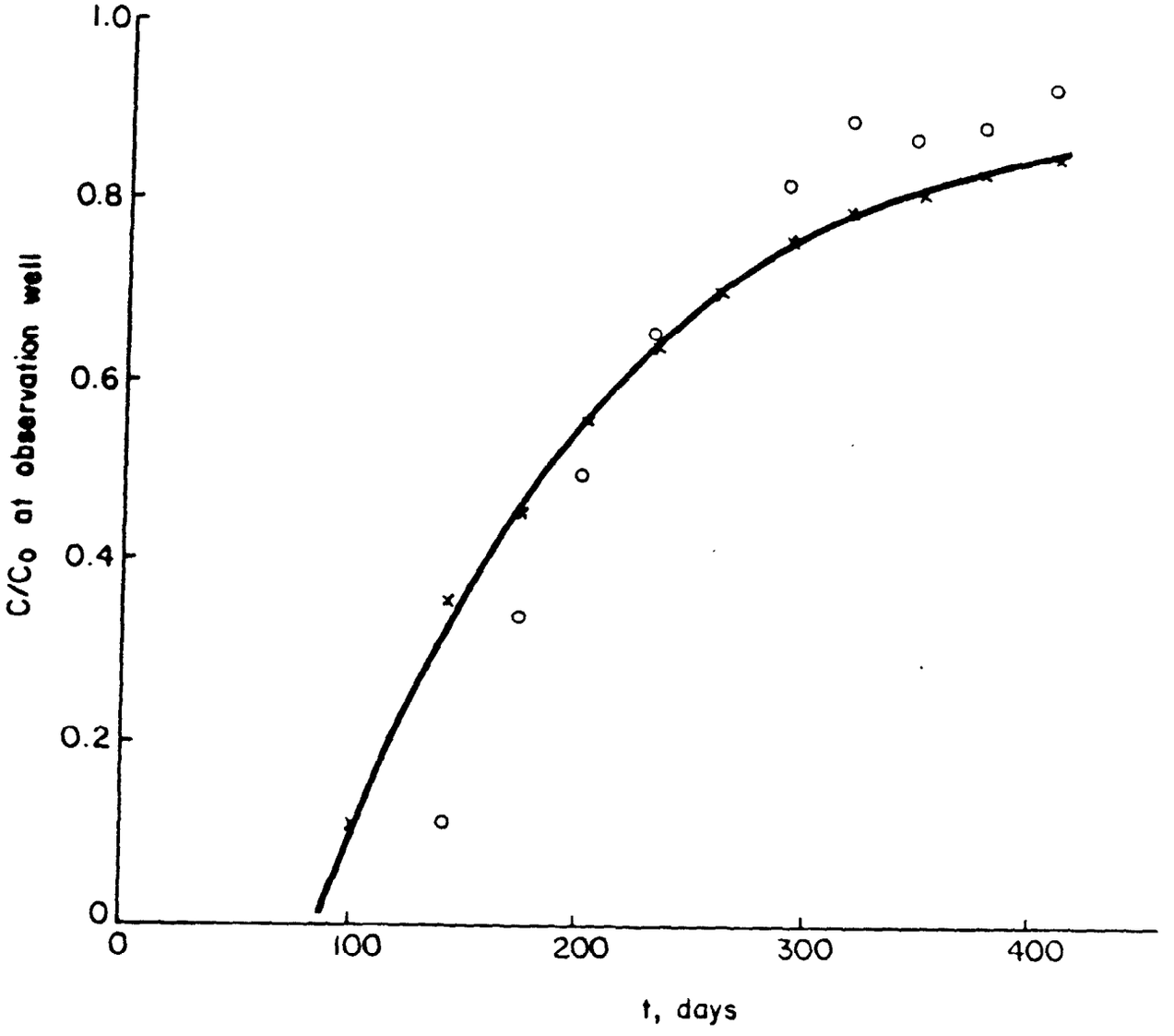

Response Curve

× Heteregeneous, α_1 = 4.0

○ Heteregeneous, α_1 = 0.0

Figure 4 - CONCENTRATION PROFILE BY LAYER

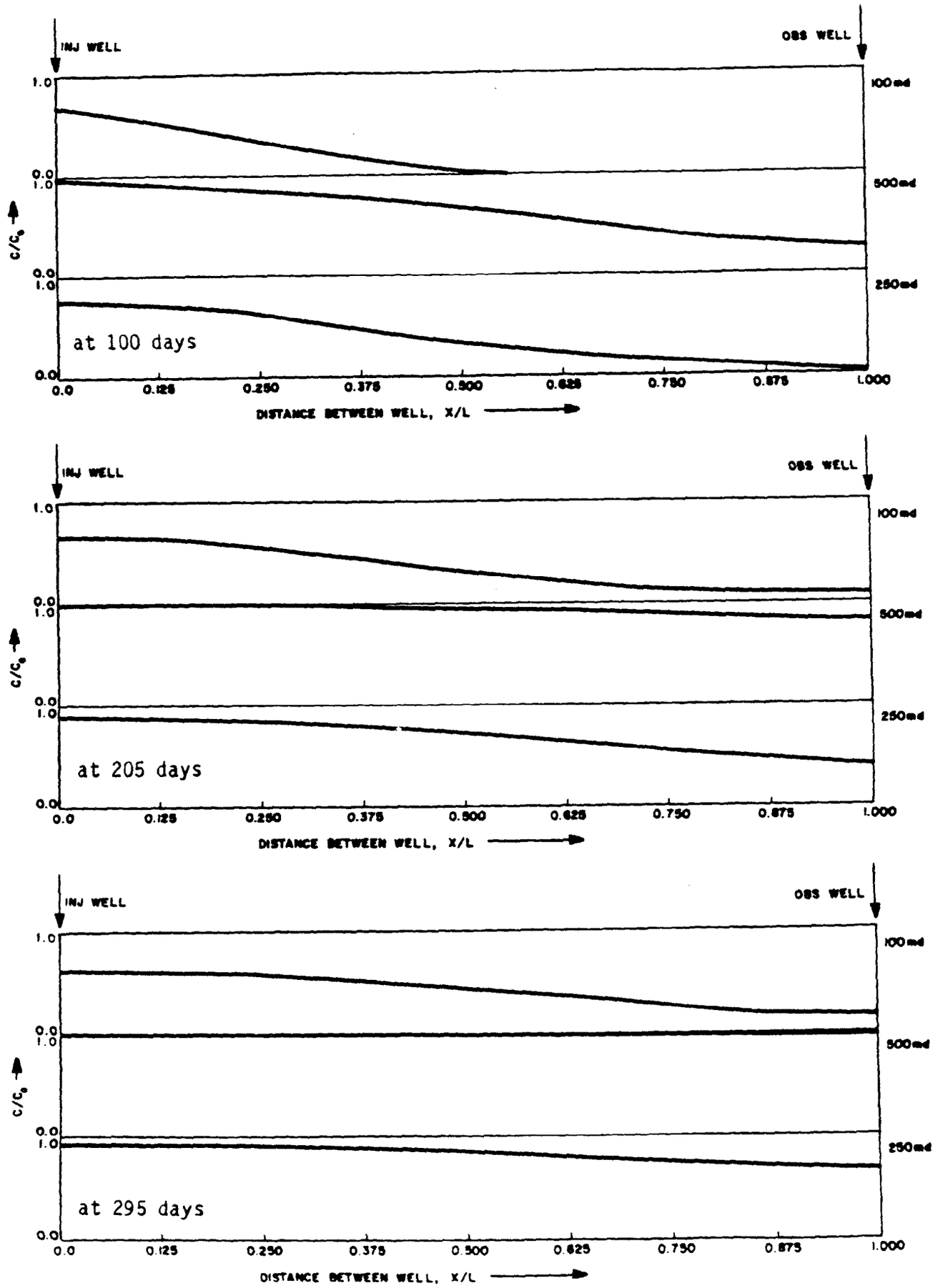

The following material has been taken from Society of Petroleum Engineers Monograph Volume 5,"Advances in Well Test Analysis" by Robert C. Earlougher, Jr.

Chapter 5

Pressure Buildup Testing

5.1 Introduction

Pressure buildup testing, probably the most familiar transient well testing technique, has been treated widely in the literature.[1-10] This type of testing was first introduced by the groundwater hydrologists,[2] but has been used extensively in the petroleum industry.

Pressure buildup testing requires shutting in a producing well. The most common and simplest analysis techniques require that the well produce at a constant rate, either from startup or long enough to establish a stabilized pressure distribution (t_{pss}), before shut-in. Fig. 5.1 schematically shows rate and pressure behavior for an ideal pressure buildup test. In that figure, and throughout this monograph, t_p is the production time and Δt is running shut-in time. The pressure is measured immediately before shut-in and is recorded as a function of time during the shut-in period. The resulting pressure buildup curve is analyzed for reservoir properties and wellbore condition; the methods used most are described in this chapter.

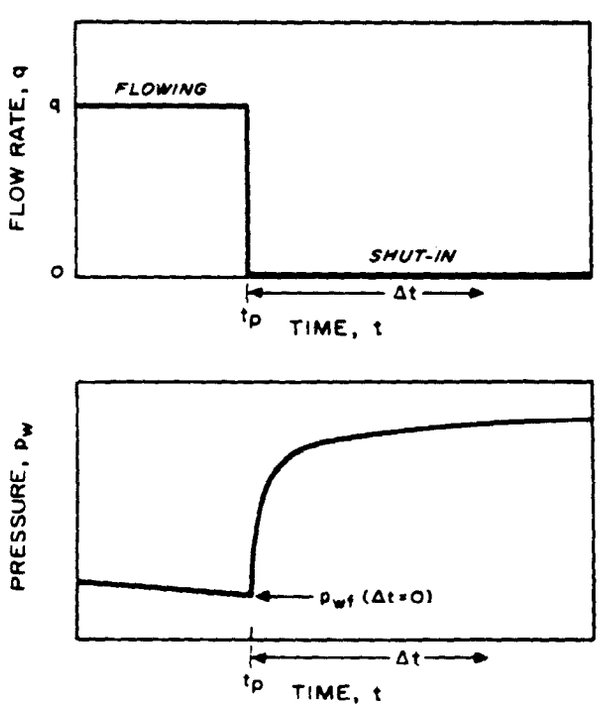

Fig. 5.1 Idealized rate and pressure history for a pressure buildup test.

As in all transient well tests, knowledge of surface and subsurface mechanical conditions is important in buildup-test data interpretation. Therefore, it is recommended that tubing and casing sizes, well depth, packer locations, etc., be determined before data interpretation starts. Short-time pressure observations usually are necessary for complete delineation of wellbore storage effects. Data may be needed at intervals as short as 15 seconds for the first few minutes of some buildup tests. As the test progresses, the data-collection interval can be expanded.

Stabilizing the well at a constant rate before testing is an important part of a pressure buildup test. If stabilization is overlooked or is impossible, standard data analysis techniques may provide erroneous information about the formation. Thus, it is important to determine the degree and adequacy of the stabilization; one way is to check the length of the pre-shut-in constant-rate period against the time required for stabilization, as given by Eqs. 2.40 and 2.42. For wells with significantly varying rates, buildup test analysis is still possible using the variable-rate methods of Chapter 4 or the modifications of those methods presented in Section 5.4.

5.2 Pressure Buildup Test Analysis During the Infinite-Acting Period

For any pressure-buildup testing situation, bottom-hole shut-in pressure in the test well may be expressed by using the principle of superposition for a well producing at rate q until time t_p, and at zero rate thereafter. At any time after shut-in,

$$p_{ws} = p_i - \frac{141.2\,qB\mu}{kh}\left\{p_D\left(\left[t_p + \Delta t\right]_D\right) - p_D(\Delta t_D)\right\}, \quad \ldots\ldots\ldots\ldots\ldots\ldots\ldots\ldots (5.1)$$

where p_D is the applicable dimensionless-pressure function and t_D is as defined by Eq. 2.3a:

$$t_D = \frac{0.0002637\,kt}{\phi\mu c_t r_w^{\,2}} \quad \ldots\ldots\ldots\ldots\ldots\ldots\ldots\ldots (5.2)$$

During the infinite-acting time period, after wellbore storage effects have diminished and providing there are no major induced fractures, p_D in Eq. 5.1 may be replaced by the logarithmic approximation to the exponential integral, Eq. 2.5b:

$$p_D = \frac{1}{2}(\ln t_D + 0.80907) \quad \ldots\ldots\ldots\ldots\ldots\ldots (5.3)$$

Eq. 5.3 applies when $t_D > 100$, which occurs after a few minutes for most unfractured systems. By using Eqs. 5.2 and 5.3, Eq. 5.1 may be rewritten:

$$p_{ws} = p_i - m \log\left(\frac{t_p + \Delta t}{\Delta t}\right) \quad \ldots\ldots\ldots\ldots\ldots\ldots (5.4)$$

Eq. 5.4 describes a straight line with intercept p_i and slope $-m$, where

$$m = \frac{162.6\, qB\mu}{kh} \quad \ldots\ldots\ldots\ldots\ldots\ldots\ldots\ldots (5.5)$$

Eq. 5.4 indicates that a plot of observed shut-in bottom-hole pressure, p_{ws}, vs $\log\left[(t_p + \Delta t)/\Delta t\right]$ should have a straight-line portion with slope $-m$ that can be used to estimate reservoir permeability,

$$k = \frac{162.6\, qB\mu}{mh} \quad \ldots\ldots\ldots\ldots\ldots\ldots\ldots\ldots (5.6)$$

Both Theis[2] and Horner[6] proposed estimating permeability in this manner. The p_{ws} vs $\log\left[(t_p + \Delta t)/\Delta t\right]$ plot is commonly called the Horner plot (graph, method) in the petroleum industry; that terminology is used in this monograph.

Fig. 5.2 is a schematic Horner plot of pressure buildup data. The straight-line section is shown. As indicated by Eq. 5.4, this straight-line portion of the Horner plot may be extrapolated to $(t_p + \Delta t)/\Delta t = 1$, $\left\{\log\left[(t_p + \Delta t)/\Delta t\right] = 0\right\}$, the equivalent of infinite shut-in time, to obtain an estimate of p_i. That is an accurate estimate only for short production periods. However, the extrapolated pressure value is useful for estimating average reservoir pressure, as indicated in Chapter 6.

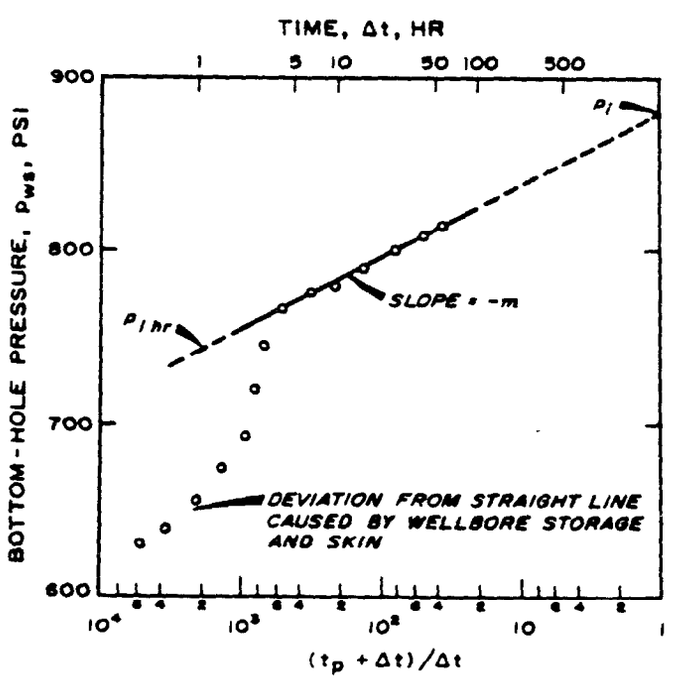

Fig. 5.2 Horner plot of pressure buildup data showing effects of wellbore storage and skin.

In Fig. 5.2, as in all other Horner plots in this monograph, the abscissa has been reversed so it increases from right to left in keeping with common practice. The reverse plotting, which is mathematically equivalent to plotting $\log\left[\Delta t/(t_p + \Delta t)\right]$, causes time to increase from left to right (see upper scale in Fig. 5.2) and gives the buildup curve the shape one would expect. However, it means that the slope, which normally would be thought of as positive, *is negative*. In Fig. 5.2, the slope is -42 psi/cycle, so $m = 42$ psi/cycle.

A result of using the superposition principle is that the skin factor, s, does not appear in the general pressure-buildup equation, Eq. 5.1. As a result, skin factor does not appear in the simplified equation for the Horner plot, Eq. 5.4. That means the Horner-plot slope is not affected by the skin factor; however, the skin factor still *does* affect the *shape* of the pressure buildup data. In fact, an early-time deviation from the straight line can be caused by skin factor as well as by wellbore storage, as indicated in Fig. 5.2 (also see Fig. E.1). The deviation can be significant for the large negative skins that occur in hydraulically fractured wells. In any case, the skin factor does affect flowing pressure before shut-in, so skin may be estimated from the buildup test data plus the flowing pressure immediately before the buildup test:[1,8,11]

$$s = 1.1513\left[\frac{p_{1hr} - p_{wf}(\Delta t = 0)}{m} - \log\left(\frac{k}{\phi\mu c_t r_w^2}\right) + 3.2275\right]. \quad \ldots\ldots\ldots\ldots\ldots\ldots (5.7)$$

In Eq. 5.7, $p_{wf}(\Delta t = 0)$ is the observed flowing bottom-hole pressure immediately before shut-in and $-m$ is the slope of the Horner plot. As a result of assumptions made in deriving Eq. 5.7,[1,8] the value of p_{1hr} must be taken from the Horner straight line. Frequently, pressure data do not fall on the straight line at 1 hour because of wellbore storage effects that allow afterflow into the well, or large negative skin factors resulting from induced fracturing, etc. In that case, the semilog line must be extrapolated to 1 hour and the pressure read. Fig. 5.2 shows the correct way to determine p_{1hr}.

In different types of transient test analysis, the slope is sometimes $+m$ and sometimes $-m$; additionally, m sometimes includes a minus sign (compare Eq. 3.6 for drawdown testing with Eq. 5.5 for buildup). This may cause some confusion in transient well test analysis. Confusion may be avoided by realizing (1) permeability must always be positive, so the sign of m may be determined from Eq. 5.5 (or its equivalent for other types of testing); (2) the first term inside the brackets of the skin equation, $\left[p_{1hr} - p_{wf}(\Delta t = 0)\right]/m$, is usually positive (the exception occurs in hydraulically fractured wells with $s << 0$); and (3) production rates are positive while injection rates are negative. There should not be a problem with analysis equations if the correct definition of m and its relation to the slope of the data

plot are used with the correct signs in the analysis equations. Appendix E gives appropriate signs for common analysis techniques for different tests.

Eq. 5.7 provides a good estimate of the skin factor as long as $t_p >> 1$ hour. But when t_p is on the order of 1 hour (for example, in drillstem testing), Eq. 5.7 should be replaced by

$$s = 1.1513 \left[\frac{p_{1hr} - p_{wf}(\Delta t=0)}{m} + \log\left(\frac{t_p + 1}{t_p}\right) - \log\left(\frac{k}{\phi\mu c_t r_w^2}\right) + 3.2275 \right]. \quad (5.8)$$

The proper t_p to use for a given well in a multiple-well reservoir has been a matter of frequent concern to practicing engineers. Eqs. 5.1 and 5.4 assume a constant production rate from time 0 to time t_p, not often a realistic assumption. Horner[6] indicated that t_p often can be approximated as the cumulative production since completion divided by the rate immediately before shut-in (when rate varies). Except shortly after well completion, it appears desirable as a matter of general practice to approximate t_p using cumulative production since the last pressure equalization (or some other convenient, relatively short time in terms of reservoir depletion) rather than total cumulative production:

$$t_p = \frac{24 V_P}{q}. \quad (5.9)$$

In Eq. 5.9, V_P is the cumulative volume produced since the *last pressure equalization* and q is the constant rate just before shut-in. If t_p on this basis is significantly greater than t_{pss}[12,13] (for example, by a factor of 2), then replotting using t_{pss} (Eq. 2.24 for a closed boundary or Eq. 2.42 for a constant-pressure boundary) may be justified. For closed boundary conditions, a Horner plot *using* t_{pss} as opposed to a Miller-Dyes-Hutchinson (MDH) plot (Section 5.3) tends to prolong the straight-line portion of the buildup curve. However, the principal importance of using t_{pss} usually is in minimizing errors in estimating average reservoir pressure (Section 6.3).

When the time at constant rate immediately before shut-in is significantly less than t_{pss} and the rate variation is significant (for example, 20 to 50 percent), accurate values of permeability, skin, and static pressure generally can be obtained only by using the methods of superposition discussed in Section 5.4. When the time at a constant production rate is significantly less than t_{pss}, but is still large (more than about four times the buildup time of interest), reasonably accurate values of skin and permeability should still be obtainable with the normal Horner plot using Eq. 5.9, even though values of estimated static pressure could be poor. This comment applies to systems with negligible fracturing in which wellbore storage effects either have died out or have been properly adjusted for (Section 11.2).

Even though the well is shut in during pressure buildup testing, the afterflow caused by wellbore storage has a significant influence on pressure buildup data. Fig. 5.2 schematically shows that pressure points fall below the semilog straight line while wellbore storage is important. The duration of those effects may be estimated by making the log-log data plot described in Section 2.6. For pressure buildup testing, plot $\log[p_{ws} - p_{wf}(\Delta t=0)]$ vs $\log \Delta t$. When wellbore storage dominates, that plot will have a unit-slope straight line; as the semilog straight line is approached, the log-log plot bends over to a gently curving line with a low slope (see Fig. 2.10). In all pressure-buildup test analyses, the log-log data plot should be made before the straight line is chosen on the semilog data plot, since it is often possible to draw a semilog straight line through wellbore-storage-dominated data. This phenomenon occurs because wellhead shut-in does not correspond to sand-face shut-in. When the surface valve is closed, fluid continues to flow into the wellbore from the formation. Thus, pressure does not build up as fast as we might expect. As the flow rate drops off to zero, the pressure increases rapidly to approach the theoretically predicted level. The semilog data plot is steep and nearly linear during this time, and may be analyzed incorrectly. The analyzable data occur after the data-plot slope has become less steep, as indicated in Fig. 5.2.

When wellbore storage effects last so long that the semilog straight line does not develop, it may be possible to analyze the test data by using type-curve matching techniques in a manner similar to that described in Section 3.3, with $\Delta p = p_{ws} - p_{wf}(\Delta t = 0)$. The type curves of Figs. C.6,[14] C.8,[15] and C.9[16,17] are particularly useful for pressure buildup testing, providing a significant change in wellbore storage coefficient is not involved (see Section 11.2). It cannot be overemphasized that type-curve matching *should not be used for test analysis if semilog analysis techniques can be applied*. Type-curve matching generally gives only approximate results (within a factor of 2 or 3). Refs. 15 and 16 give examples of type-curve matching for pressure buildup analysis. The Gladfelter-Tracy-Wilsey[1,18] or Russell[1,9] approaches can also give good results for data nearing the semilog straight line (after q is less than 20 percent of the previous rate). However, curve-matching techniques, particularly Fig. C.8, can also give good quantitative results in this region.

Example 5.1 Pressure Buildup Test Analysis—Horner Method

Table 5.1 shows pressure buildup data from an oil well with an estimated drainage radius of 2,640 ft. Before shut-in the well had produced at a stabilized rate of 4,900 STB/D for 310 hours. Known reservoir data are

depth = 10,476 ft
r_w = (4.25/12) ft
$c_t = 22.6 \times 10^{-6}$ psi^{-1}
q_o = 4,900 STB/D
h = 482 ft
$p_{wf}(\Delta t = 0)$ = 2,761 psig
μ_o = 0.20 cp
ϕ = 0.09
B_o = 1.55 RB/STB
casing ID = (6.276/12) ft
t_p = 310 hours.

Wellbore storage affects transient pressure behavior and,

therefore, should be considered in all transient test analyses. Failure to do so may result in analyzing the wrong portion of the data. Fig. 5.3, the log-log plot of the buildup data in Table 5.1, is used to check the significance of wellbore storage. Since there is no unit-slope line, we conclude that dominant wellbore storage has ended by 0.1 hour. However, the rapid pressure increase shown in Fig. 5.4 does indicate that wellbore storage or skin effects are significant until about 0.75 hour. The data obtained after 0.75 hour can be analyzed.

The Horner plot is shown as Fig. 5.4. Residual wellbore storage or skin effects at shut-in times of less than 0.75 hour are apparent. The straight line, drawn after $\Delta t = 0.75$ hour, has a slope of -40 psig/cycle, so $m = 40$ psig/cycle.

Eq. 5.6 is used to estimate permeability:

$$k = \frac{162.6(4{,}900)(1.55)(0.20)}{(40)(482)} = 12.8 \text{ md}.$$

Skin factor is estimated from Eq. 5.7 using $p_{1\text{hr}} = 3{,}266$ psig from Fig. 5.4:

$$s = 1.1513\left[\frac{3{,}266 - 2{,}761}{40} - \log\left(\frac{(12.8)(12)^2}{(0.09)(0.20)(22.6 \times 10^{-6})(4.25)^2}\right) + 3.2275\right] = 8.6.$$

We can estimate Δp across the skin from Eq. 2.9:

$$\Delta p_s = \frac{(141.2)(4{,}900)(1.55)(0.20)(8.6)}{(12.8)(482)} = 300 \text{ psi}.$$

TABLE 5.1—PRESSURE BUILDUP TEST DATA FOR EXAMPLE 5.1, $t_p = 310$ HOURS.

Δt (hours)	$t_p + \Delta t$ (hours)	$\frac{(t_p+\Delta t)}{\Delta t}$	p_{ws} (psig)	$p_{ws} - p_{wf}$ (psig)
0.0	—	—	2,761	—
0.10	310.10	3,101	3,057	296
0.21	310.21	1,477	3,153	392
0.31	310.31	1,001	3,234	473
0.52	310.52	597	3,249	488
0.63	310.63	493	3,256	495
0.73	310.73	426	3,260	499
0.84	310.84	370	3,263	502
0.94	310.94	331	3,266	505
1.05	311.05	296	3,267	506
1.15	311.15	271	3,268	507
1.36	311.36	229	3,271	510
1.68	311.68	186	3,274	513
1.99	311.99	157	3,276	515
2.51	312.51	125	3,280	519
3.04	313.04	103	3,283	522
3.46	313.46	90.6	3,286	525
4.08	314.08	77.0	3,289	528
5.03	315.03	62.6	3,293	532
5.97	315.97	52.9	3,297	536
6.07	316.07	52.1	3,297	536
7.01	317.01	45.2	3,300	539
8.06	318.06	39.5	3,303	542
9.00	319.00	35.4	3,305	544
10.05	320.05	31.8	3,306	545
13.09	323.09	24.7	3,310	549
16.02	326.02	20.4	3,313	552
20.00	330.00	16.5	3,317	556
26.07	336.07	12.9	3,320	559
31.03	341.03	11.0	3,322	561
34.98	344.98	9.9	3,323	562
37.54	347.54	9.3	3,323	562

Thus, pressure drop across the skin in this damaged well is about one-half the total pressure drop. The flow efficiency may be estimated from Eq. 2.12, using $\bar{p} = 3{,}342$ psig (as estimated in Example 6.1, Section 6.3). Flow efficiency is calculated as

$$\frac{3{,}342 - 2{,}761 - 300}{3{,}342 - 2{,}761} = 0.48.$$

This suggests that the production rate could be more than doubled by simply removing the damage, or possibly could be tripled with an acid or fracture treatment, depending on conditions around the well and on rock type.

5.3 Pressure Buildup Test Analysis in Finite and Developed Reservoirs

When wells being tested do not act like a single well in an infinite system, the equations in Section 5.2 require modification. In this section, we consider pressure buildup testing of a single well in a bounded reservoir and of a well in a developed reservoir. During the initial discussion, we will not consider the effects of changing offset-well drainage areas on the developed reservoir situation.

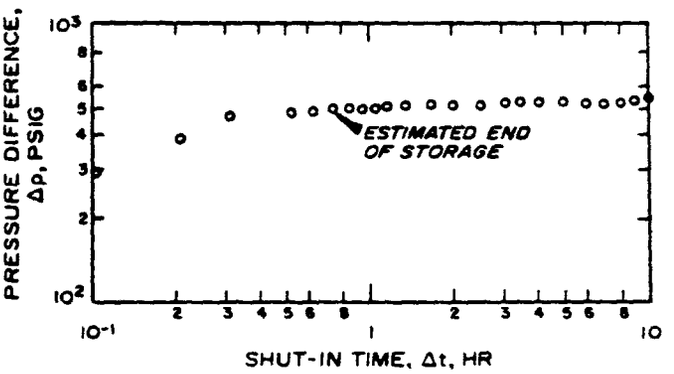

Fig. 5.3 Log-log data plot for the buildup test of Example 5.1.

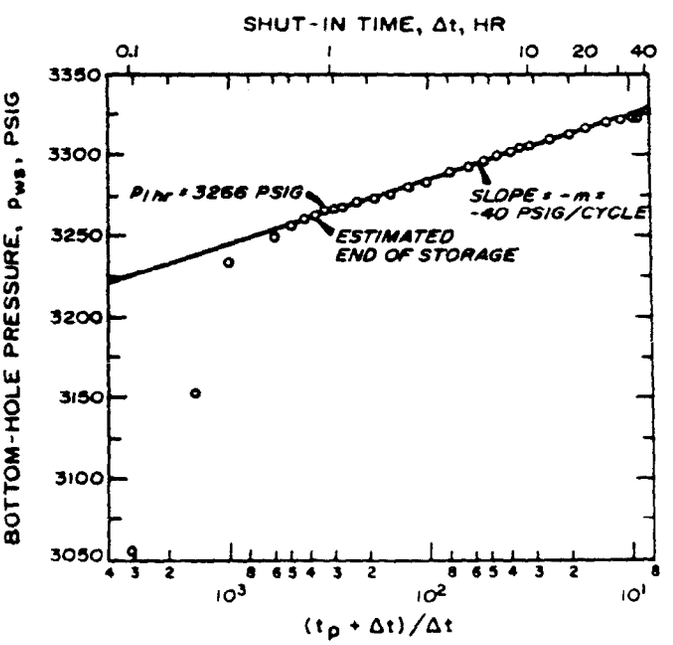

Fig. 5.4 Horner plot of pressure buildup data for Example 5.1.

Horner Plot

The Horner pressure-buildup test data analysis can be used to estimate permeability and skin in finite reservoirs just as in infinite-acting reservoirs, since boundary effects influence only late-time data. The data plot is as described in Section 5.2 and Fig. 5.2; Eqs. 5.6, 5.7, and 5.9 apply. Section 5.2 states that an estimate of p_i is obtained by extrapolating the straight-line section of the Horner plot to infinite shut-in time. For finite and developed reservoirs, the extrapolated pressure is not a good estimate of p_i and generally has been called the "false pressure," p^*.[1,6,9,10] Fig. 5.5 shows pressure buildup data for a well in a finite reservoir. The extrapolated false pressure, p^*, is higher than the average pressure at the instant of shut-in unless the drainage region is highly skewed.

Using the concept of the false pressure, we may rewrite Eq. 5.4:

$$p_{ws} = p^* - m \log \left(\frac{t_p + \Delta t}{\Delta t} \right) . \quad \ldots\ldots\ldots\ldots (5.10)$$

Ramey and Cobb[10] show that p^* is related to p_i by

$$p^* = p_i - \frac{141.2\, qB\mu}{kh} \left[p_D(t_{pD}) - \frac{1}{2} (\ln t_{pD} + 0.80907) \right] . \quad \ldots\ldots\ldots\ldots (5.11)$$

When the logarithmic approximation, Eq. 5.3, can be used for $p_D(t_{pD})$ in Eq. 5.11, p^* is identical to p_i.

Eq. 5.10 indicates that the normal Horner plot, p_{ws} vs log $\left[(t_p + \Delta t)/\Delta t\right]$, should have a straight-line section with slope $-m$, as schematically illustrated in Figs. 5.2 and 5.5. Although it is commonly believed that the Horner plot should be used only for new wells or when t_p is relatively small, Ramey and Cobb[10] and Cobb and Smith[19] indicate that the Horner plot may *always* be used for pressure-buildup data analysis. However, since it requires more work than the Miller-Dyes-Hutchinson method, the Horner plot is generally not used unless $t_p < t_{pss}$.

Chapter 7

Injection Well Testing

7.1 Introduction

In many reservoirs, the number of injection wells approaches the number of producing wells, so the topic of testing those wells is important. That is particularly true when tertiary recovery projects are being considered or are in progress. When an input well receives an expensive fluid, its ability to accept that fluid uniformly for a long time is important to the economics of the tertiary recovery project. In particular, increasing wellbore damage must be detected and corrected promptly.

The information available about injection well testing is much less abundant than information about production well testing. Matthews and Russell[1] summarize injection well testing, but emphasize falloff testing. Injectivity testing is rarely discussed in the literature, but it can be important.[2] Falloff testing is treated[3-7] rather thoroughly, particularly for systems with unit mobility ratio. Gas-well falloff testing, especially in association with in-situ combustion, also has been discussed.[8,9]

Injection-well transient testing and analysis are basically simple — as long as the *mobility ratio* between the injected and the in-situ fluids is about unity. Fortunately, that is a reasonable approximation for many waterfloods. It also is a reasonable approximation in watered-out waterfloods that initially had mobility ratios significantly different from unity, and early in the life of tertiary recovery projects when so little fluid has been injected that it appears only as a skin effect. When the unit-mobility-ratio condition is satisfied, injection well testing for liquid-filled systems is analogous to production well testing. Injection is analogous to production (but the rate, q, used in equations is negative for injection while it is positive for production), so an injectivity test (Section 7.2) parallels a drawdown test (Chapter 3). Shutting in an injection well results in a pressure falloff (Section 7.3) that is analogous to a pressure buildup (Chapter 5). The equations for production well testing in Chapters 3 through 5 apply to injection well testing as long as sign conventions are observed. The analogy should become clear in the next two sections.

When the unit-mobility-ratio assumption is not satisfied, the analogy between production well testing and injection well testing is not so complete. In that situation, analysis depends on the relative sizes of the water bank and the oil bank; generally, analysis is possible only when $r_{ob} > 10r_{wb}$ (see Section 7.5). Fracturing effects, which can have a significant effect on analysis, are discussed in Section 11.3.

Reservoirs with injection wells can reach true steady-state conditions when total injection rate equals total production rate. In that situation, or when the situation is approached, the steady-state analysis techniques of Section 7.7 may be useful.

7.2 Injectivity Test Analysis in Liquid-Filled, Unit-Mobility-Ratio Reservoirs

Injectivity testing is pressure transient testing during injection into a well. It is analogous to drawdown testing, for both constant and variable injection rates. Although sometimes called "injection pressure buildup" or simply "pressure buildup," we prefer to use the term "injectivity testing" to avoid confusion with production-well pressure buildup testing. This section applies to liquid-filled reservoirs with mobility of the injected fluid essentially equal to the mobility of the in-situ fluid. If the unit-mobility-ratio condition is not satisfied, results of analysis by techniques in this section may not be valid. Even in that situation, if the radius of investigation is not beyond the water (injected-fluid) bank, valid analysis can be made for permeability and skin, but not necessarily for static reservoir pressure.

Fig. 7.1 shows an ideal rate schedule and pressure response for injectivity testing. The well is initially shut in and pressure is stabilized at the initial reservoir pressure, p_i. At time zero, injection starts at constant rate, q. Fig. 7.1 illustrates the convention that $q < 0$ for injection. It is advisable to monitor the injection rate carefully so the methods of Chapter 4 (variable-rate analysis) may be applied if the rate varies significantly.

Since unit-mobility-ratio injection well testing is analogous to production well testing, the analysis methods in Chapters 3 and 4 for drawdown and multiple-rate testing may be applied directly to injection well testing. Of course, while pressure at a production well declines during drawdown, pressure at an injection well increases during injec-

tion. That difference is accounted for in the analysis methods by using $q < 0$ for injection and $q > 0$ for production.

For the constant-rate injectivity test illustrated in Fig. 7.1, the bottom-hole injection pressure is given by Eq. 3.5:

$$p_{wf} = p_{1hr} + m \log t. \quad \ldots\ldots\ldots\ldots\ldots\ldots\ldots\ldots (7.1)$$

Eq. 7.1 indicates that a plot of bottom-hole injection pressure vs the logarithm of injection time should have a straight-line section, as shown in Fig. 7.2. The intercept, p_{1hr}, is given by Eq. 3.7; the slope is m and is given by Eq. 3.6:

$$m = \frac{-162.6\,qB\mu}{kh} \quad \ldots\ldots\ldots\ldots\ldots\ldots\ldots\ldots (7.2)$$

As in drawdown testing, wellbore storage may be an important factor in injection well testing. Often, reservoir pressure is low enough so that there is a free liquid surface in the shut-in well. In that case, the wellbore storage coefficient is given by Eq. 2.16 and can be expected to be relatively large. Therefore, we recommend that all injectivity test analyses start with the $\log(p_{wf} - p_i)$ vs $\log t$ plot so the duration of wellbore storage effects may be estimated as explained in Sections 2.6 and 3.2. As indicated in Fig. 7.2, wellbore effects may appear as a semilog straight line on the p_{wf} vs $\log t$ plot; if such a line is analyzed, low values of permeability will be obtained and calculated skin factor will be shifted in the negative direction. Eq. 3.8 may be used to estimate the beginning of the semilog straight line shown in Fig. 7.2:

$$t > \frac{(200{,}000 + 12{,}000\,s)\,C}{(kh/\mu)} \quad \ldots\ldots\ldots\ldots\ldots\ldots (7.3)$$

Once the semilog straight line is determined, reservoir permeability is estimated from Eq. 3.9:

$$k = \frac{-162.6\,qB\mu}{mh} \quad \ldots\ldots\ldots\ldots\ldots\ldots\ldots\ldots (7.4)$$

Skin factor is estimated with Eq. 3.10:

$$s = 1.1513\left[\frac{p_{1hr} - p_i}{m} - \log\left(\frac{k}{\phi\mu c_t r_w^2}\right) + 3.2275\right]. \quad \ldots\ldots\ldots\ldots\ldots\ldots\ldots\ldots (7.5)$$

Example 7.1 Injectivity Test Analysis in an Infinite-Acting Reservoir

Figs. 7.3 and 7.4 show pressure response data for an injectivity test in a waterflooded reservoir. Before the test, all wells in the reservoir had been shut in for several weeks and pressure had stabilized. Known reservoir data are

depth = 1,002 ft	$h = 16$ ft
$c_t = 6.67 \times 10^{-6}$ psi^{-1}	$\mu = 1.0$ cp
$\phi = 0.15$	$B = 1.0$ RB/STB
$\rho_w = 62.4$ lb$_m$/cu ft	$q = -100$ STB/D
$p_i = 194$ psig	$r_w = 0.25$ ft.

The well is completed with 2-in. tubing set on a packer. The reservoir had been under waterflood for several years. We can safely assume that the unit-mobility-ratio assumption is satisfied, since the test radius of investigation is less than the distance to the water bank, as shown by calculations later in this example.

The log-log data plot, Fig. 7.3, indicates that wellbore storage is important for about 2 to 3 hours. The deviation of the data above the unit-slope line suggests that the wellbore storage coefficient decreased at about 0.55 hour. Sections 2.6 and 11.2 and Figs. 2.12 and 11.5 through 11.7 discuss such changing wellbore storage conditions. The data in Fig. 7.3 start deviating upward from the unit-slope straight line when $\Delta p = 230$ psi and $p_{wf} = 424$ psig. Since the column of water in the well is equivalent to about 434 psi, it appears that the apparent decrease in storage coefficient corresponds to fillup of the tubing.

From the unit-slope portion of Fig. 7.3, $\Delta p = 408$ psig when $\Delta t = 1$ hour. Using Eq. 2.20, we estimate the apparent wellbore storage coefficient:

$$C = \frac{(100)(1.0)}{24}\,\frac{(1.0)}{(408)} = 0.0102 \text{ bbl/psi}.$$

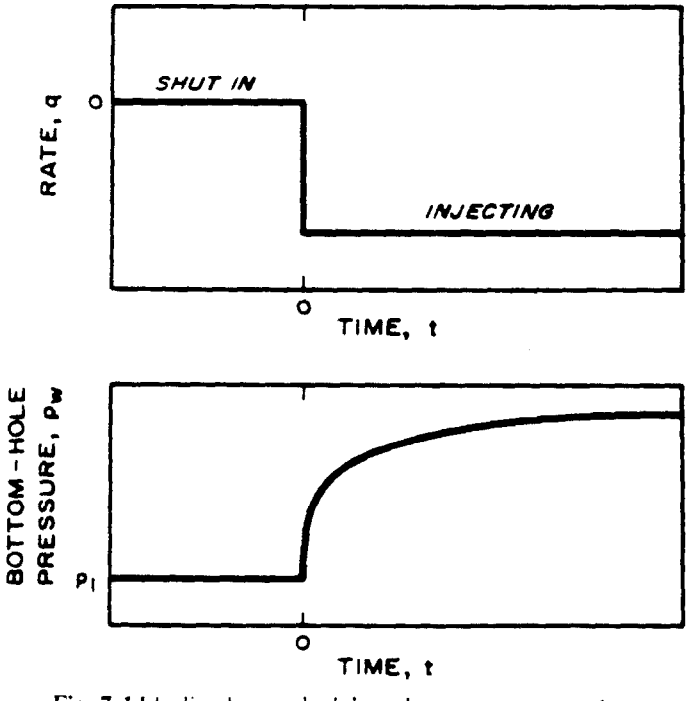

Fig. 7.1 Idealized rate schedule and pressure response for injectivity testing.

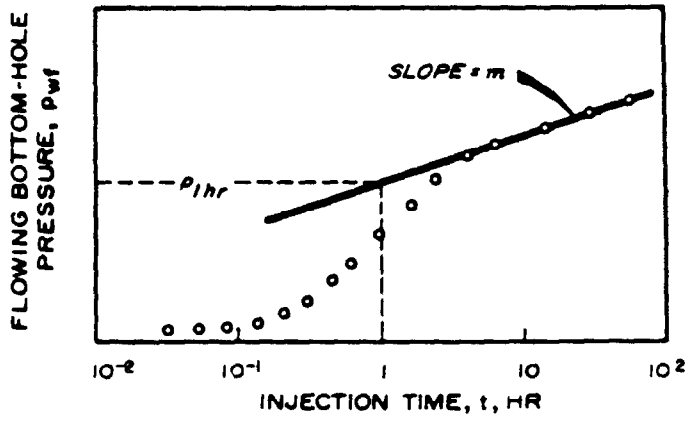

Fig. 7.2 Semilog plot of typical injectivity test data.

(C is always positive.) Wellbore capacity for a rising fluid level can be estimated (from Eq. 2.16) to get $V_u = 0.0044$ bbl/ft. Two-inch tubing has a capacity of about 0.004 bbl/ft, so the unit-slope straight line does correspond to a rising fluid level in the tubing. If we use $C = 0.0102$ in Eq. 7.3, or if we go 1 to 1.5 cycles in Δt after the data start deviating from the unit-slope line (Section 2.6), we would decide that the semilog straight line should not start for 5 to 10 hours of testing. Those rules indicate too long a time for a *decreasing* wellbore storage condition. Figs. 7.3 and 7.4 clearly show that wellbore storage effects have died out after about 2 to 3 hours.

Fig. 7.4 shows a semilog straight line through the data after 3 hours of injection. From this line, $m = 80$ psig/cycle and $p_{1hr} = 770$ psig. Permeability is estimated using Eq. 7.4:

$$k = \frac{-(162.6)(-100)(1.0)(1.0)}{(80)(16)} = 12.7 \text{ md.}$$

We may now determine if the unit-mobility-ratio analysis applies. The estimated permeability is used to estimate a radius of investigation from Eq. 2.41:

$$r_d \simeq 0.029\sqrt{\frac{kt}{\phi\mu c_t}}$$

$$\simeq 0.029\sqrt{\frac{(12.7)(7)}{(0.15)(1.0)(6.67\times 10^{-6})}}$$

$$\simeq 273 \text{ ft.}$$

A volumetric balance provides an estimate of the distance to the water bank. The volume injected is

$$W_i = \frac{\pi r_{wb}^2 h\phi\Delta S_w}{5.6146},$$

so

$$r_{wb} = \sqrt{\frac{5.6146\, W_i}{\pi h\phi\Delta S_w}}.$$

Assuming that $\Delta S_w = 0.4$ and that injection has been under way for at least 2 years,

$$W_i \simeq (100 \text{ STB/D})(1.0 \text{ RB/STB})(2 \text{ years})(365 \text{ D/year})$$

$$\simeq 73{,}000 \text{ res bbl}$$

and

$$r_{wb} = \sqrt{\frac{(5.6146)(73{,}000)}{\pi(16)(0.15)(0.4)}} \simeq 369 \text{ ft.}$$

Since $r_d < r_{wb}$, we are justified in using the unit-mobility-ratio analysis.

Eq. 7.5 provides an estimate of the skin factor:

$$s = 1.1513\left\{\frac{770-194}{80} - \log\left[\frac{12.7}{(0.15)(1.0)(6.67\times 10^{-6})(0.25)^2}\right] + 3.2275\right\}$$

$$= 2.4.$$

The well is damaged; the pressure drop across the skin may be estimated from Eq. 2.9:

$$\Delta p_s = \frac{(141.2)(-100)(1.0)(1.0)(2.4)}{(12.7)(16)}$$

$$= -167 \text{ psi.}$$

The negative sign here indicates damage since the pressure decreases away from the well (in the positive r direction) for injection while it increases for production. This is seen by computing the flow efficiency from Eq. 2.12. Assume $\bar{p} = p_i = 194$ psi, since the reservoir is stabilized before injection. Using $p_{wf} = 835$ psig from the last available data point, the *flow efficiency* is

$$\frac{194 - 835 - (-167)}{194 - 835} = 0.74.$$

If we had ignored the sign on q when estimating Δp_s, we would have incorrectly computed a flow efficiency of 1.26, indicating improvement instead of damage.

Multiple-rate injection testing, constant-pressure injection testing, injectivity testing after falloff testing, etc., are all performed and analyzed as explained for production well

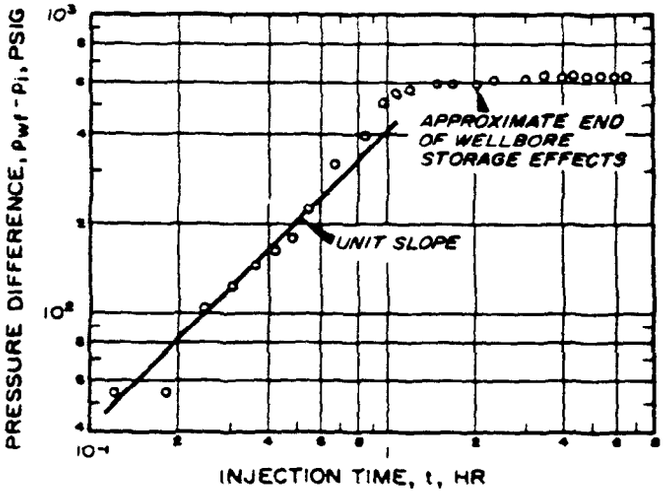

Fig. 7.3 Log-log data plot for the injectivity test of Example 7.1. Water injection into a reservoir at static conditions.

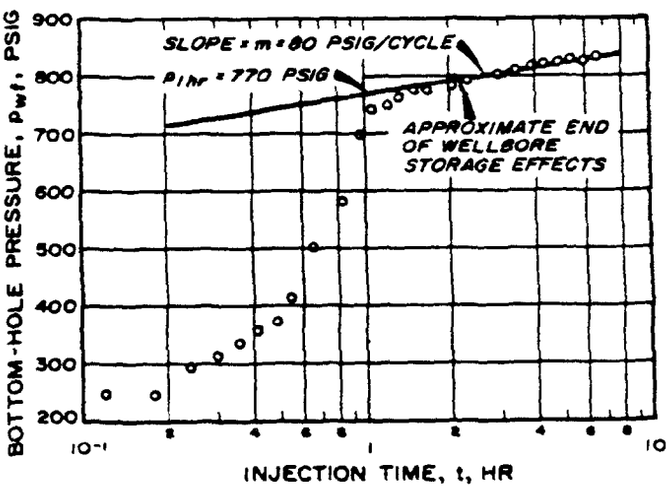

Fig. 7.4 Semilog plot for the injectivity test of Example 7.1. Water injection into a reservoir at static conditions.

testing in Chapters 3 and 4. Type-curve matching for injection well testing is done just as it is for production well testing (Section 3.3); the Δp used must be positive for plotting the log scale, although it is actually a negative number. The signs must be considered in analysis.

Eqs. 7.1 through 7.5 apply to injectivity testing in infinite-acting reservoirs, just as do Eqs. 3.5 through 3.10 for drawdown testing. When an injection well in a developed reservoir shows the effects of interference from other wells, the infinite-acting analysis may not be strictly applicable. In that case, the techniques presented in Section 3.4 should be used.

7.3 Falloff Test Analysis for Liquid-Filled, Unit-Mobility-Ratio Reservoirs

Falloff testing, illustrated schematically in Fig. 7.5, is analogous to pressure buildup testing in a production well. Injection is at a constant rate, q, until the well is shut in at time t_p. Pressure data taken immediately before and during the shut-in period are analyzed as pressure buildup data are analyzed. The pressure falloff behavior can be expressed by Eq. 5.10 for both infinite-acting and developed reservoirs:

$$p_{ws} = p^* - m \log\left(\frac{t_p + \Delta t}{\Delta t}\right) \quad \ldots\ldots\ldots\ldots\ldots (7.6)$$

The false pressure, p^*, is equivalent to the initial pressure, p_i, for an infinite-acting system. As illustrated in Fig. 7.6, Eq. 7.6 indicates that a plot of p_{ws} vs $\log[(t_p + \Delta t)/\Delta t]$ should have a straight-line portion with intercept p^* at infinite shut-in time $[(t_p + \Delta t)/\Delta t = 1]$ and with slope $-m$, where m is given by Eq. 5.5:

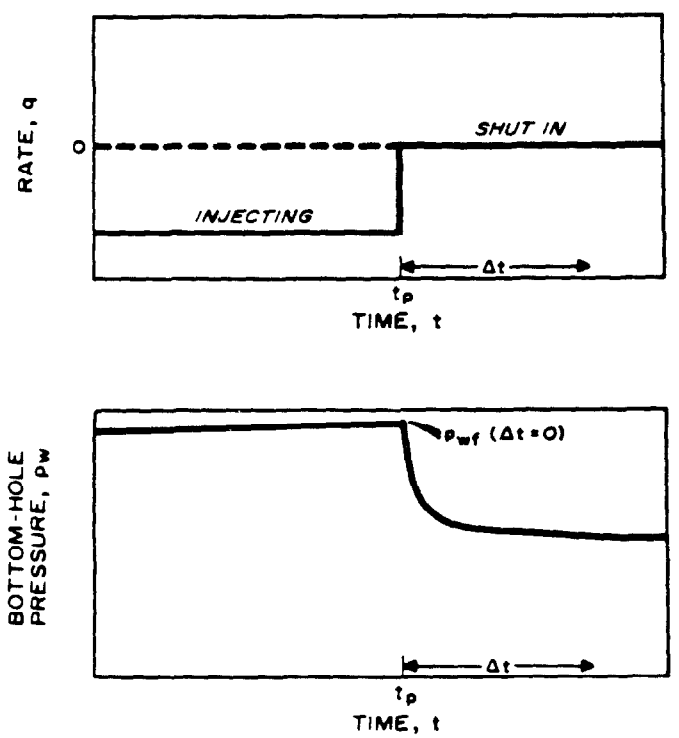

Fig. 7.5 Idealized rate schedule and pressure response for falloff testing.

$$m = \frac{162.6\,qB\mu}{kh} \quad \ldots\ldots\ldots\ldots\ldots (7.7)$$

As in buildup testing, the Horner graph is plotted with the horizontal scale increasing from right to left (Fig. 7.6). Thus, although the slope appears to be negative, it is actually positive because of the reverse plotting; m is negative since $m = -$slope.

As for other transient well tests, the log-log data plot should be made so the end of wellbore storage effects may be estimated and the proper semilog straight line (Fig. 7.6) can be chosen. Eq. 5.15b may be used to estimate the beginning of the semilog straight line for falloff testing:

$$t = \frac{170{,}000\,Ce^{0.14s}}{(kh/\mu)} \quad \ldots\ldots\ldots\ldots\ldots (7.8)$$

but the log-log plot is preferred.

Once the correct semilog straight line has been determined, reservoir permeability and skin factor are estimated from Eqs. 5.6 and 5.7:

$$k = \frac{162.6\,qB\mu}{mh} \quad \ldots\ldots\ldots\ldots\ldots (7.9)$$

and

$$s = 1.1513\left[\frac{p_{1hr} - p_{wf}(\Delta t = 0)}{m} - \log\left(\frac{k}{\phi\mu c_t r_w^2}\right) + 3.2275\right] \quad \ldots\ldots\ldots\ldots\ldots (7.10)$$

As is the case in pressure buildup testing, if the injection rate varies before the falloff test, the equivalent injection time may be approximated from Eq. 5.9:

$$t_p = \frac{24\,V_p}{q} \quad \ldots\ldots\ldots\ldots\ldots (7.11)$$

where V_p is the cumulative volume injected since the *last pressure equalization* and q is the constant rate just before shut-in. Comments made in Sections 5.2 and 6.3 about the proper t_p to use for a Horner-type analysis also apply here. In Eq. 7.11, the numerator is usually the cumulative injection since the last pressure equalization rather than the cumula-

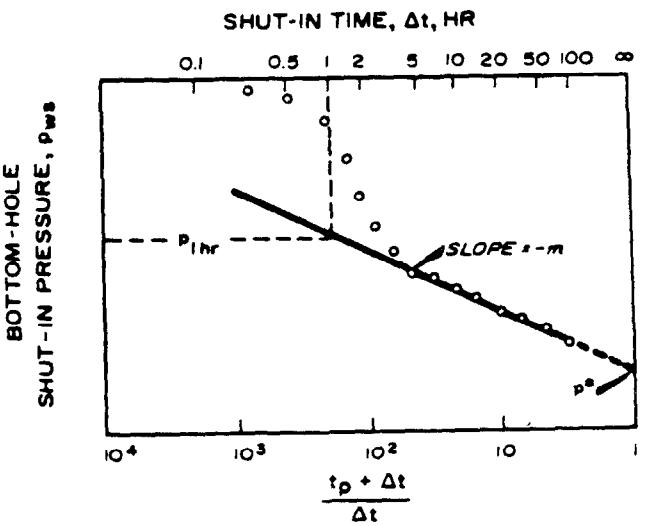

Fig. 7.6 Horner plot of a typical falloff test.

tive injection since the well was put on injection. If $t_p > 2t_{pss}$, then, for reasons discussed in Sections 5.2 and 6.3, the time to reach pseudosteady state (or steady state, which for a five-spot system[10] occurs at $t_{DA} = 0.25$ with A = the area per well, not per pattern) should be used[11,12] in place of t_p.

Miller-Dyes-Hutchinson-type plotting of falloff data, as suggested by Eq. 5.13,

$$p_{ws} = p_{1hr} + m \log \Delta t \ , \quad \ldots\ldots\ldots\ldots\ldots\ldots\ldots\ldots (7.12)$$

also applies to falloff testing. The analysis method of Section 5.3 applies: m in Eq. 7.12 is the slope of the p_{ws} vs log Δt straight line and is defined by Eq. 7.7; k is estimated from Eq. 7.9; skin factor is estimated from Eq. 7.10; and the false pressure, p^*, may be estimated from Eq. 5.14. The end of the semilog straight line (either Horner or MDH) may be estimated by using Eq. 5.16 and Figs. 5.6 and 5.7. Because it is less work, the MDH plot is more practical unless t_p is less than about twice the maximum shut-in time. If necessary, the Horner plot may be used for a second pass to estimate average pressure.

Muskat-type plotting may be used to analyze pressure falloff tests, but this is generally not recommended since the boundary conditions in injection well testing are more complicated than the simple single-well closed systems assumed in the analysis technique described in Section 5.3. The information in Section 6.4 indicates that a Muskat plot may provide good results if there is essentially a constant-pressure boundary between production and injection wells.

Example 7.2 Pressure Falloff in a Liquid-Filled, Infinite-Acting Reservoir

During a stimulation treatment, brine was injected into a well and the falloff data shown in Figs. 7.7 through 7.9 were taken.[6] Other data include

$t_p = 6.82$ hours

total falloff time = 0.67 hour

$p_{tf}(\Delta t = 0) = 1{,}310$ psig
$q_w = -807$ STB/D
$B_w = 1.0$ RB/STB
$\mu_w = 1.0$ cp
$c_t = 1.0 \times 10^{-5}$ psi^{-1}
$c_w = 3.0 \times 10^{-6}$ psi^{-1}
$\phi = 0.25$
$r_w = 0.4$ ft
$\rho_w = 67.46$ lb$_m$/cu ft
$h = 28$ ft
depth = 4,819 ft
$A = 20$ acres = 871,200 sq ft.

Fig. 7.7 is the log-log plot for the test data. From the shape of the curve, it appears that the semilog straight line should begin by 0.1 to 0.2 hour. Using $\Delta p = 238$ psi and $\Delta t = 0.01$ hour from the unit-slope straight line, we estimate the wellbore storage coefficient from Eq. 2.20:

$$C = \frac{(807)(1.0)(0.01)}{(24)(238)} = 0.0014 \text{ RB/psi}.$$

C must be positive, so we disregard the sign convention here. Since wellhead pressure was always above atmospheric, the wellbore remained full during the test. Thus, Eq. 2.17 and a wellbore compressibility of $c_w = 3.0 \times 10^{-6}$ psi^{-1} can be used to estimate the wellbore volume corresponding to $C = 0.0014$ bbl/psi: $V_w = 467$ bbl. Using the depth of 4,819 ft, we compute a casing radius of 0.42 ft, which is too large for a hole of radius 0.4 ft. Nevertheless,

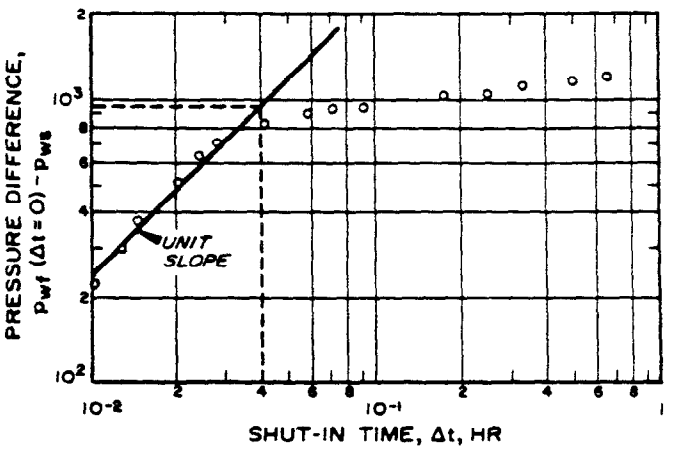

Fig. 7.7 Log-log data plot for a falloff test after brine injection, Example 7.2.

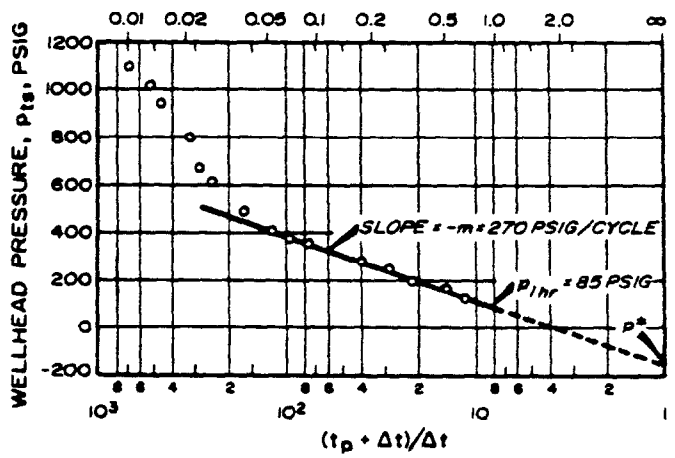

Fig. 7.8 Horner plot of pressure falloff after brine injection, Example 7.2.

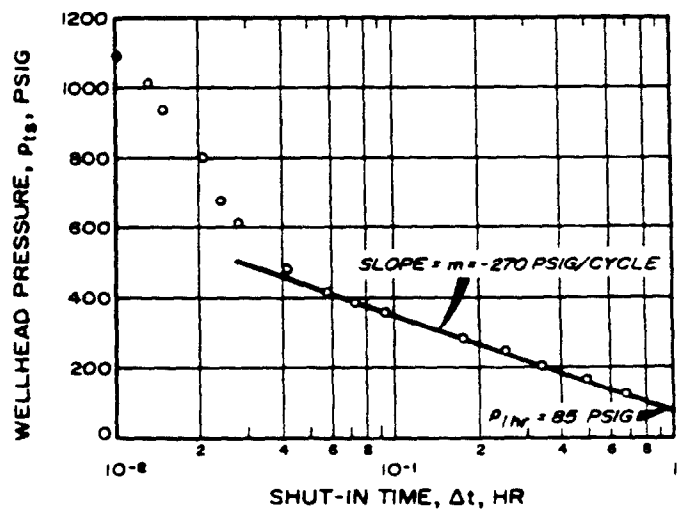

Fig. 7.9 Miller-Dyes-Hutchinson plot of pressure falloff after brine injection, Example 7.2.

the agreement is within reason. If the well was shut in at the injection pump rather than at the wellhead, the connecting lines would cause the storage coefficient to be larger than that resulting from the wellbore only. Unfortunately, we do not have all the information necessary to know if such speculation is correct. This clearly indicates the *need* for a diagram or a sketch of the well completion equipment and surface connecting lines.

Wellhead pressures are plotted vs $\log[(t_p + \Delta t)/\Delta t]$ in Fig. 7.8. That Horner plot can be used to estimate k, s, and p^*. Since the falloff time (0.67 hour) is much smaller than the flow time (6.82 hours), the log Δt (MDH) plot shown in Fig. 7.9 also may be used. The correct straight line in Figs. 7.8 and 7.9 indicates $m = -270$ psig/cycle and $p_{1hr} = 85$ psig. Thus, using Eq. 7.9,

$$k = \frac{(162.6)(-807)(1.0)(1.0)}{(-270)(28)} = 17.4 \text{ md.}$$

The skin factor is estimated from Eq. 7.10:

$$s = 1.1513 \left\{ \frac{85 - 1,310}{-270} - \log \left[\frac{17.4}{(0.25)(1.0)(1.0 \times 10^{-5})(0.4)^2} \right] + 3.2275 \right\}$$

$$= 0.15.$$

From Fig. 7.8, $p_{ts}^* = -151$ psig. This is the false pressure at the *surface*. Using the hydrostatic gradient of 0.4685 psi/ft and the depth of 4,819 ft, the initial bottom-hole pressure is estimated:

$$p^* = (4,819)(0.4685) - 151 = 2,107 \text{ psig.}$$

Since injection time t_p is short, we can safely assume that $p^* = \bar{p}$, so $\bar{p} = 2,107$ psig.

10.5 Layered Reservoir Systems

Layered reservoirs can be divided into two groups: *layered reservoirs with crossflow*, in which layers are hydrodynamically communicating at the contact planes (Fig. 10.11), and *layered reservoirs without crossflow*, in which layers communicate only through the wellbore (Fig. 10.12). The latter type of system also has been called a "commingled system".

Layered Reservoirs With Crossflow

Fig. 10.11 schematically shows a three-layer reservoir with crossflow allowed between the layers. Many papers discuss pressure transient testing in such reservoirs; Russell and Prats[27] summarize the practical aspects of those papers. They conclude that pressure transient behavior of a layered reservoir is the same as the behavior of the *equivalent homogeneous system*. Thus, the layered system with crossflow behaves like a homogeneous system with an arithmetic total permeability-thickness product,

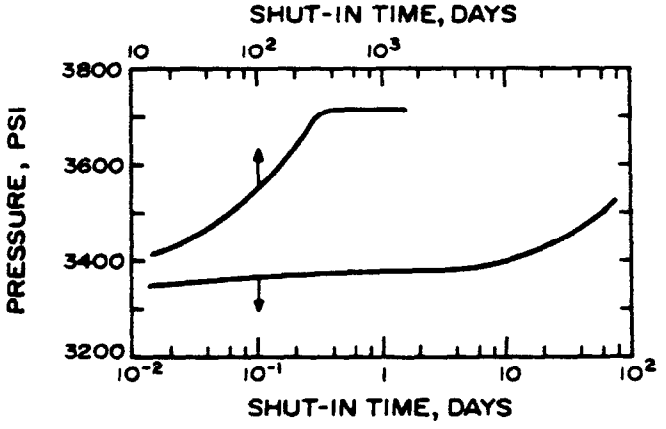

Fig. 10.10 Pressure buildup for a composite gas reservoir with $k_1 = 10$ md, $k_2 = 0.01$ md, $r_{f1} = 500$ ft, $r_e = 1{,}000$ ft, $\phi_1 = \phi_2$, $\mu_1 = \mu_2$, and $c_{t1} = c_{t2}$. After Carter.[22]

$$(kh)_t = \sum_{j=1}^{n} (kh)_j, \quad \ldots\ldots\ldots\ldots\ldots\ldots (10.14)$$

substituted for kh and an arithmetic total porosity-compressibility-thickness product,

$$(\phi c_t h)_t = \sum_{j=1}^{n} (\phi c_t h)_j, \quad \ldots\ldots\ldots\ldots\ldots\ldots (10.15)$$

substituted for $\phi c_t h$. The total number of layers is n. As a result, the appropriate semilog plot for any pressure transient test can be analyzed just like it can for homogeneous systems.

Kazemi and Seth[28] show how a series of drillstem tests on sequential intervals can be used to estimate the average permeability of the tested intervals and, thus, provide a gross picture of layering. A flow profile, such as a spinner survey, may also indicate gross reservoir stratification. If $(kh)_t$ is known from a well test, individual layer permeabilities may be approximated from[29]

$$k_j = (q_j/q)\left[(kh)_t/h_j\right], \quad j = 1, 2, \ldots, n. \quad \ldots\ldots\ldots\ldots\ldots\ldots (10.16)$$

Layered Reservoirs Without Crossflow

Fig. 10.12 schematically illustrates a two-layer reservoir with the layers separated by a flow barrier. Production is commingled at the well so layers communicate only through the well. Early-time pressure drawdown in such a system yields a straight line on the semilog plot,[30-35] as illustrated in Fig. 10.13. Nothing distinguishes the drawdown curve from that for a single-layer, homogeneous reservoir. The slope of the semilog straight line may be used to estimate $(kh)_t$ and average skin factor with normal drawdown equations. The drawdown curves shown in Fig. 10.13 are for a layered system with no skin damage or with equal skin damage in each layer. If the damage varies from layer to layer, the behavior may differ from that shown. Unfortunately, there is little information available about that situation.

The upward bending in Fig. 10.13 is caused by boundary effects. After a long enough production time, pseudosteady-state conditions prevail and the pressure behavior will be linear with time. Pseudosteady-state flow generally begins much later in a commingled system than in the equivalent single-layer system because of the complex variation in flow contribution of each layer and the different times required for boundary effects to be felt in each layer. Cobb, Ramey, and Miller[33] indicate that pseudosteady-state flow begins at approximately

$$(t_{DA})_{pss} \simeq 23.5\,(k_1/k_2), \quad k_1 > k_2, \quad \ldots\ldots\ldots (10.17)$$

for a single well in the center of a closed, circular, two-layered reservoir with porosity, compressibility, viscosity, and thickness equal in each layer. (Recall that $(t_{DA})_{pss} \simeq 0.1$ for a single-layer, closed, circular system.) Earlougher, Kersch, and Kunzman[35] indicate that the time to the beginning of pseudosteady state also depends on the relationship between the porosity, thickness, and compressibility in the various layers. We should also expect that time to depend on reservoir shape, number of layers, and well location.

A Horner or Miller-Dyes-Hutchinson plot of pressure buildup data for a single-well, closed, layered, no-crossflow system has an initial straight-line section with slope proportional to $(kh)_t$.[1,30-35] It has been stated that, after the initial semilog straight line, the buildup curve flattens, then steepens, and finally flattens toward static pressure,[1,30,33] as

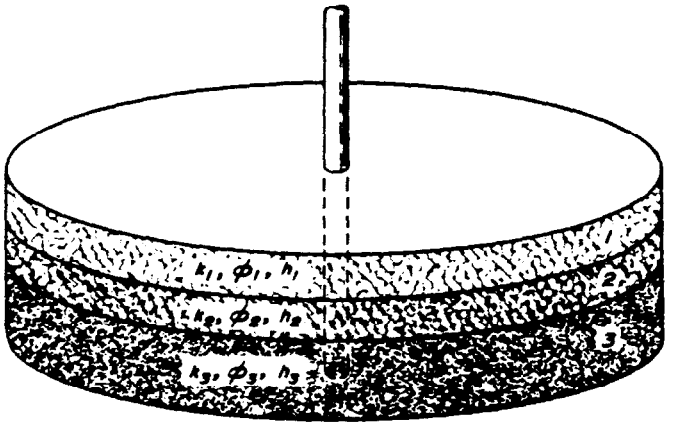

Fig. 10.11 Three-layer reservoir with crossflow.

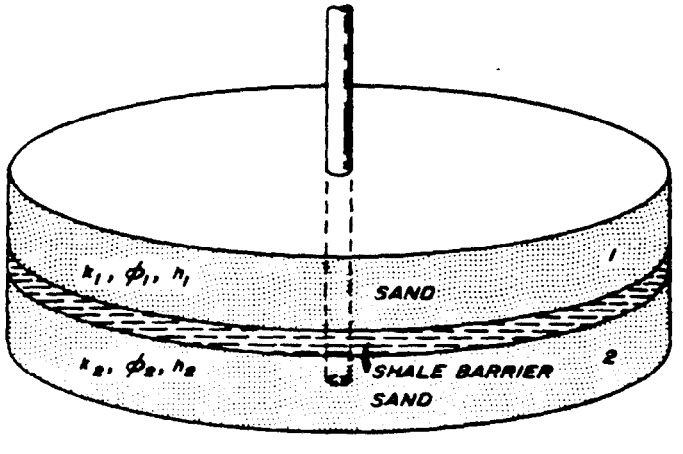

Fig. 10.12 Two-layer reservoir without crossflow.

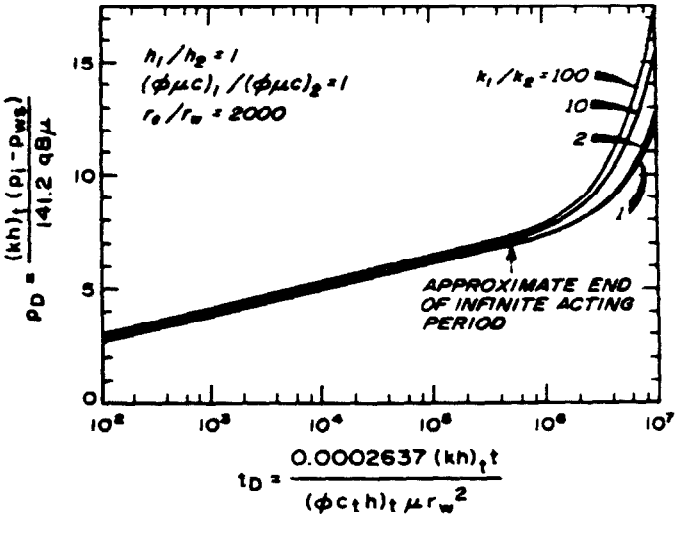

Fig. 10.13 Dimensionless drawdown behavior for a well in the center of a closed, circular, commingled, layered reservoir. After Cobb, Ramey, and Miller.[33]

indicated schematically in Fig. 10.14. *This is not always correct.* Several studies [32-35] show that the first flattening of the buildup curve, F-G in Fig. 10.14, can be insignificant for some systems. That is particularly true for large contrasts in thickness or porosity, for more than two layers, or for nonsymmetrical systems. Figs. 10.15 and 10.16 illustrate flattening and its absence. In Fig. 10.15, the flattening and secondary pressure rise are definitely apparent for the two lower curves. However, in the upper curve, where the *kh* ratio is the result of a large thickness ratio rather than a high permeability ratio, the buildup curve is indistinguishable from that for a single-layer system. Fig. 10.16 shows that the flattening does not occur for a 4:1 rectangle. Rather, the buildup curves take on a shape dominated by the drainage-area shape and the well location. Nevertheless, in all cases, the initial semilog straight-line segment may be used to estimate the total permeability-thickness product.[35] The second (steep) slope is not analyzable by known methods.

An additional danger lies in attributing the shape shown in Fig. 10.14 to layered reservoirs. Fig. 10.10, for a composite reservoir system, has the shape shown in Fig. 10.14. (There is no wellbore storage effect in Figs. 10.10, 10.15, and 10.16.) Changing wellbore storage can also cause the early part of a pressure buildup curve to be similar to the curve shown in Fig. 10.14; for examples, see Fig. 2.12 or Fig. 11.2, and Ref. 36.

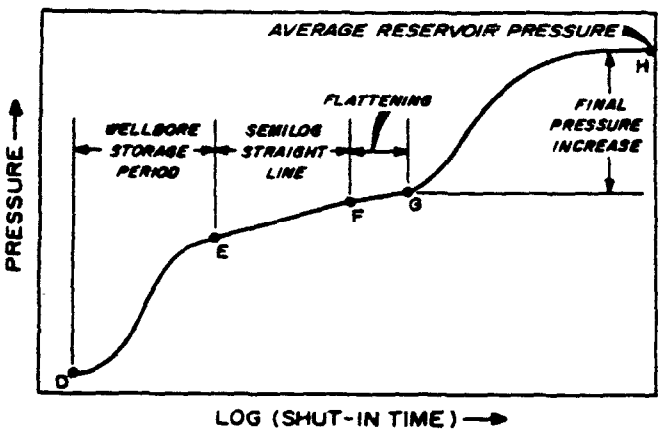

Fig. 10.14 Hypothetical pressure buildup curve for an ideal single-well, multiple-layer, bounded reservoir. After Earlougher, Kersch, and Kunzman.[35]

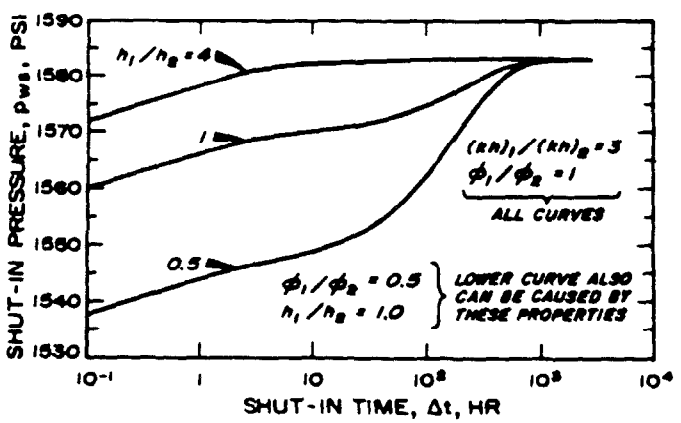

Fig. 10.15 Pressure buildup behavior as a function of thickness ratio for a well in the center of a square, two-layer reservoir; $(kh)_1/(kh)_2 = 3$, $\phi_1/\phi_2 = 1$. After Earlougher, Kersch and Kunzman.[35]

Almost all the published material about layered systems is for a single well in the center of a symmetrical bounded system. If there are other wells in the reservoir, and if they continue producing while one well is shut in for a buildup test, none of the pressure response characteristics described in Refs. 30 through 35 and illustrated in Figs. 10.14 through 10.16 necessarily occur. Fig. 10.17 shows pressure behavior when a single well in a developed, two-layer, commingled reservoir is shut in for pressure buildup testing. The initial semilog straight line is observed and may be used to estimate $(kh)_t$. However, neither the flattening nor the secondary pressure rise and eventual leveling to average reservoir pressure occur. Rather, the influence of adjacent producing wells causes the pressure to decline at the shut-in well, completely obscuring evidence of possible layered behavior.

Raghavan *et al.*[34] propose a technique for estimating the *kh* ratio between layers for a single well in the center of a circular, two-layer, commingled system. The method re-

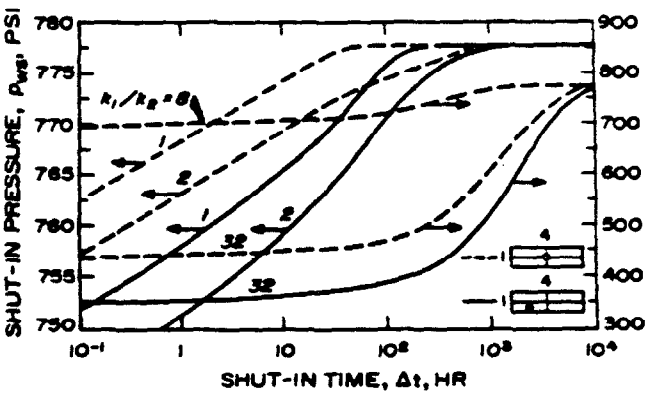

Fig. 10.16 Pressure buildup behavior as a function of permeability ratio for two different well locations in a two-layer, 4:1, rectangular reservoir; $\phi_1/\phi_2 = 1$, $h_1/h_2 = 1$. After Earlougher, Kersch, and Kunzman.[35]

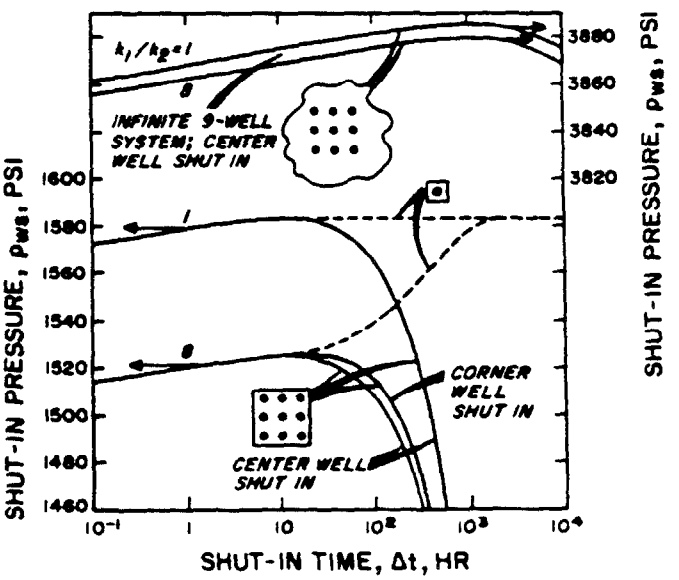

Fig. 10.17 Comparison of pressure buildup behavior in single-well and multiple-well layered systems; $\phi_1/\phi_2 = 1$, $h_1/h_2 = 1$. After Earlougher, Kersch, and Kunzman.[35]

quires a relatively long production time and requires that buildup data be taken *through* the final pressure rise.

Refs. 33 through 35 may be used to estimate average reservoir pressure from buildup tests in commingled systems. The techniques do require some knowledge of the layer properties and utilize correlations for specific systems.

Woods[29] has studied pulse-test behavior in a two-layer reservoir system. His studies include the commingled case, the full-communication case, and intermediate situations. He shows how a combination of single-well tests, pulse tests, and flowmeter surveys may be used to estimate individual-zone properties for two-layer reservoirs with communication only at the wellbores. He points out that the wellbores must be undamaged or uniformly damaged. He extensively studied *pulse-test* behavior in such reservoirs, with the following conclusions:

1. Apparent kh/μ is always equal to or greater than the actual total kh/μ for the reservoir.
2. Apparent $\phi c_t h$ is always equal to or less than total $\phi c_t h$ for the reservoir.
3. The deviation of apparent values from actual total values depends on the pulse duration (see Section 9.3).
4. When wells are undamaged or have uniform damage, the ratio of flow rates into the zones is a good estimator of kh/μ of the zones for noncommunicating systems. The estimate is usually valid within ±15 percent when the zones are partially communicating.